

GENERAL ATOMIC
DIVISION OF
GENERAL DYNAMICS

JOHN JAY HOPKINS LABORATORY FOR PURE AND APPLIED SCIENCE

P.O. BOX 608, SAN DIEGO, CALIFORNIA 92112

GA-5009, Vol. IV
Supplement



NUCLEAR PULSE SPACE VEHICLE STUDY

Vol. IV -- MISSION VELOCITY REQUIREMENTS
AND SYSTEM COMPARISONS
(SUPPLEMENT)

George C. Marshall Space Flight Center
Future Projects Office
National Aeronautics and Space Administration
Huntsville, Alabama

Contract NAS 8-11053

Issued February 28, 1966



[REDACTED]

[REDACTED]

FOREWORD

This report is a supplement to Vol. IV, Mission Velocity Requirements and System Comparisons (Unclassified) of the report on the Nuclear Pulse Vehicle Study performed under National Aeronautics and Space Administration Contract NAS8-11053. This supplement, referred to as Vol. IVA contains mission velocity and mass ratio charts which are background material for some of the missions studied under the above mentioned contract and which in part also represent relevant results of in-house studies.

The report is divided into six sections, one for each planet from Mercury to Saturn, including Earth. For Mercury, Venus and Jupiter, both, hyperbolic departure and arrival data, as well as planetocentric data are presented. For Saturn, only hyperbolic data, and for Earth and Mars only planetocentric data are presented. The hyperbolic departure and arrival data refer to mono-elliptic heliocentric transfer paths between Earth and target planet, and vice versa. In the case of Venus they are presented as impulsive velocity changes Δv (10^3 ft/sec) at 1.1 planet radii distance. By conversion to EMOS (97,700 ft/sec = 1 EMOS), the associated hyperbolic excess velocity v_{∞}^* (both in EMOS) can be read from $\Delta v^*/v_{\infty}^*$ (both in EMOS) versus v_{∞}^* charts for the respective capture conditions (1.1 planet radii, circular capture orbit). For Mercury, Jupiter and Saturn, the hyperbolic excess velocities are shown (in EMOS). The associated impulsive capture or departure maneuver is readily found from $\Delta v^*/v_{\infty}^*$ charts for a large range of planetocentric distances and capture orbit ellipticities.

The planetocentric data for Mercury, Venus and Jupiter refer to the (impulsive) maneuvers required for transition into circular orbit at the apopsis of elliptic capture orbits. Those for Earth and Mars refer to powered flight time and mass ratio versus hyperbolic excess velocity ranging from $F/W_0 = 0.001$ to 0.1 g at various specific impulses ranging from 1000 to 10,000 seconds. For Earth, four out of the five charts presented refer to departure operations, one ($0.05g$) to arrival at Earth. In comparing the chart for departure at 0.05 g with that for arrival at 0.05 g, it is seen that, for equal values of v_{∞}^* and I_{sp} , the mass ratio for the arrival maneuver is slightly higher than for the departure maneuver. The reason for this is that, for departure maneuvers, the thrust acceleration (thrust/weight ratio F/W_0) refers to the initial value, whereas, for the arrival maneuver, it designates the terminal value. The same definition applies to the Mars charts all of which pertain to arrival maneuvers. Therefore, the designation on the arrival maneuver charts should say F/W_1 , rather than F/W_0 . Initial and terminal conditions are circular orbit at 1.1 Earth radii and 1.3 Mars radii. Since, at Mars the gravitational losses are lower, the differences between departure and arrival maneuvers

of finite burning time (i. e. non-impulsive) is even smaller than for Earth. Therefore, the arrival maneuver charts for Mars are representative (though slightly conservative) also for Mars departure. For Venus, the values are sufficiently close to those for Earth to permit use of the Earth charts for the accuracy level required in this study.

It should be emphasized, that the thrust accelerations specified on top of each chart are in Earth surface g-values, not in local g-values. In other words, the thrust acceleration is given in units of 32.17 ft/sec² or 9.81 m/sec². The thrust direction is taken as tangential to the instantaneous velocity vector throughout the powered flight period. This is not the optimum, but is sufficiently close to it, to be representative for the actual powered flight path, if the latter would be optimized by varying the thrust vector between aximuthal and local tangential direction.

Only a few hyperbolic data are given for Venus and none for Mars, because values for missions to these planets are abundantly available¹⁾. In the chart for Earth departure to Venus in 1980, the designation $r_{\text{♂}}^* = 1.3$ on the upper left hand side should be changed to $r_{\text{♀}}^* = 1.1$.

1) cf., for instance, National Aeronautics and Space Administration, Space Flight Handbooks, Vol. 3, Planetary Flight Handbook, Part 1, 2 & 3, NASA, SP-35, Washington, D. C., 1963

TABLE OF CONTENTS

Part I: Mercury (Me)

Ea - Me; Me - Ea: 1980, 81, 82, 83, 84, 85, 86, 87

Mercury Capture: Δv vs v_{∞} ; $r^* = 1.1, 1.5, 2.0$

Mercury - centric: Apoapsis impulse for ell. -to-circ. orbit change

Part II: Venus (Ve)

Ea - Ve; Ve - Ea: 1975, 77, 78, 80, 81

Venus: Atmospheric entry velocity vs. v

Venus capture: Δv vs v_{∞} ; $r^* = 1.1, 1.3, 1.5, 2.0, 3.0, 5.0$

Venus - centric: Apoapsis impulse for ell. -to-circ. orbit change

Part III: Earth (Ea)

Earth departure mass ratio and burning time vs. v_{∞} for $1000 \leq I_{sp} \leq 10,000$ sec and initial thrust accelerations of: 0.001, 0.005, 0.01, 0.05, 0.1 g.

Earth arrival mass ratio and burning time vs. v_{∞} for $1000 \leq I_{sp} \leq 10,000$ sec and terminal thrust acceleration of 0.05 g.

Part IV: Mars (Ma)

Mars arrival mass ratio and burning time vs v_{∞} for $1000 \leq I_{sp} \leq 10,000$ sec and terminal thrust accelerations of 0.001, 0.005, 0.01

0.05 Earth-g

Part V: Jupiter (Ju)

Jupiter capture $\frac{\Delta v}{v_{\infty}}$ vs v_{∞} ; $r^* = 1.1, 2, 4, 6, 8, 10, 15, 20, 25, 30, 50, 100$

Jupiter capture: Δv vs v_{∞} ; $r^* = 1.1, 2.4$

Part VI: Saturn (Sa)

Ea - Sa; Sa - Ea: 1985, 86, 87, 88.

Saturn capture $\frac{\Delta v}{v_{\infty}}$ vs v_{∞} ; $r^* = 1.1, 2, 4, 6, 8, 10, 15, 20, 25, 30, 50$

Δv vs v_{∞} ; $r^* = 1.1, 2, 4, 6, 8, 19, 15, 20, 25, 30, 50, 70, 100$

NOMENCLATURE AND DEFINITIONS

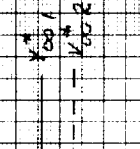
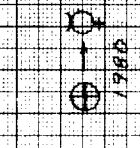
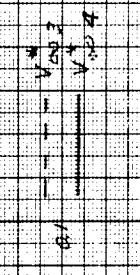
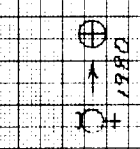
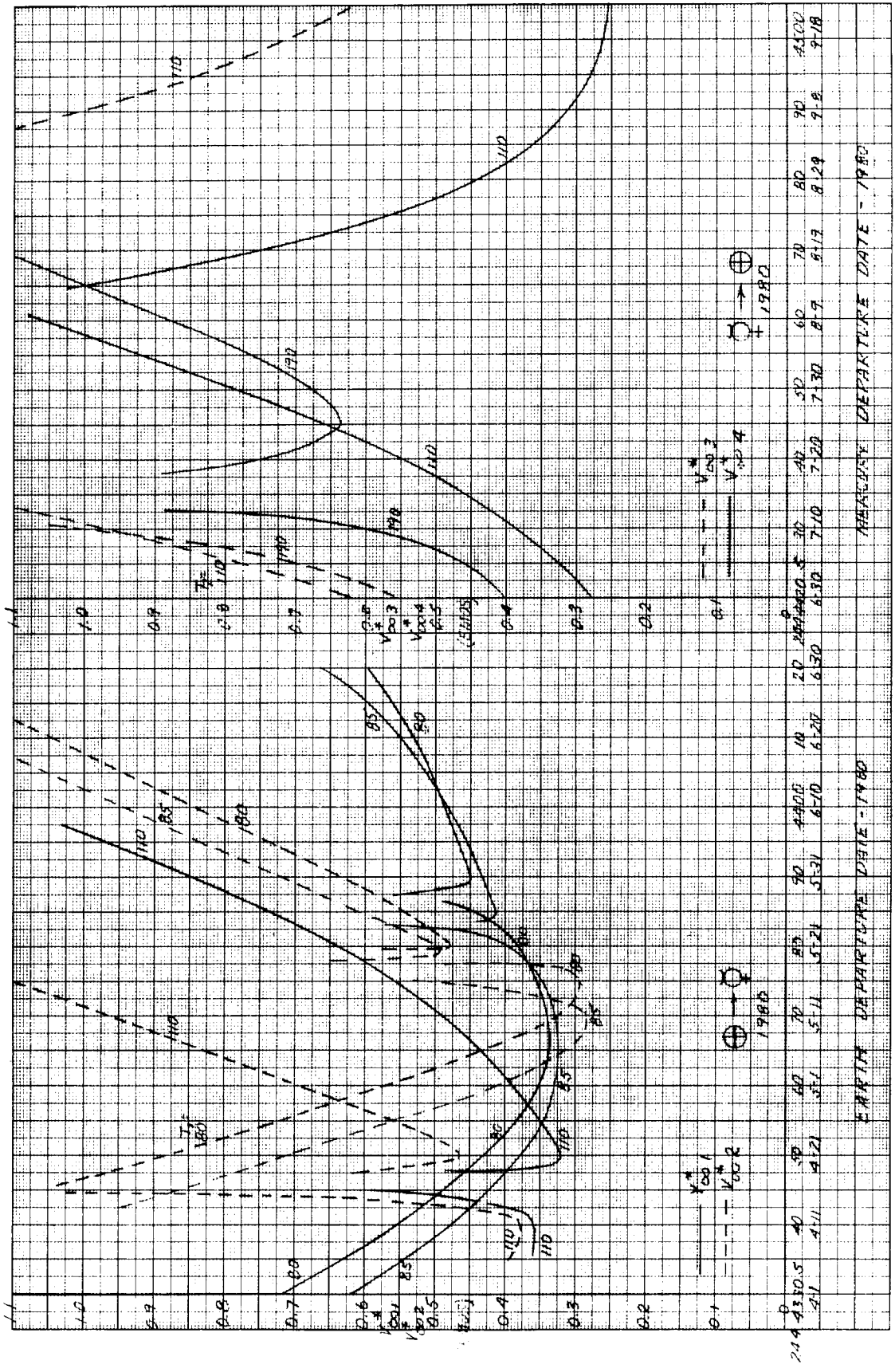
I_{sp}	= Specific impulse (sec)
n	= Ratio of apoapsis to periapsis distance of elliptic capture orbit
r^*	= Distance (planet radii)
r_P^*	= Periapsis distance (planet radii)
T_1	= Transfer period Earth to target planet (days)
T_2	= Transfer period target planet to Earth (days)
t_1	= Time of powered flight
v_E^*	= Earth atmospheric entry velocity following unretarded hyperbolic approach (nominally taken as the vacuum velocity along the approach hyperbola at 100 km apogee altitude) (EMOS)
W	= Weight (Earth pounds)
y	= Altitude (km)
Δv	= Impulsive velocity change (10^3 ft/sec)
Δv^*	= Impulsive velocity change (EMOS)
Δv_A	= Apoapsis impulse for change from elliptic to circular orbit (ft/sec)
	= Mass ratio (ignition to engine cut-off mass)
v_∞^*	= Hyperbolic excess velocity (EMOS)

Subscripts:

1	Earth departure
2	Target planet arrival
3	Target planet departure
4	Earth arrival

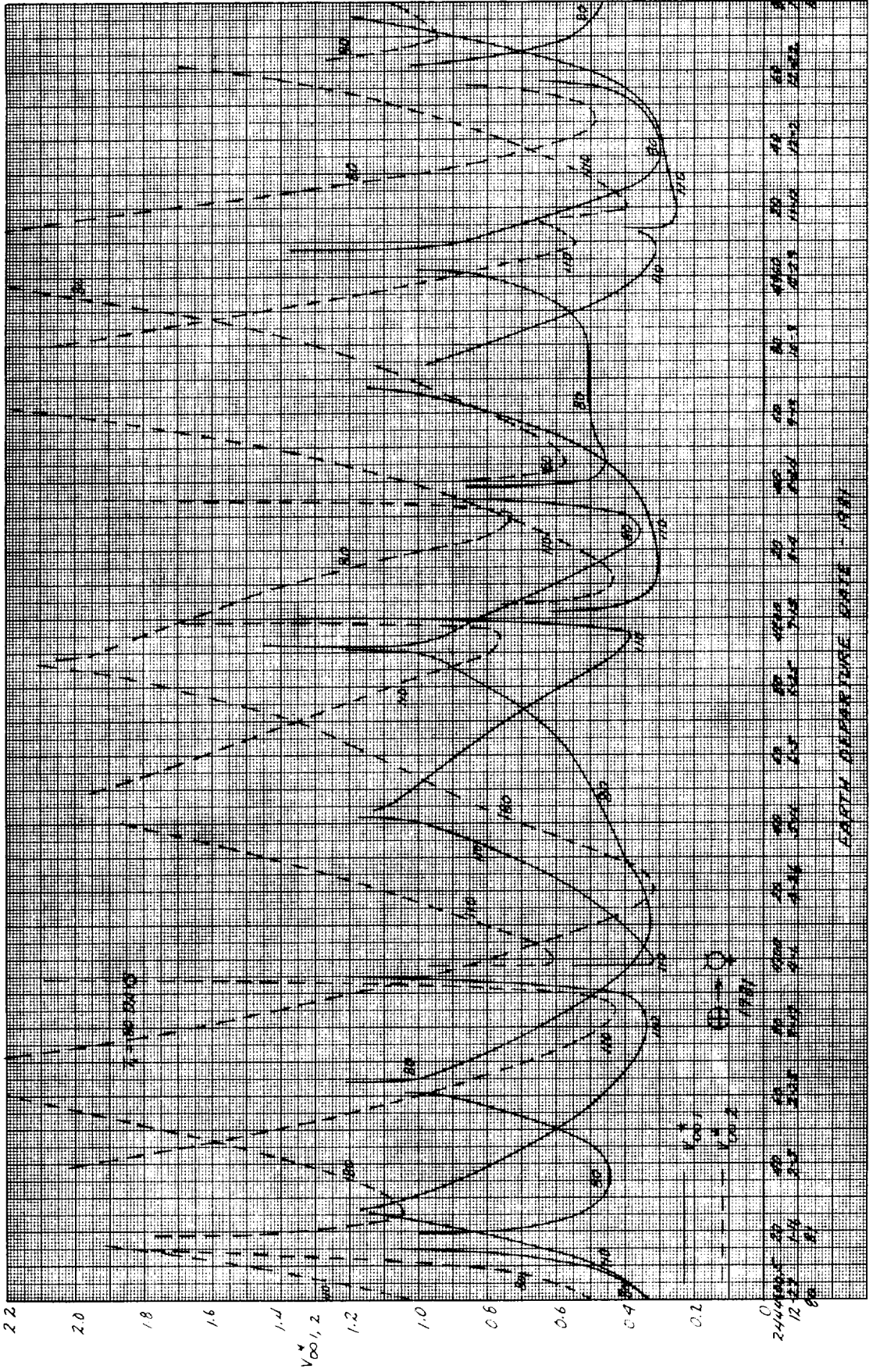
PART I MERCURY

640.1055

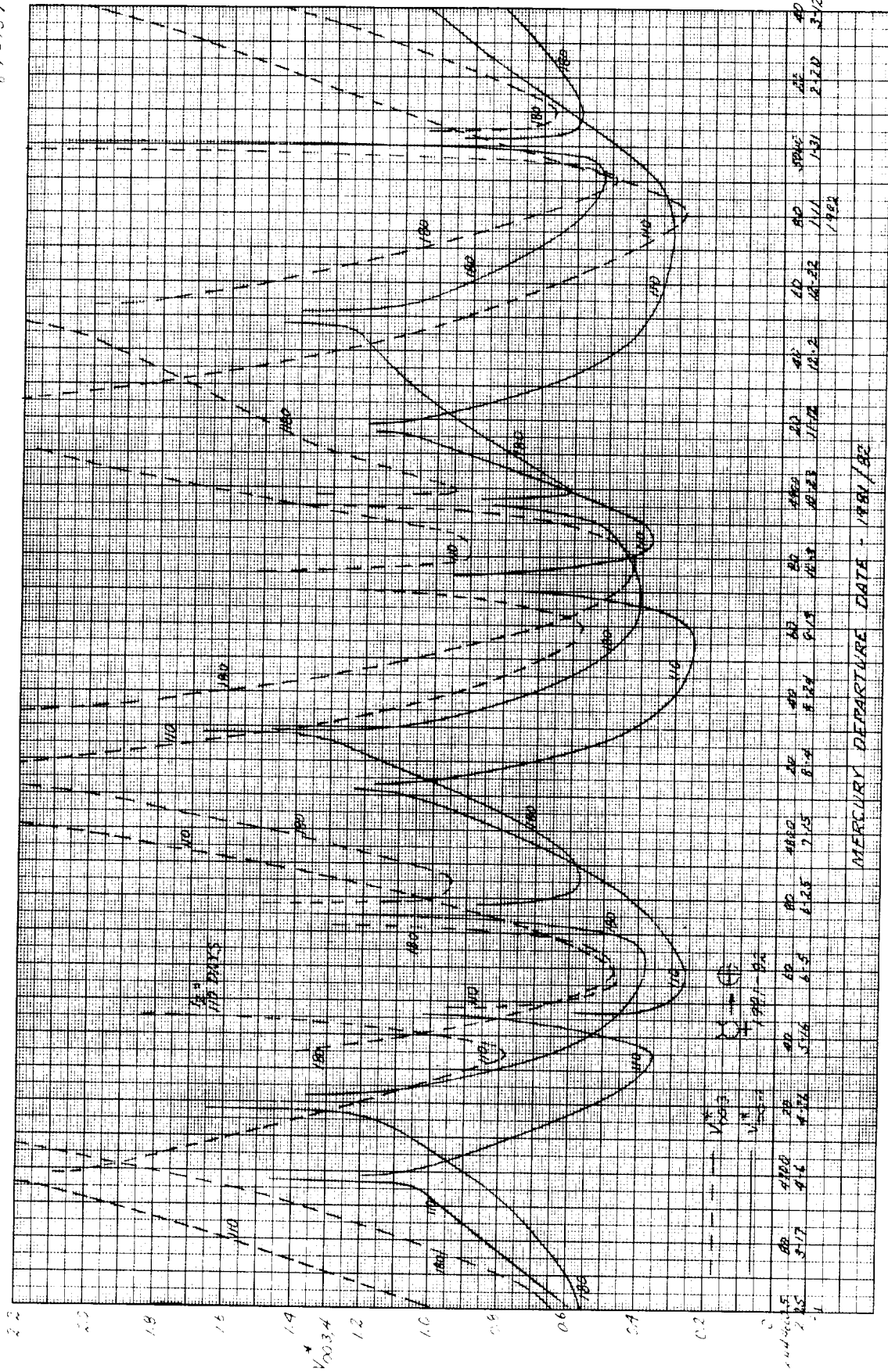


DATE	DEPARTURE	DATE	DEPARTURE
24 43 30.5	40	40	40
41	41	41	41
42	42	42	42
43	43	43	43
44	44	44	44
45	45	45	45
46	46	46	46
47	47	47	47
48	48	48	48
49	49	49	49
50	50	50	50
51	51	51	51
52	52	52	52
53	53	53	53
54	54	54	54
55	55	55	55
56	56	56	56
57	57	57	57
58	58	58	58
59	59	59	59
60	60	60	60
61	61	61	61
62	62	62	62
63	63	63	63
64	64	64	64
65	65	65	65
66	66	66	66
67	67	67	67
68	68	68	68
69	69	69	69
70	70	70	70
71	71	71	71
72	72	72	72
73	73	73	73
74	74	74	74
75	75	75	75
76	76	76	76
77	77	77	77
78	78	78	78
79	79	79	79
80	80	80	80
81	81	81	81
82	82	82	82
83	83	83	83
84	84	84	84
85	85	85	85
86	86	86	86
87	87	87	87
88	88	88	88
89	89	89	89
90	90	90	90
91	91	91	91
92	92	92	92
93	93	93	93
94	94	94	94
95	95	95	95
96	96	96	96
97	97	97	97
98	98	98	98
99	99	99	99
100	100	100	100

64-156

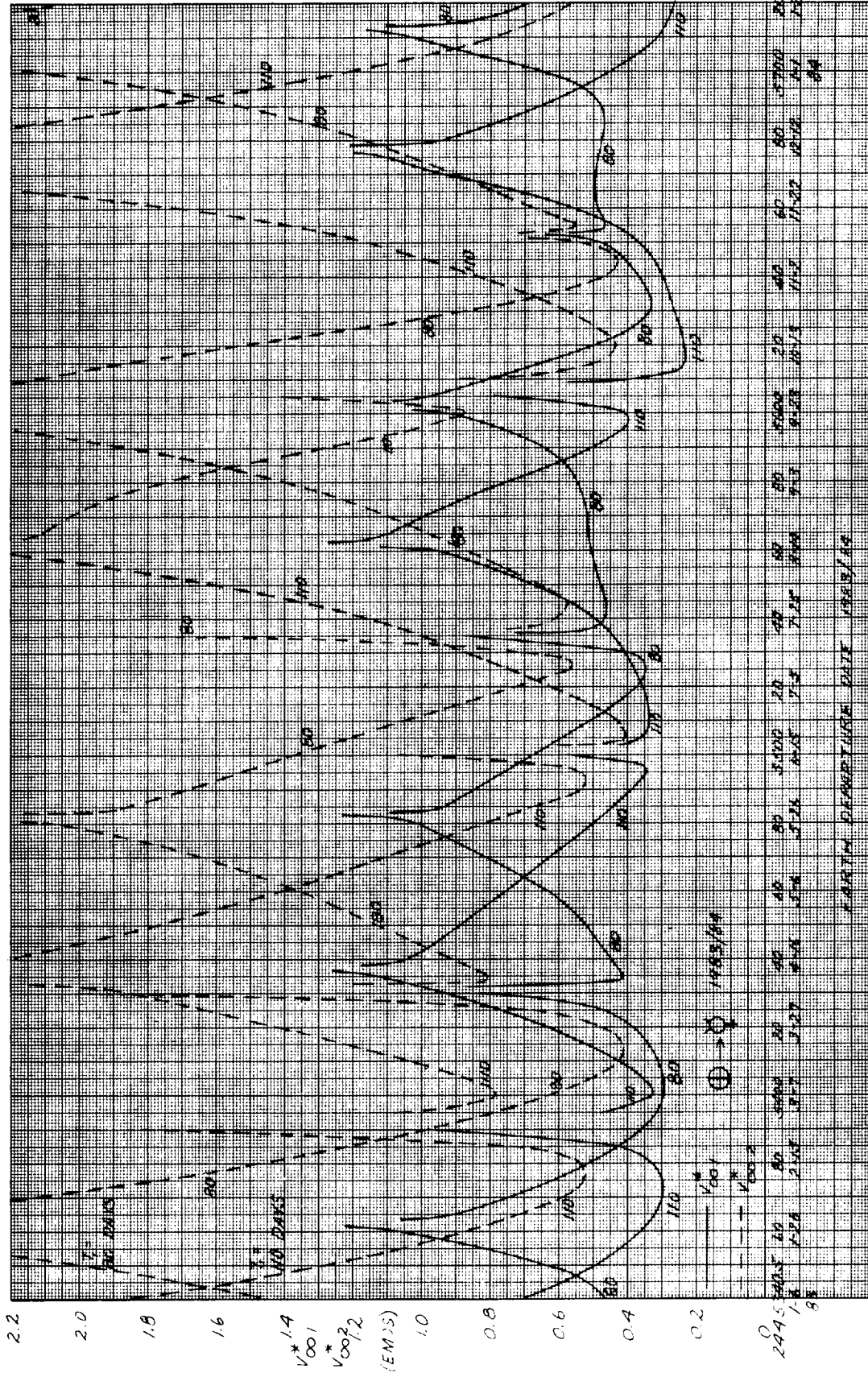


6-11-15-7

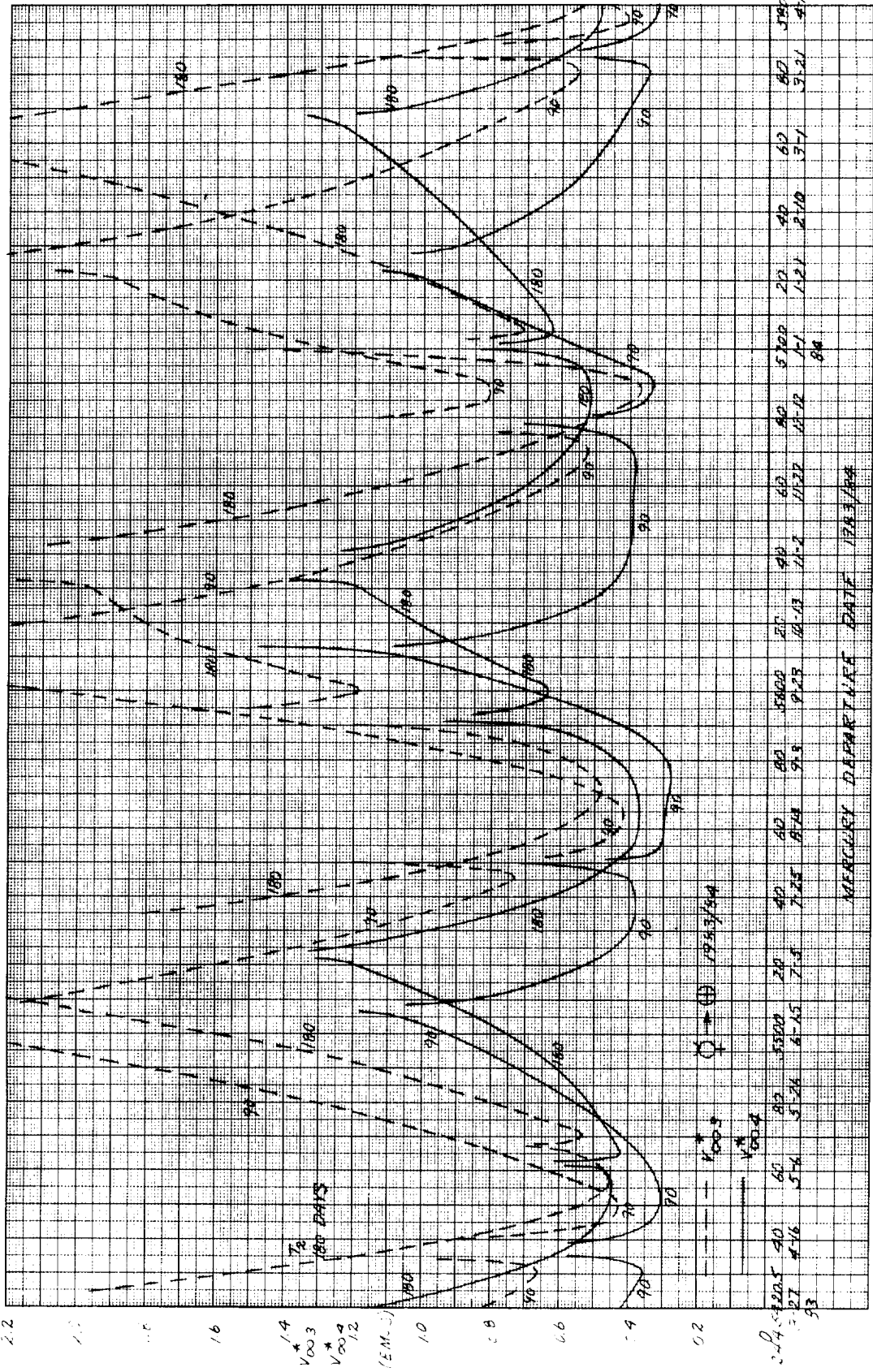


MERCURY DEPARTURE DATA - 1981/82

64-160

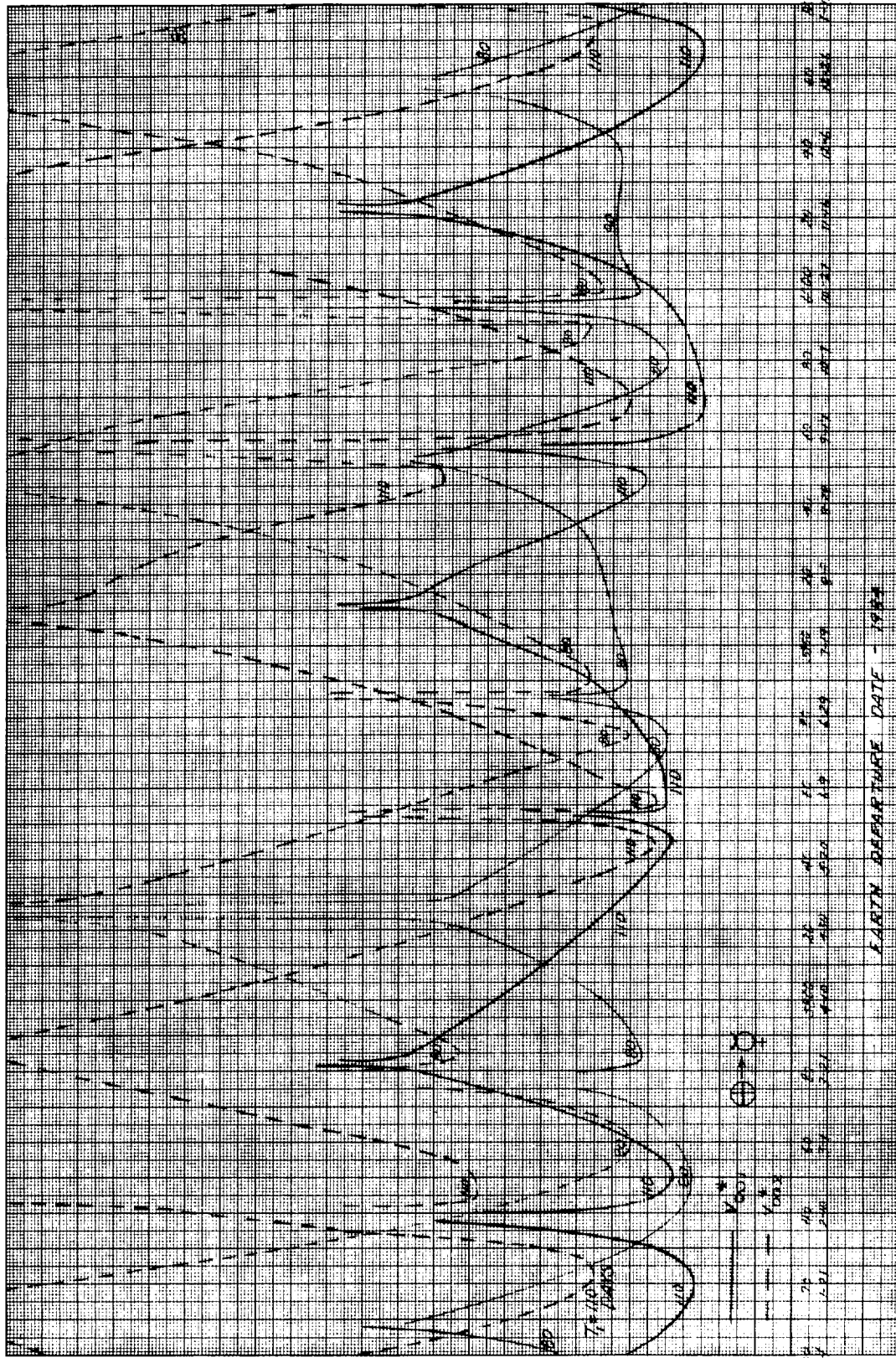


64-161

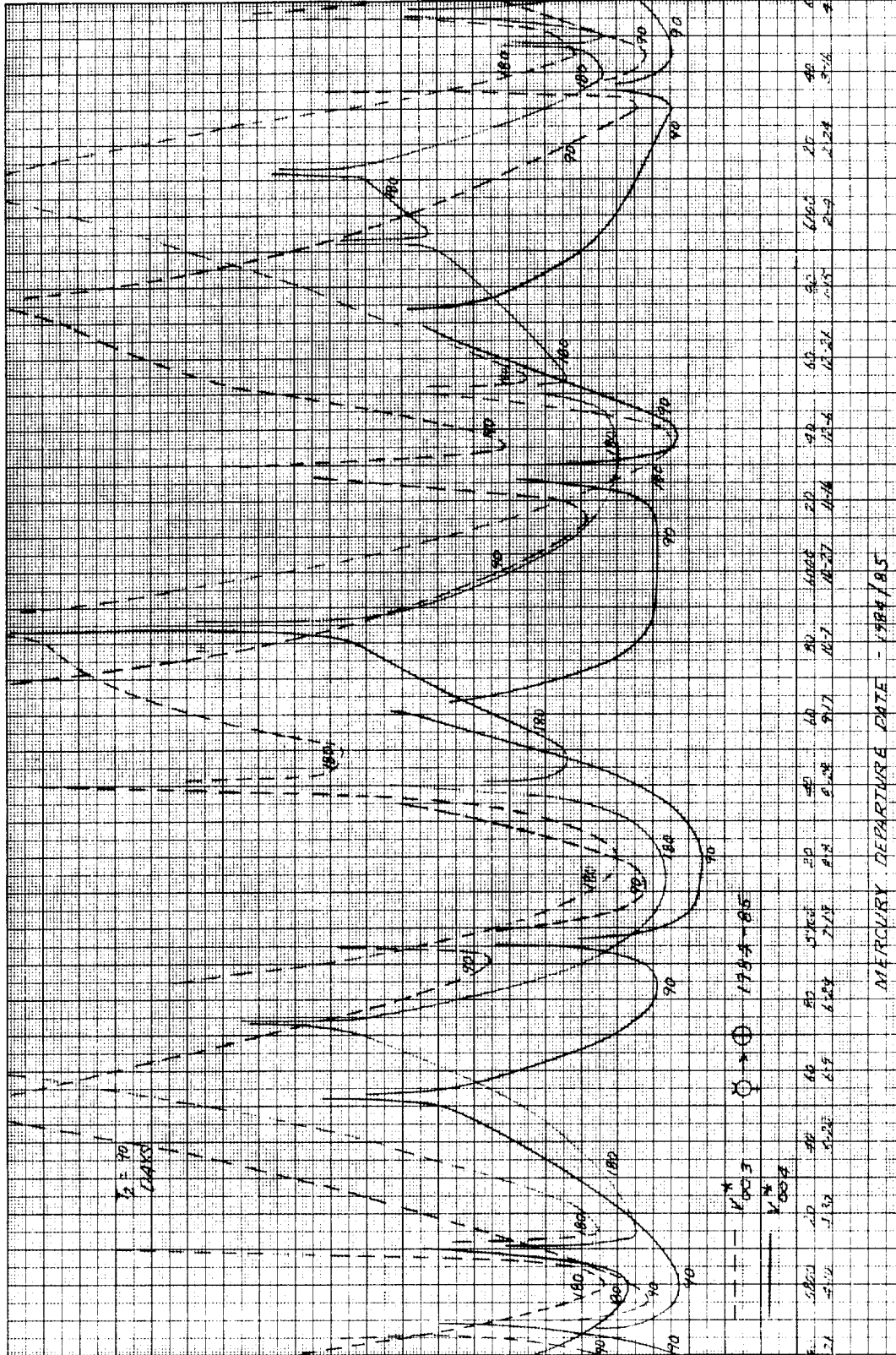


DATE	TIME	1000	1100	1200	1300
27	4:16	5.76	5.26	6.15	7.5
28	5:20.5	6.0	5.500	7.0	8.0
29	5:50	7.25	8.75	9.5	10.5
30	5:20.2	8.0	9.0	10.0	11.0
31	5:21	8.0	9.0	10.0	11.0

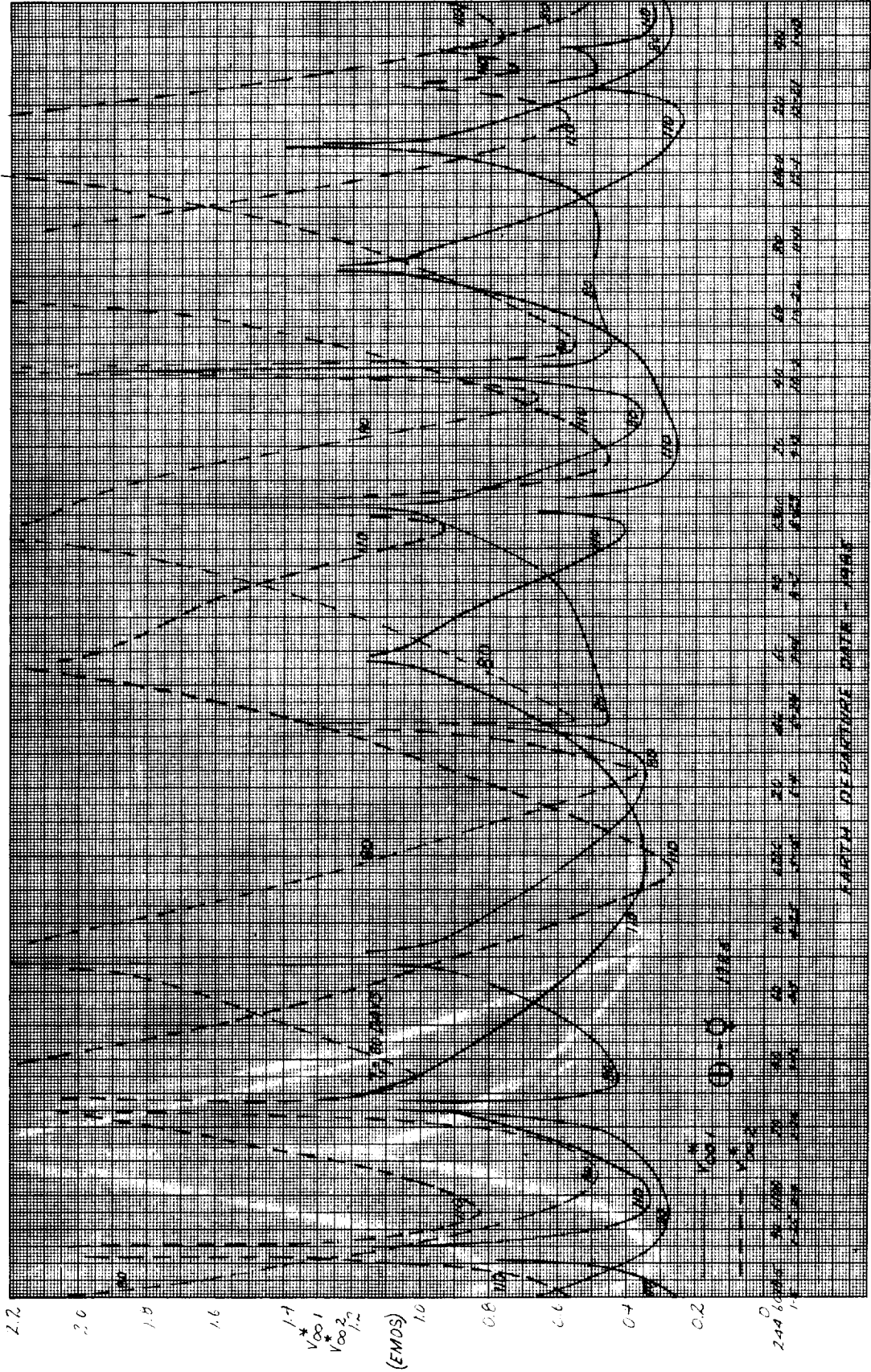
64-162



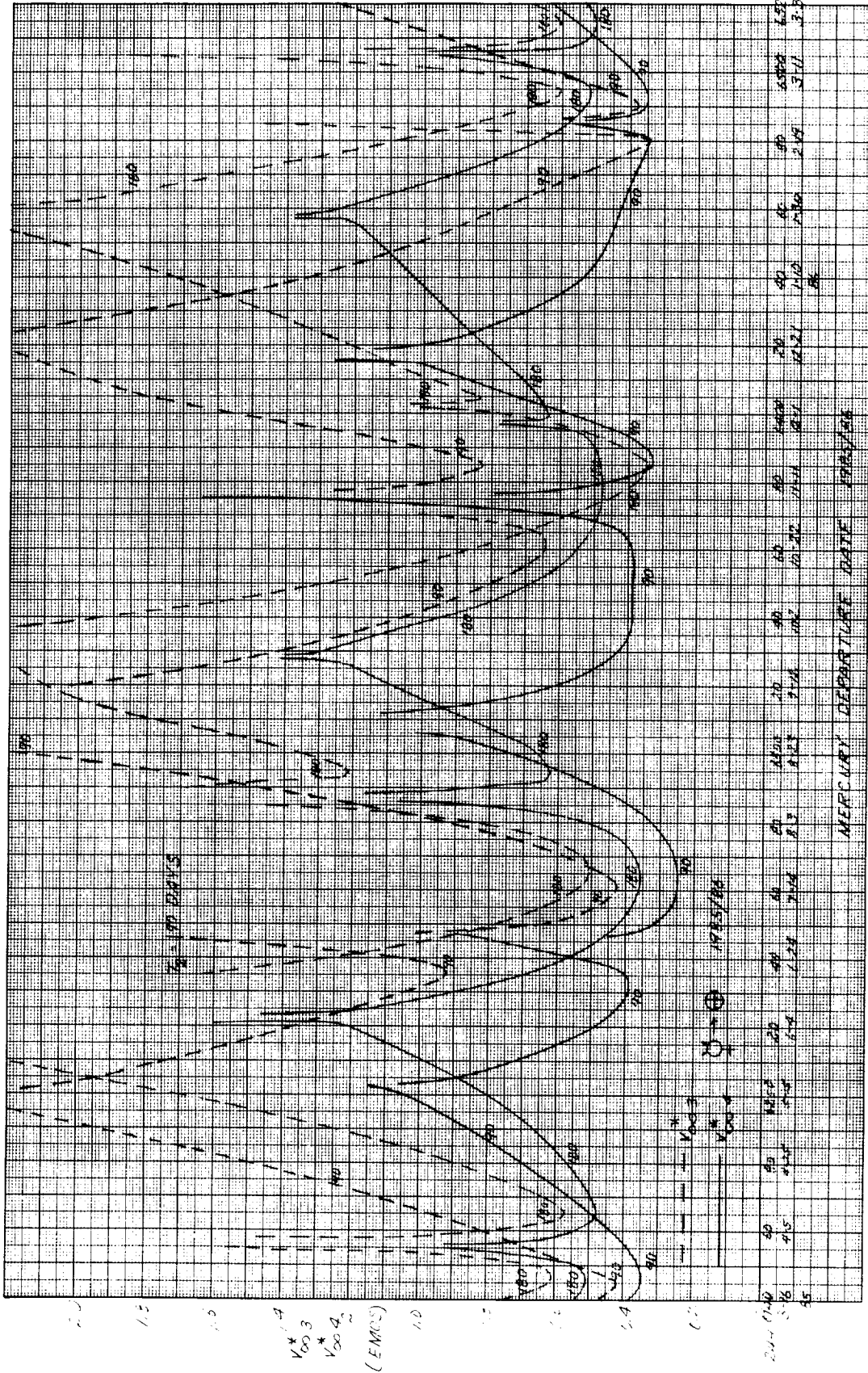
V_{001}
 V_{002}
 (E:0)



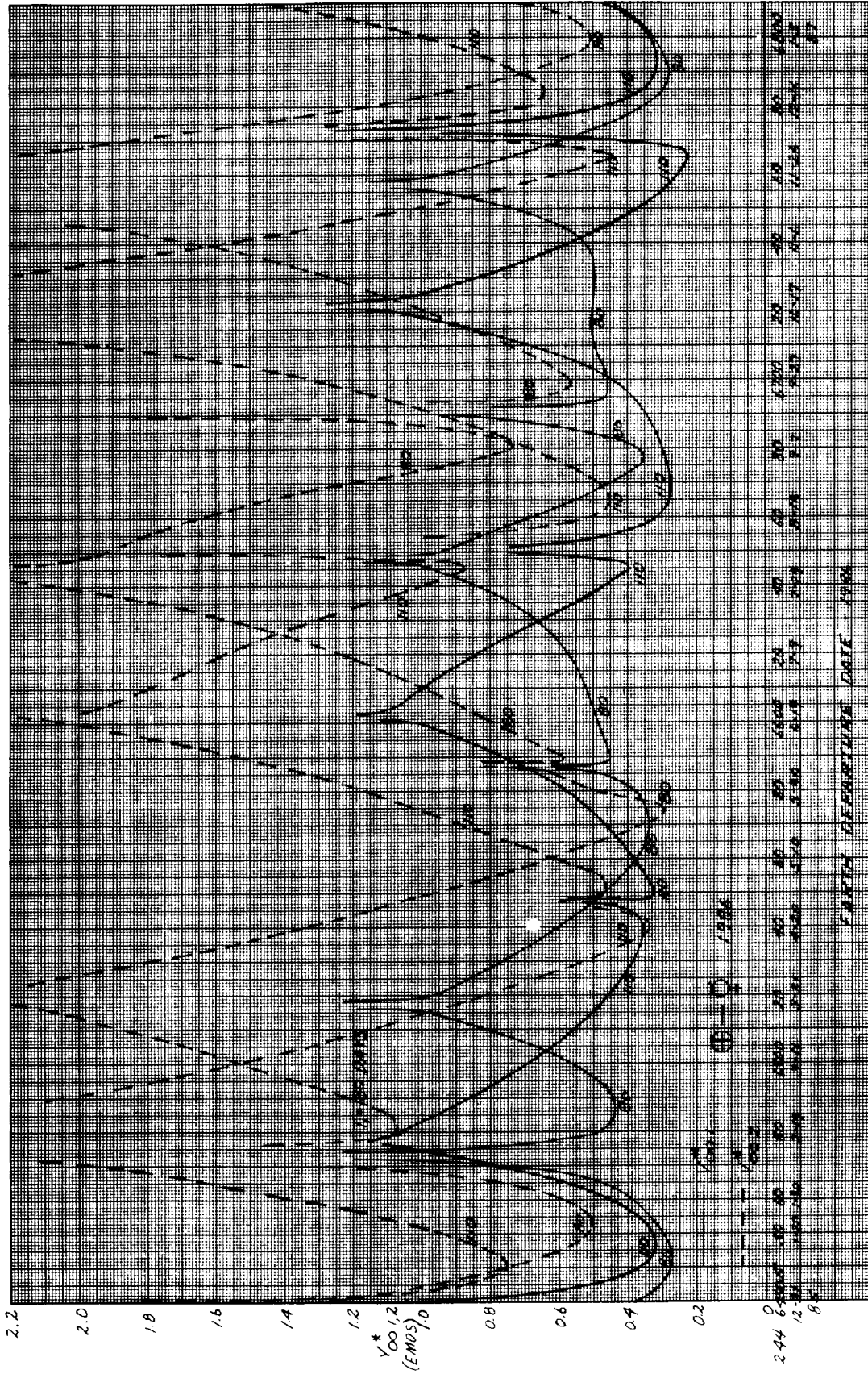
64-164



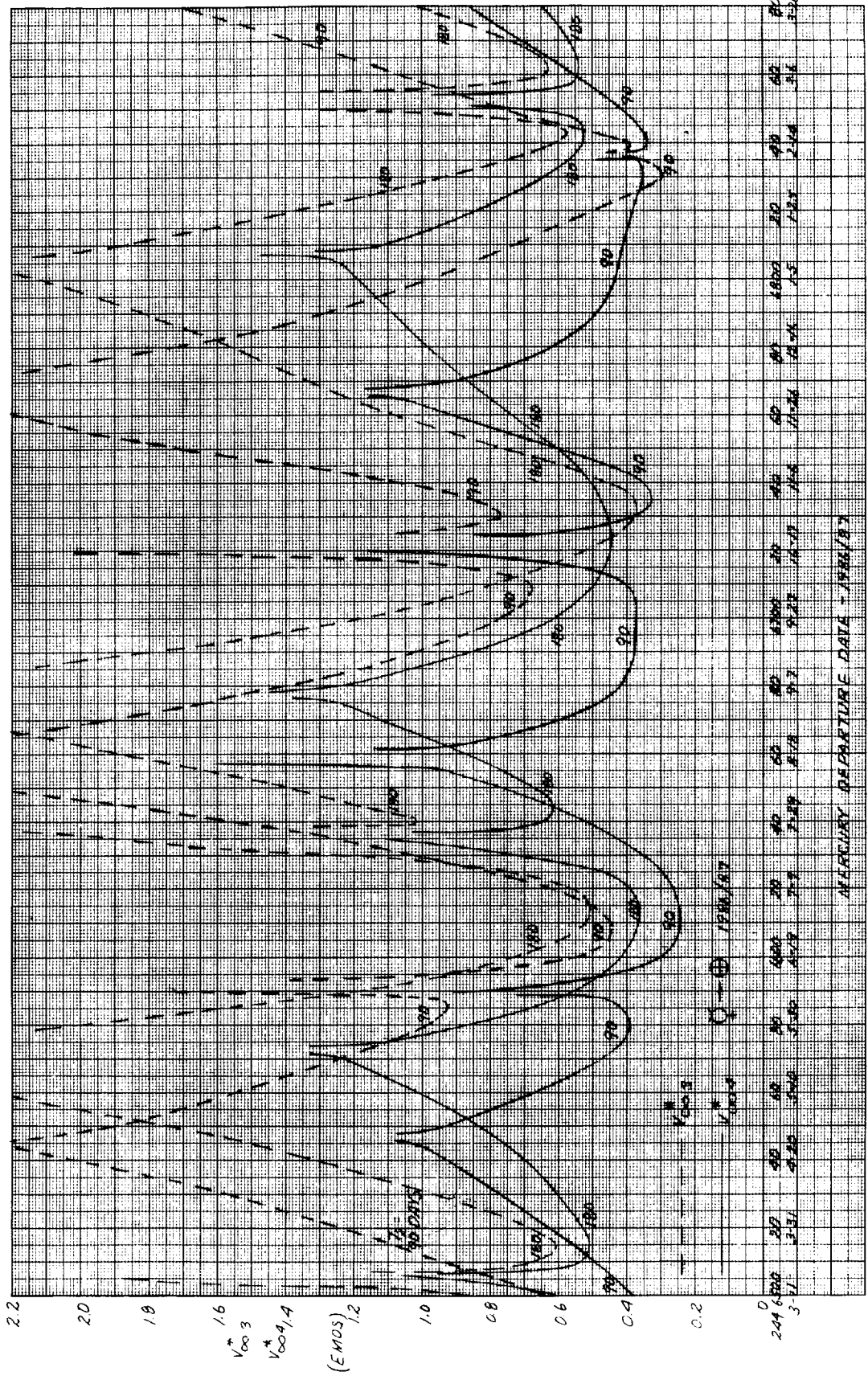
64-165

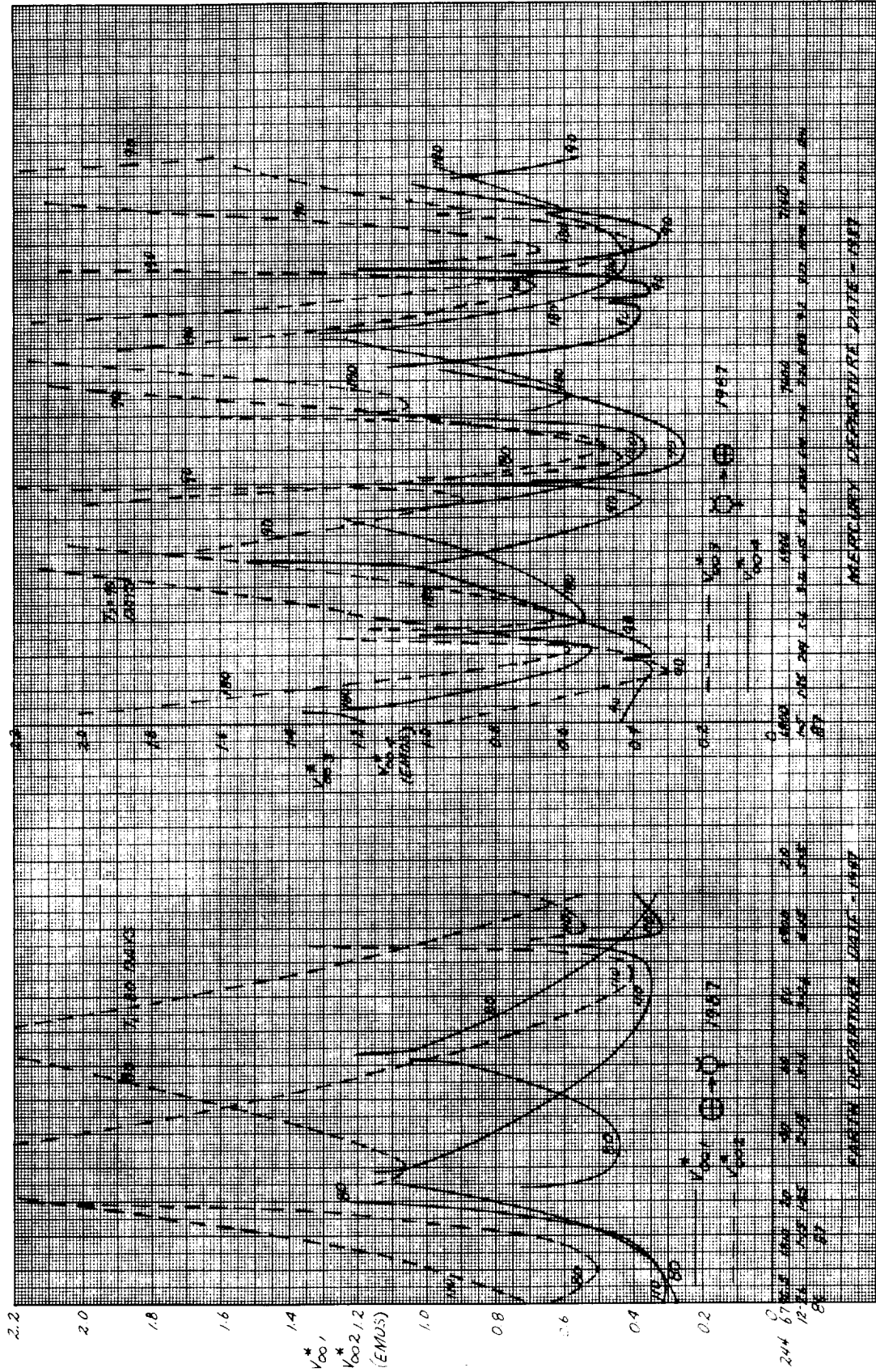


64-166



64-167





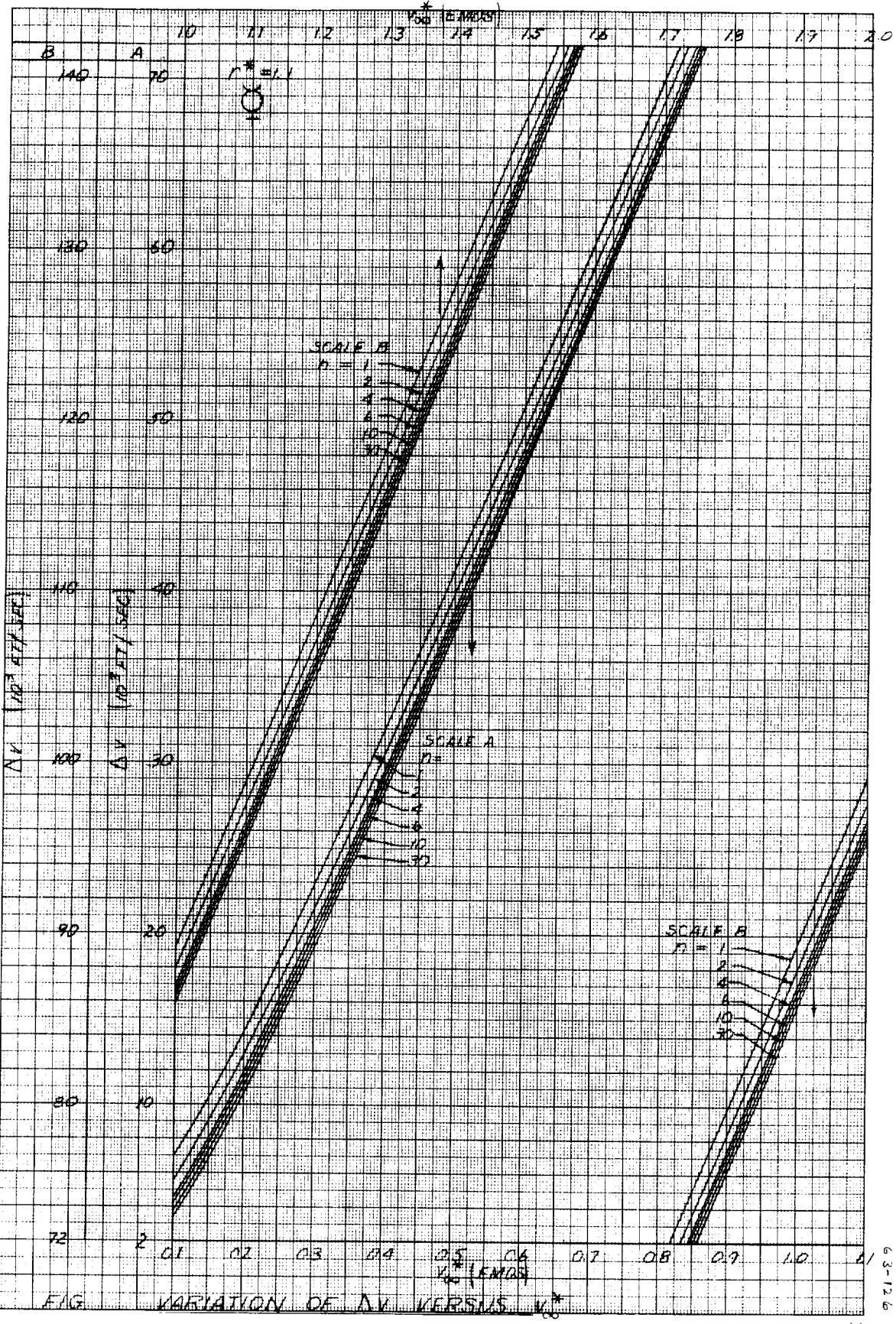


FIG. VARIATION OF ΔV VERSUS V_0^*

6.3-12.6

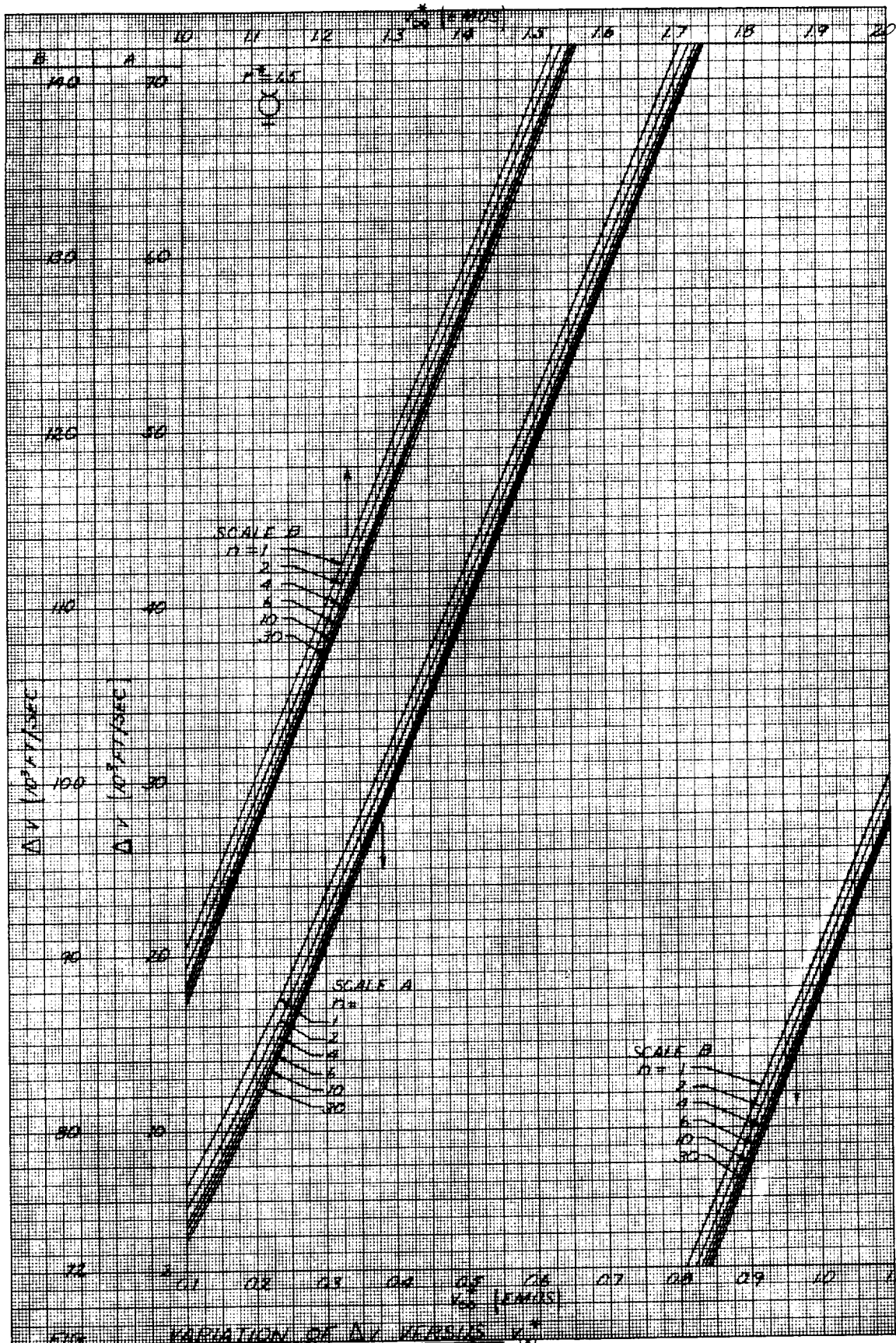
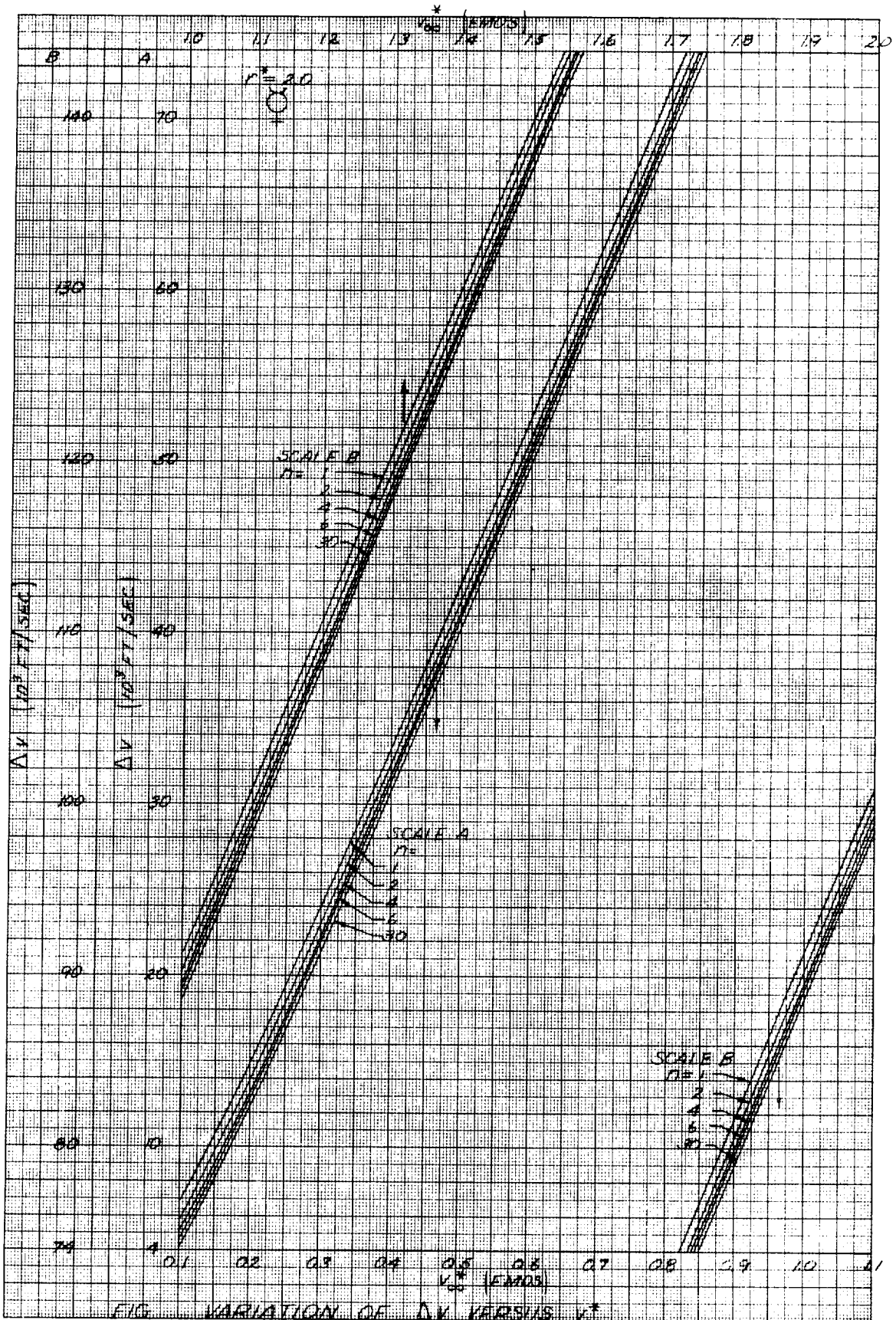


FIG. VARIATION OF DV VERSUS V_0^2

63-127



63-120

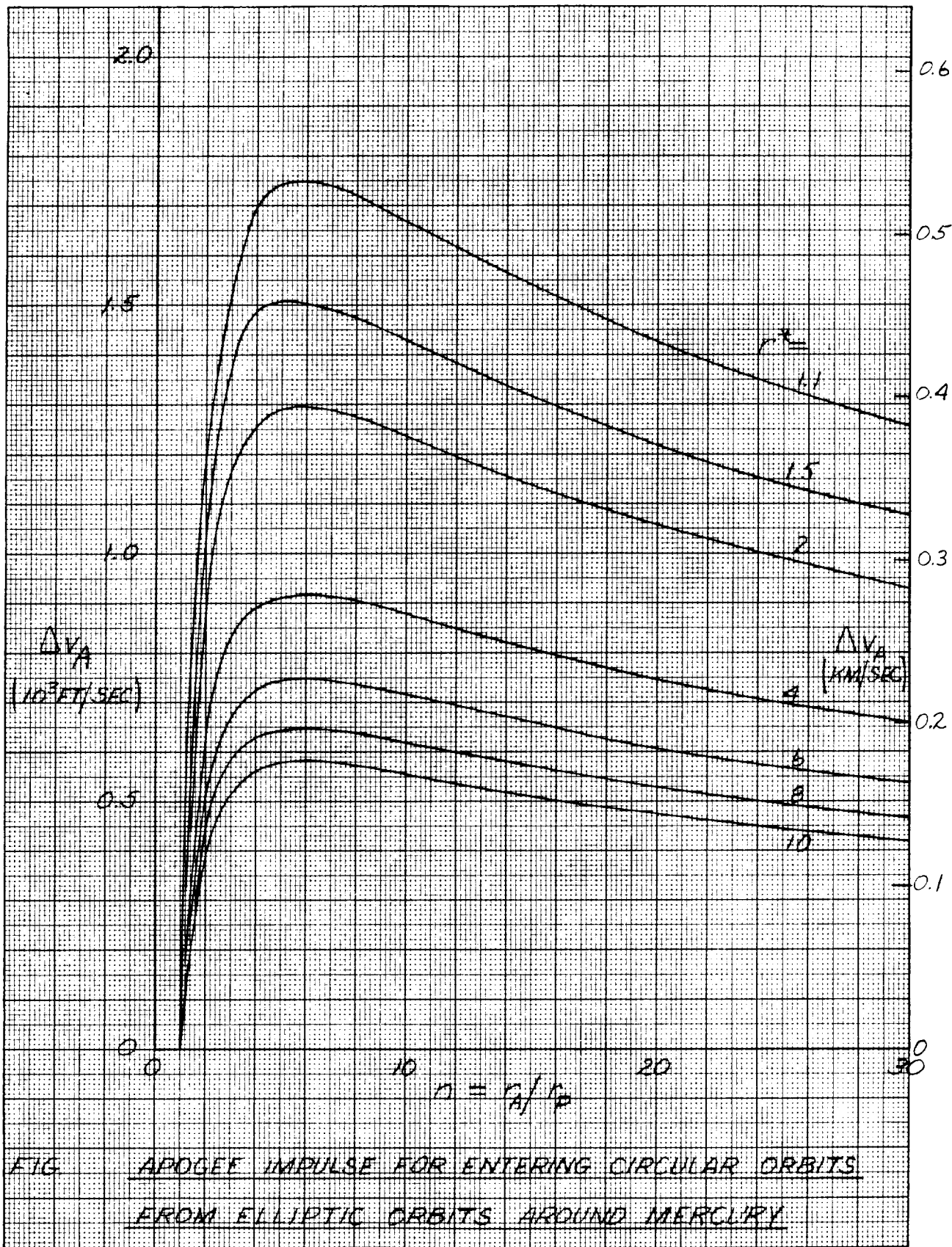
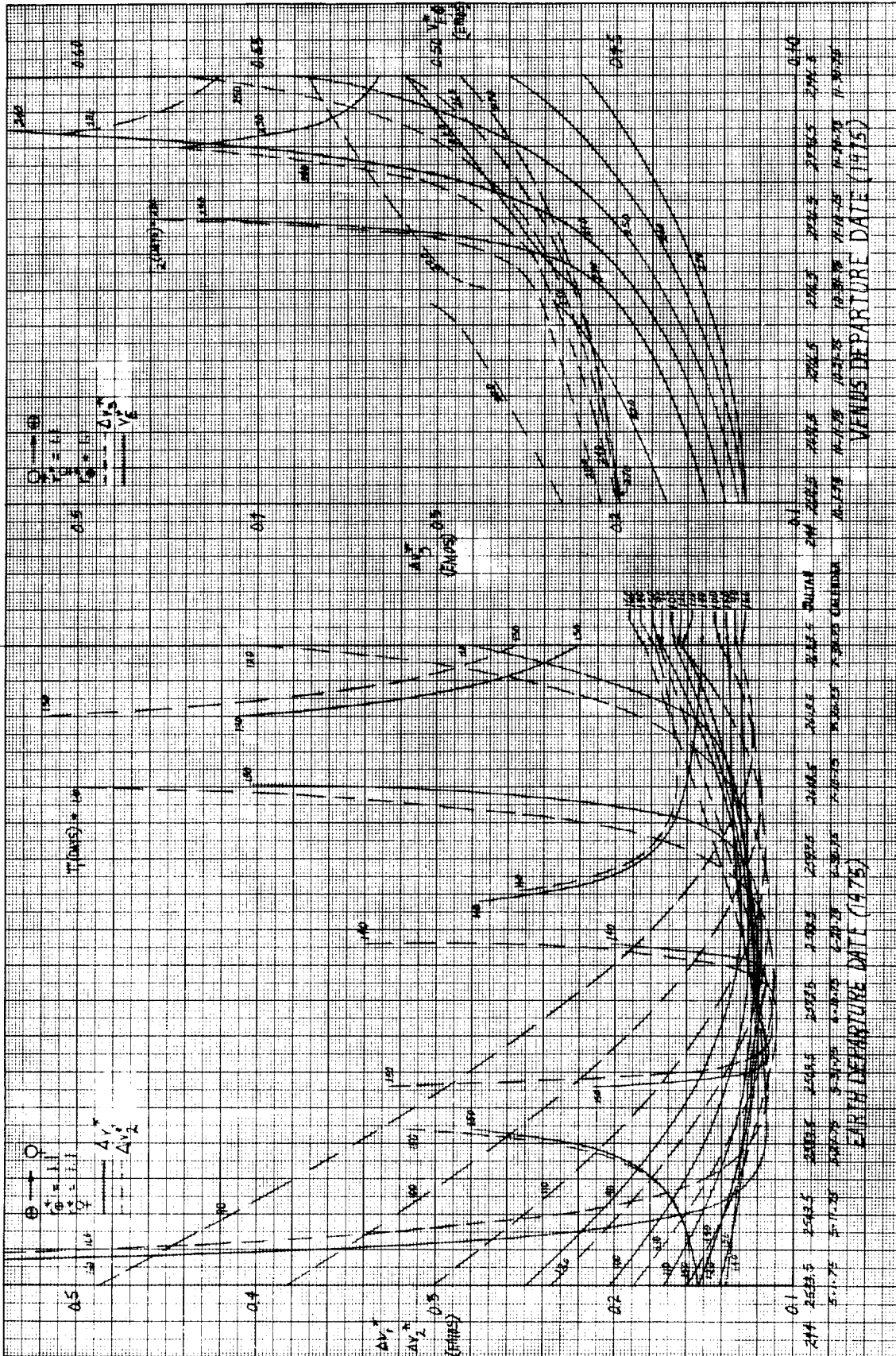
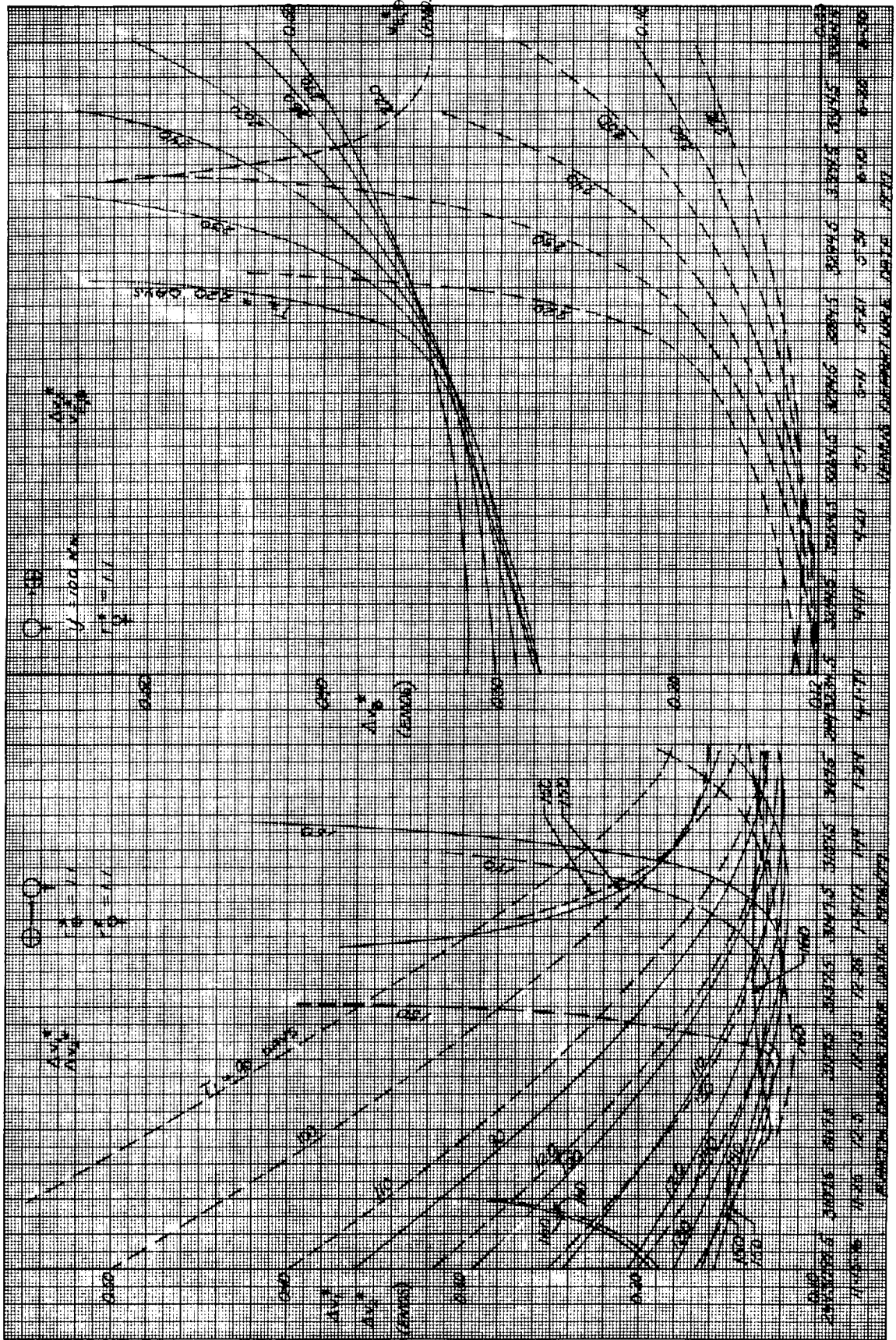
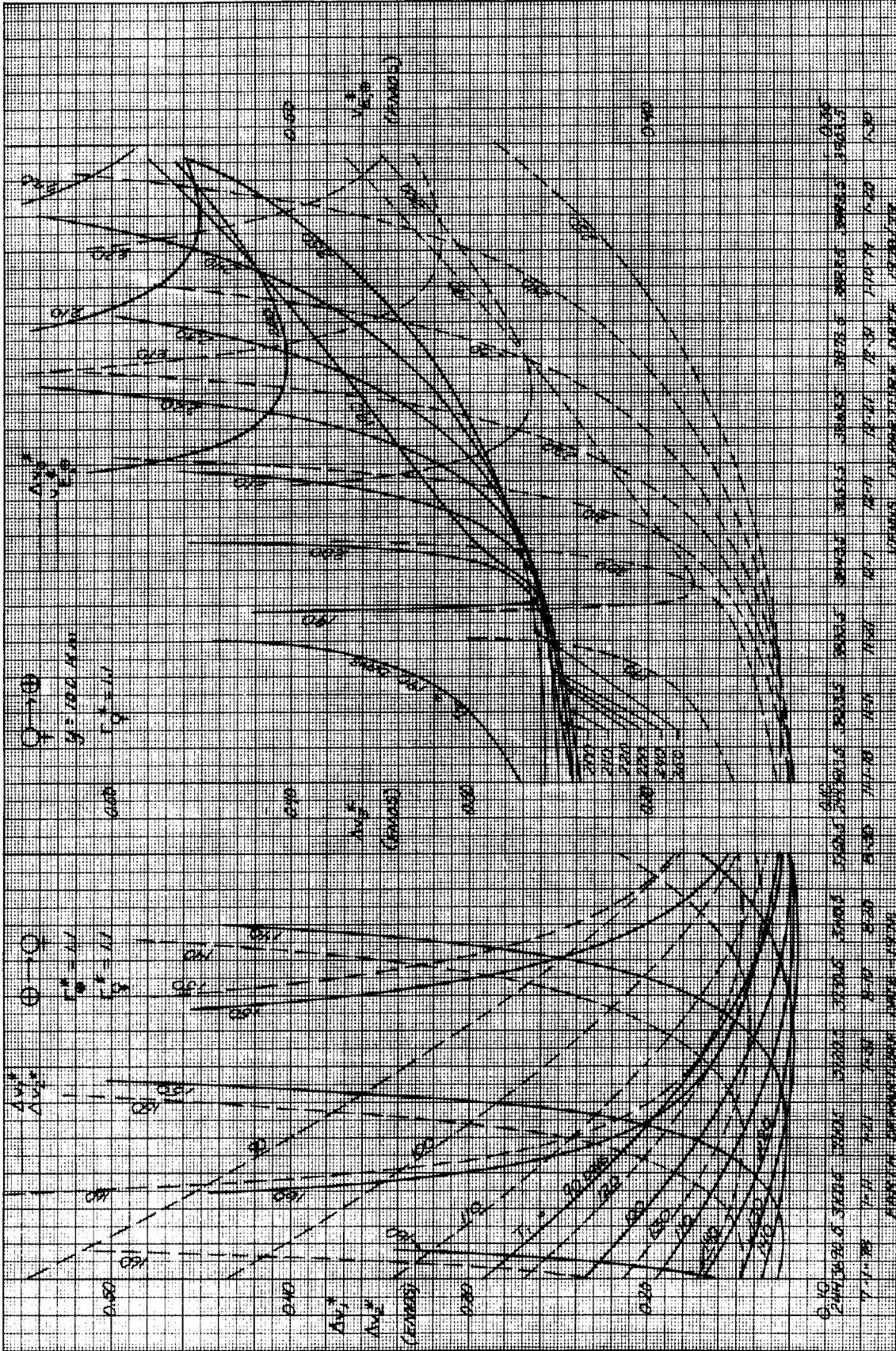


FIG APOGEE IMPULSE FOR ENTERING CIRCULAR ORBITS FROM ELLIPTIC ORBITS AROUND MERCURY

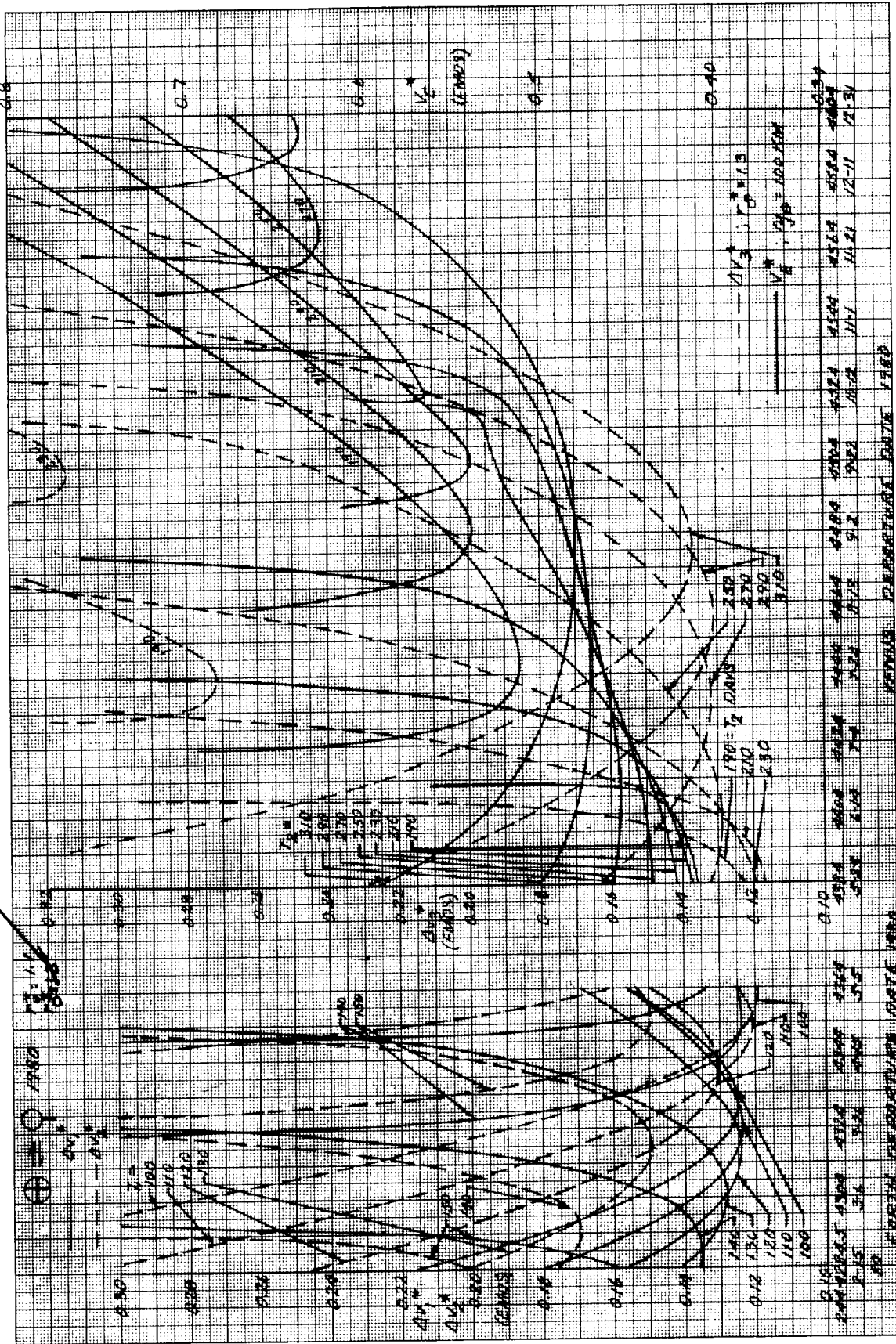
PART II VENUS







1.1



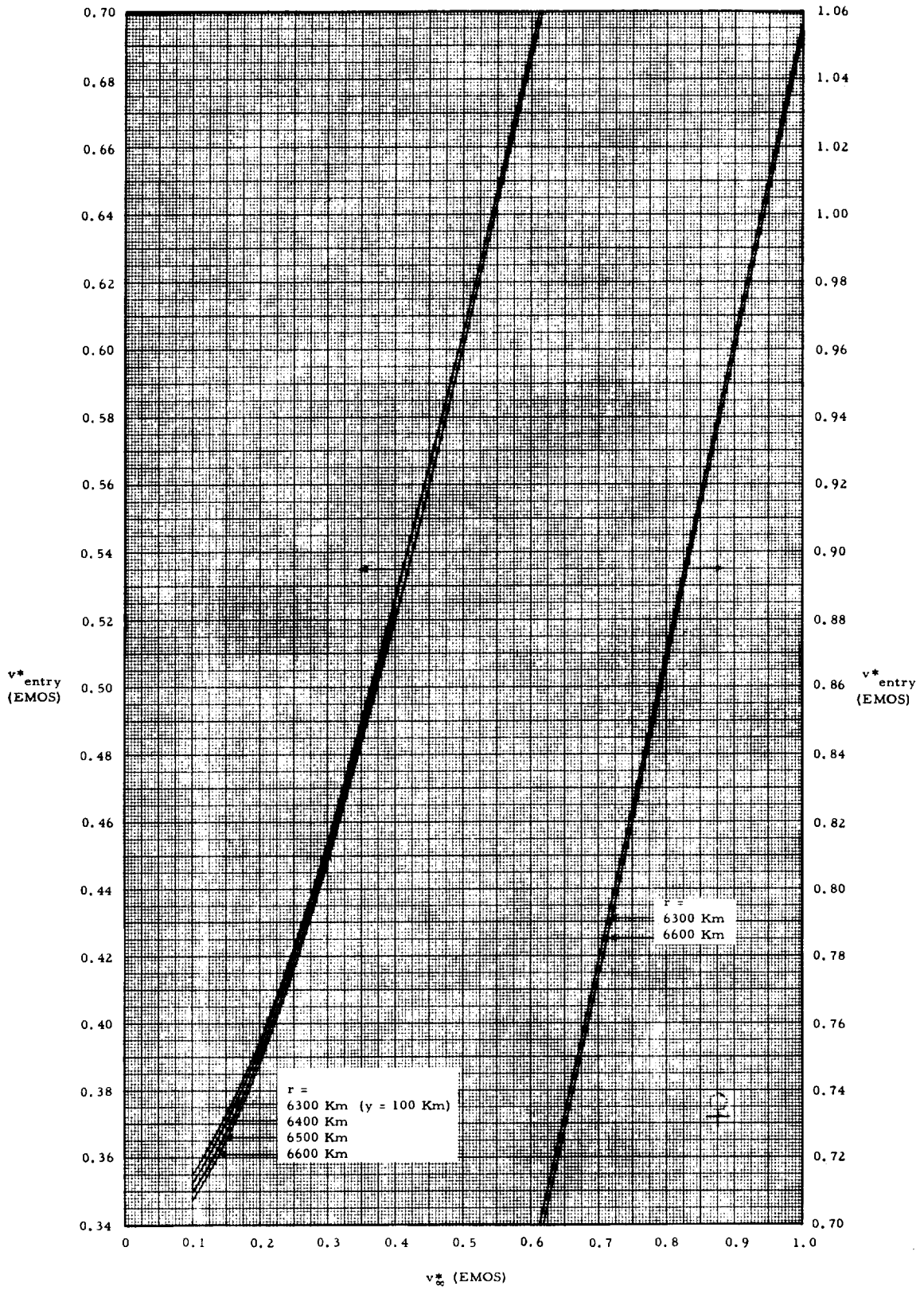


Fig. B-3 CORRELATION BETWEEN HYPERBOLIC EXCESS VELOCITY (v_{∞}^*) TO ATMOSPHERIC ENTRY VELOCITY (v_{E}^*) AT DIFFERENT ALTITUDES FOR PLANET VENUS

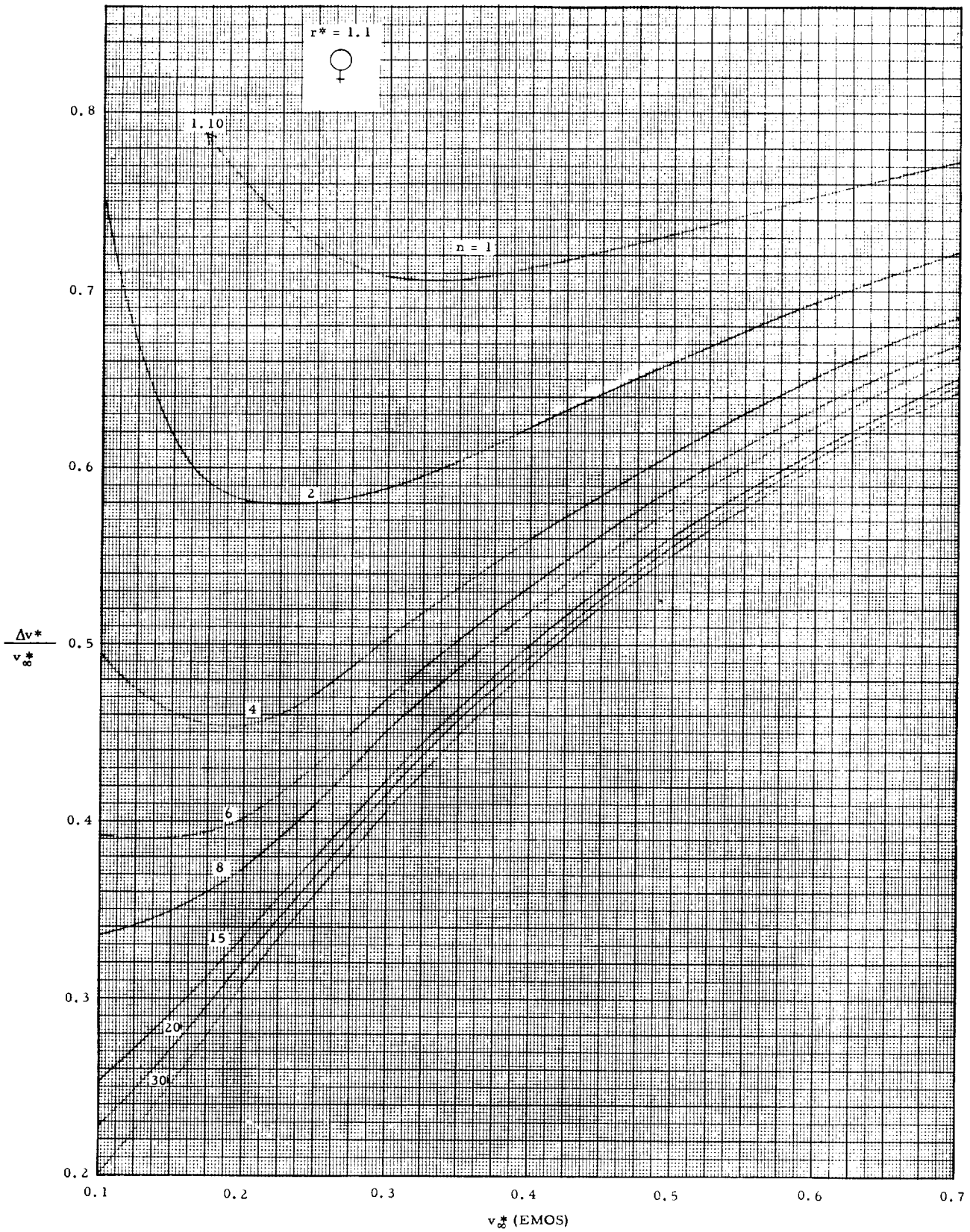


Fig. B-4 VARIATION OF $\frac{\Delta v^*}{v_{\infty}^*}$ VERSUS v_{∞}^* FOR CAPTURE IN CIRCULAR AND ELLIPTIC ORBITS AROUND VENUS (PERIAPSIS DISTANCE: $r^* = 1.1$)

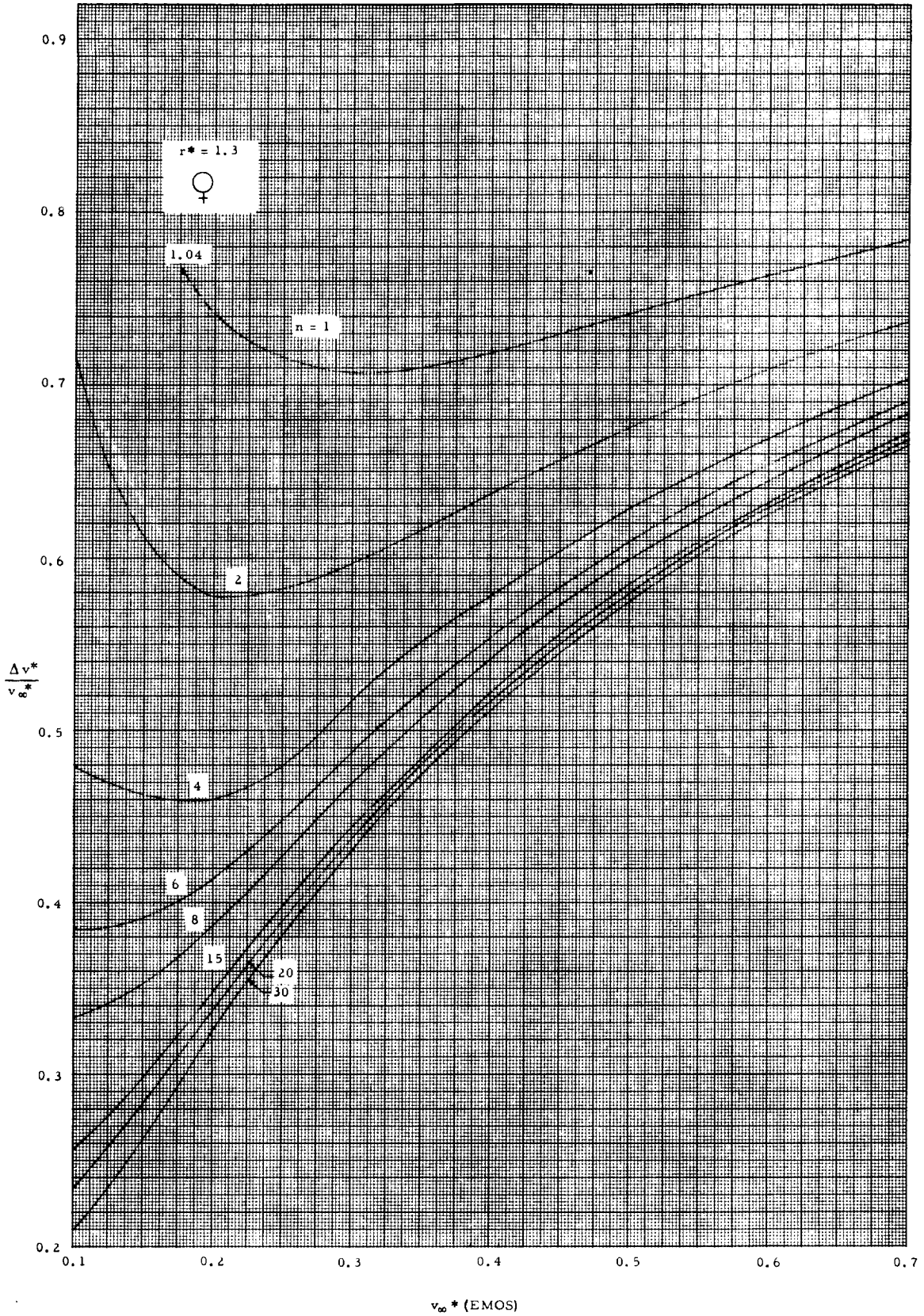


Fig. B-5 VARIATION OF $\Delta v^*/v_{\infty}^*$ VERSUS v_{∞}^* FOR CAPTURE IN CIRCULAR AND ELLIPTIC ORBITS AROUND VENUS (PERIAPSIS DISTANCE: $r^* = 1.3$)

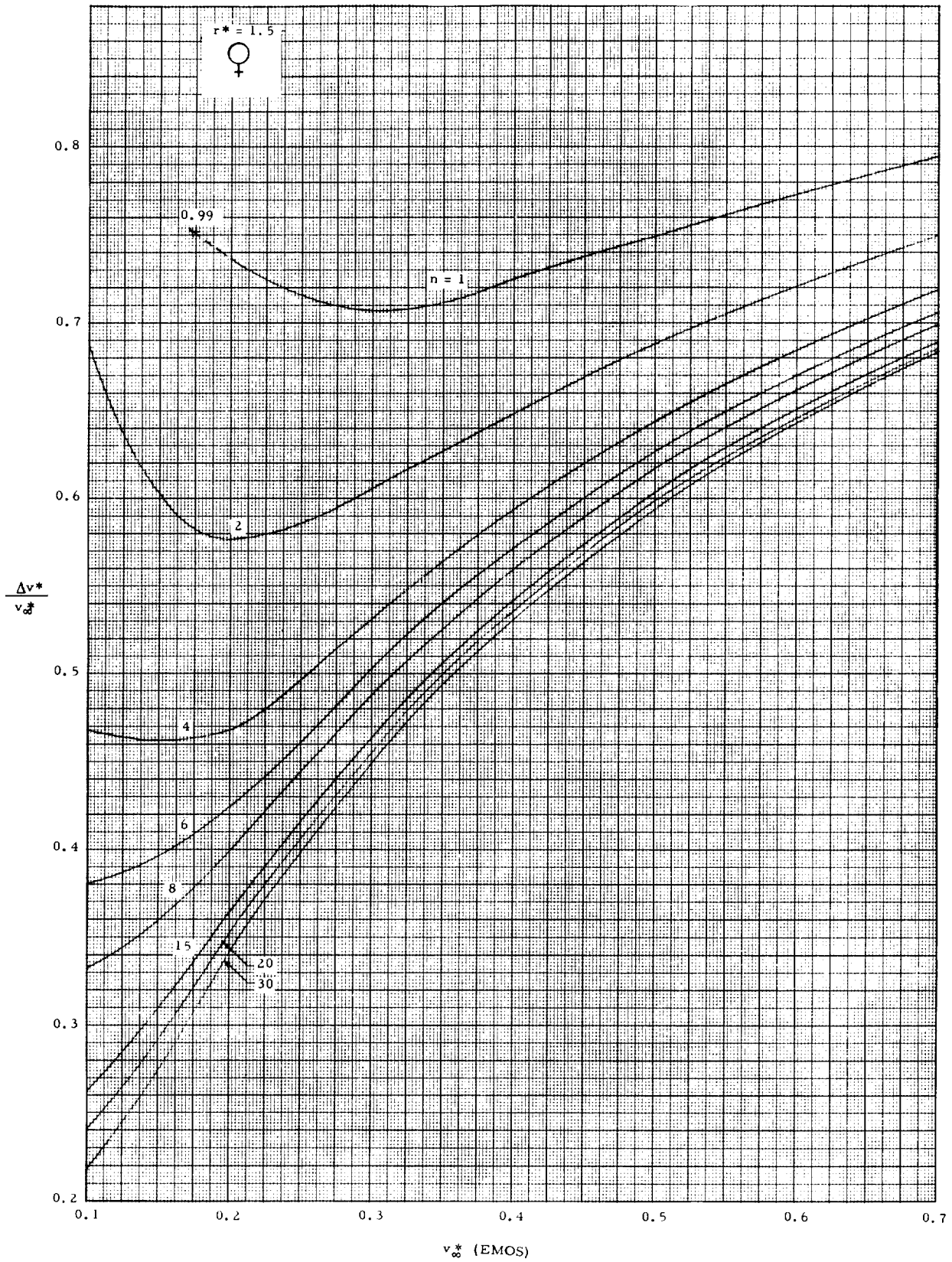


Fig. B-6 VARIATION OF $\frac{\Delta v^*}{v_{\infty}^*}$ VERSUS v_{∞}^* FOR CAPTURE IN CIRCULAR AND ELLIPTIC ORBITS AROUND VENUS (PERIAPSIS DISTANCE: $r^* = 1.5$)

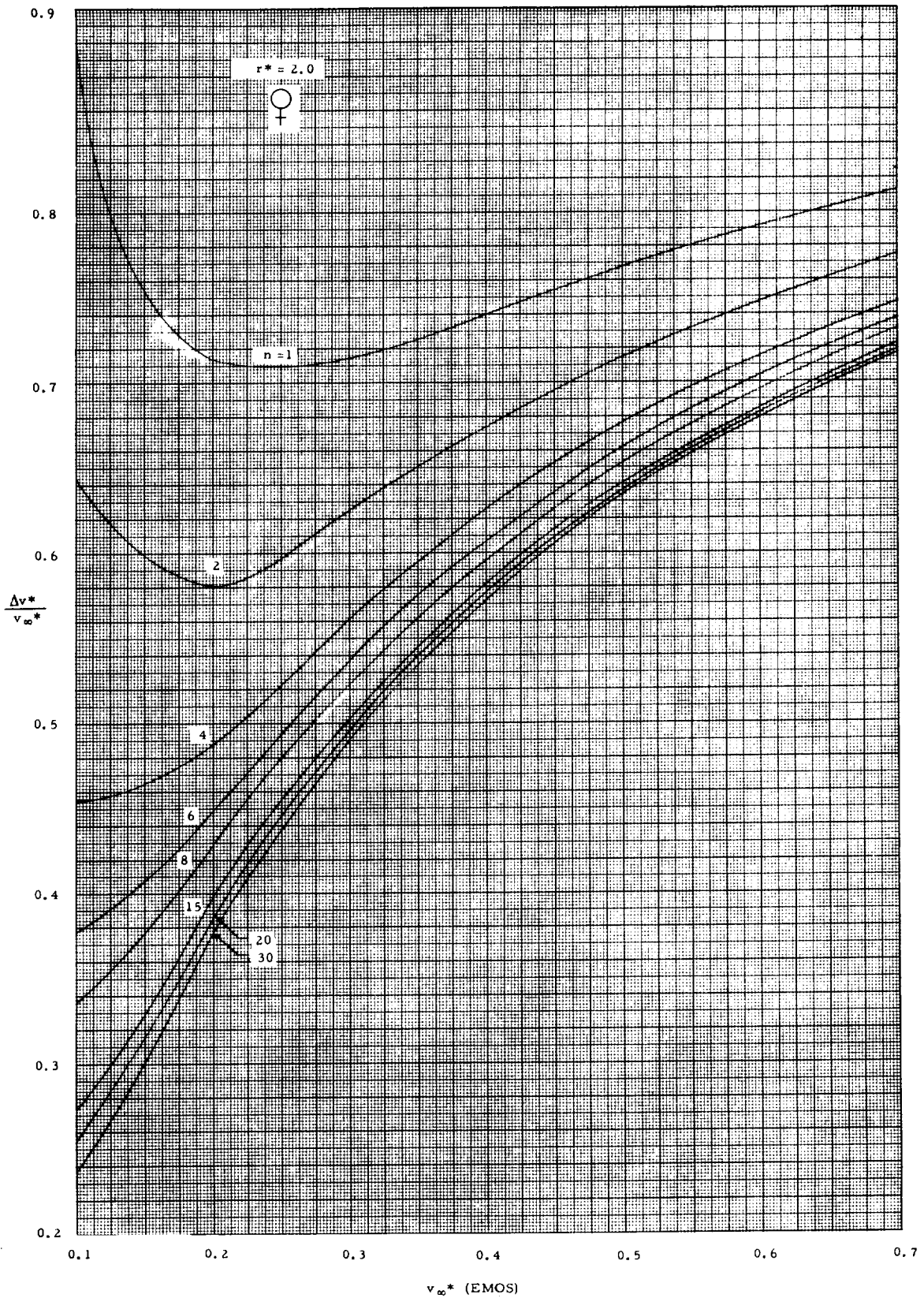


Fig. B-7 VARIATION OF $\frac{\Delta v^*}{v_{\infty}^*}$ VERSUS v_{∞}^* FOR CAPTURE IN CIRCULAR AND ELLIPTIC ORBITS AROUND VENUS (PERIAPSIS DISTANCE: $r^* = 2.0$)

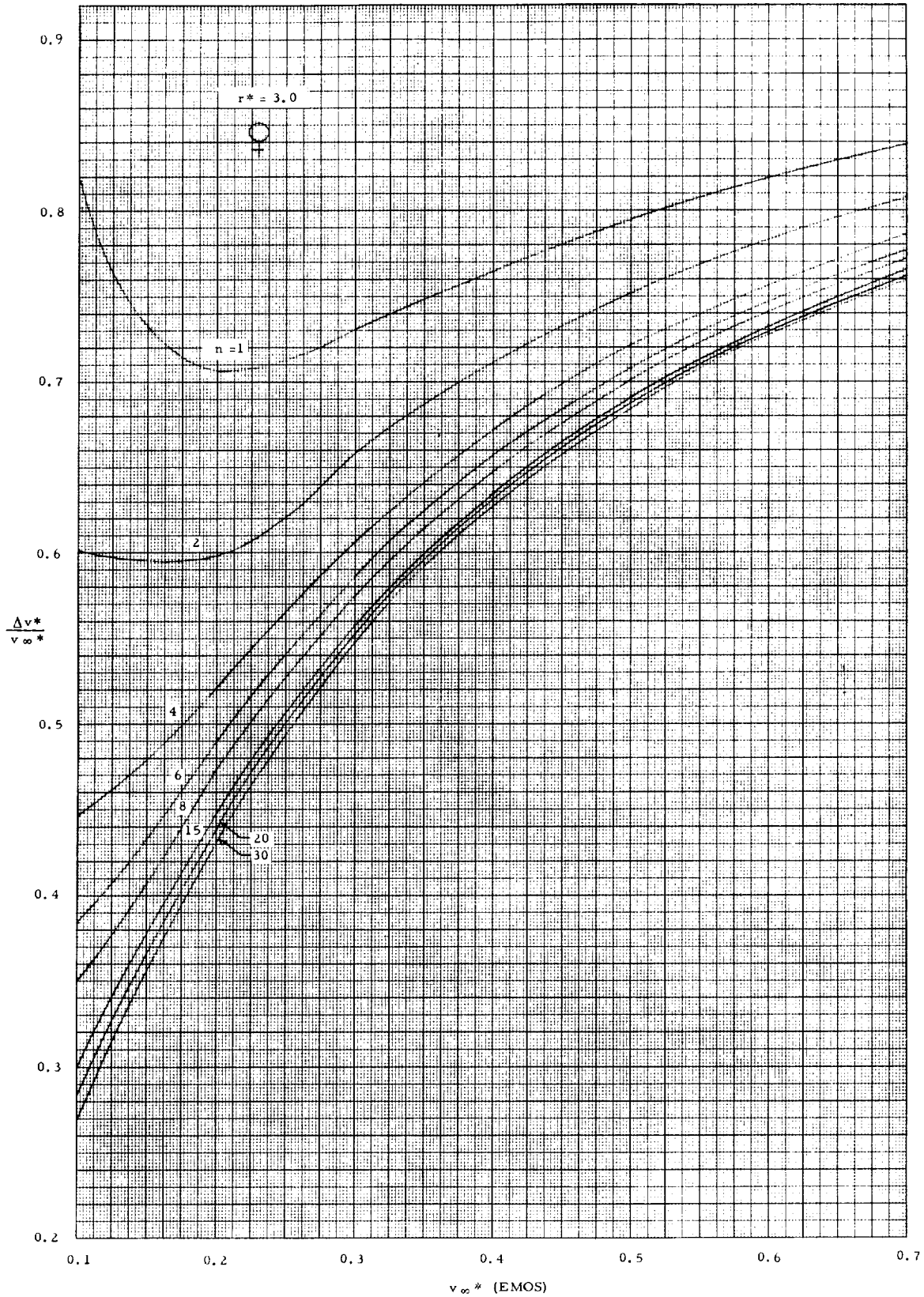


Fig. B-8 VARIATION OF $\frac{\Delta v^*}{v_{\infty}^*}$ VERSUS v_{∞}^* FOR CAPTURE IN CIRCULAR AND ELLIPTIC ORBITS AROUND VENUS (PERIAPSIS DISTANCE: $r^*=3.0$)

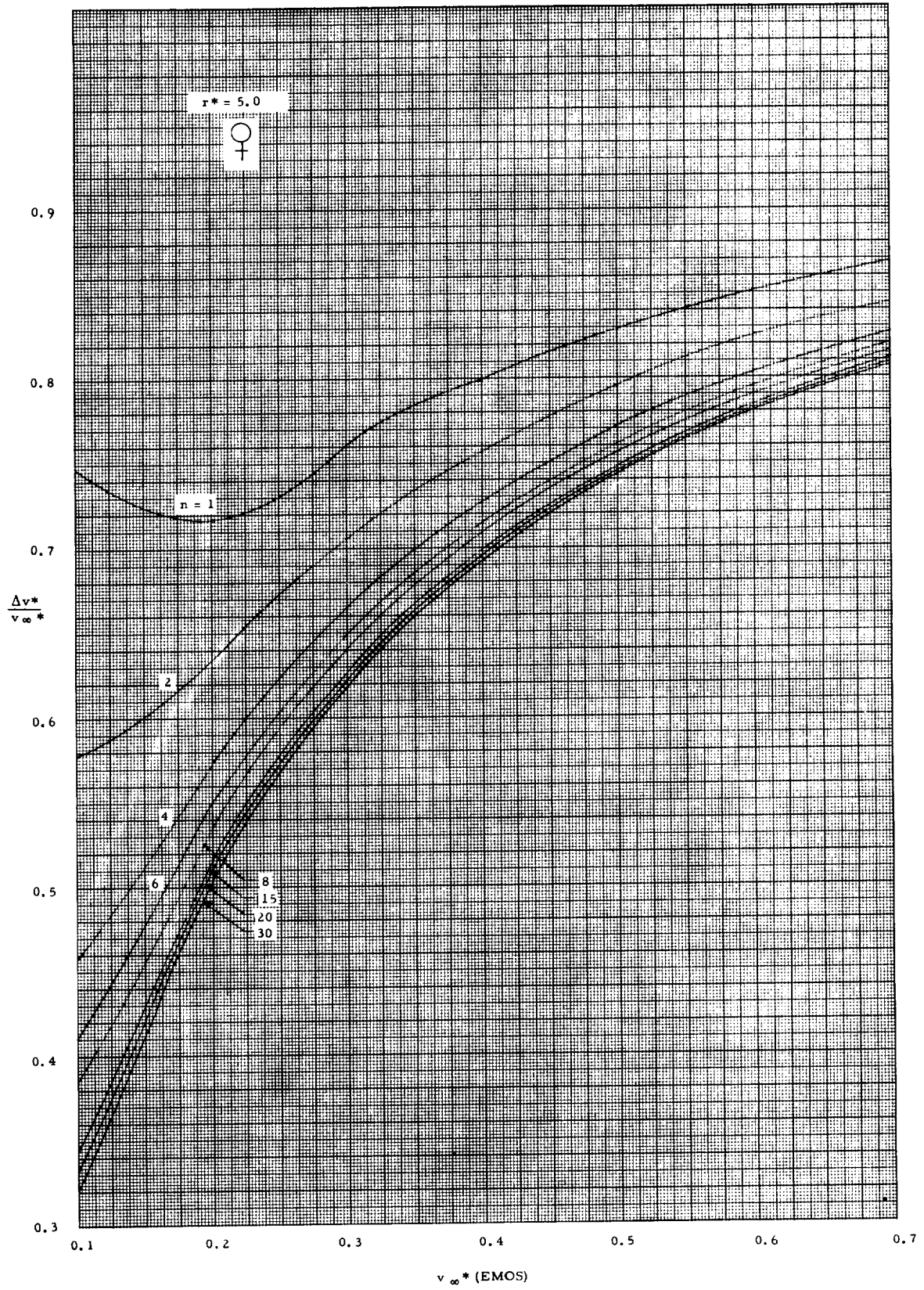


Fig. B-9 VARIATION OF $\frac{\Delta v^*}{v_{\infty}^*}$ VERSUS v_{∞}^* FOR CAPTURE IN CIRCULAR AND ELLIPTIC ORBITS AROUND VENUS (PERIAPSIS DISTANCE: $r^*=5.0$)

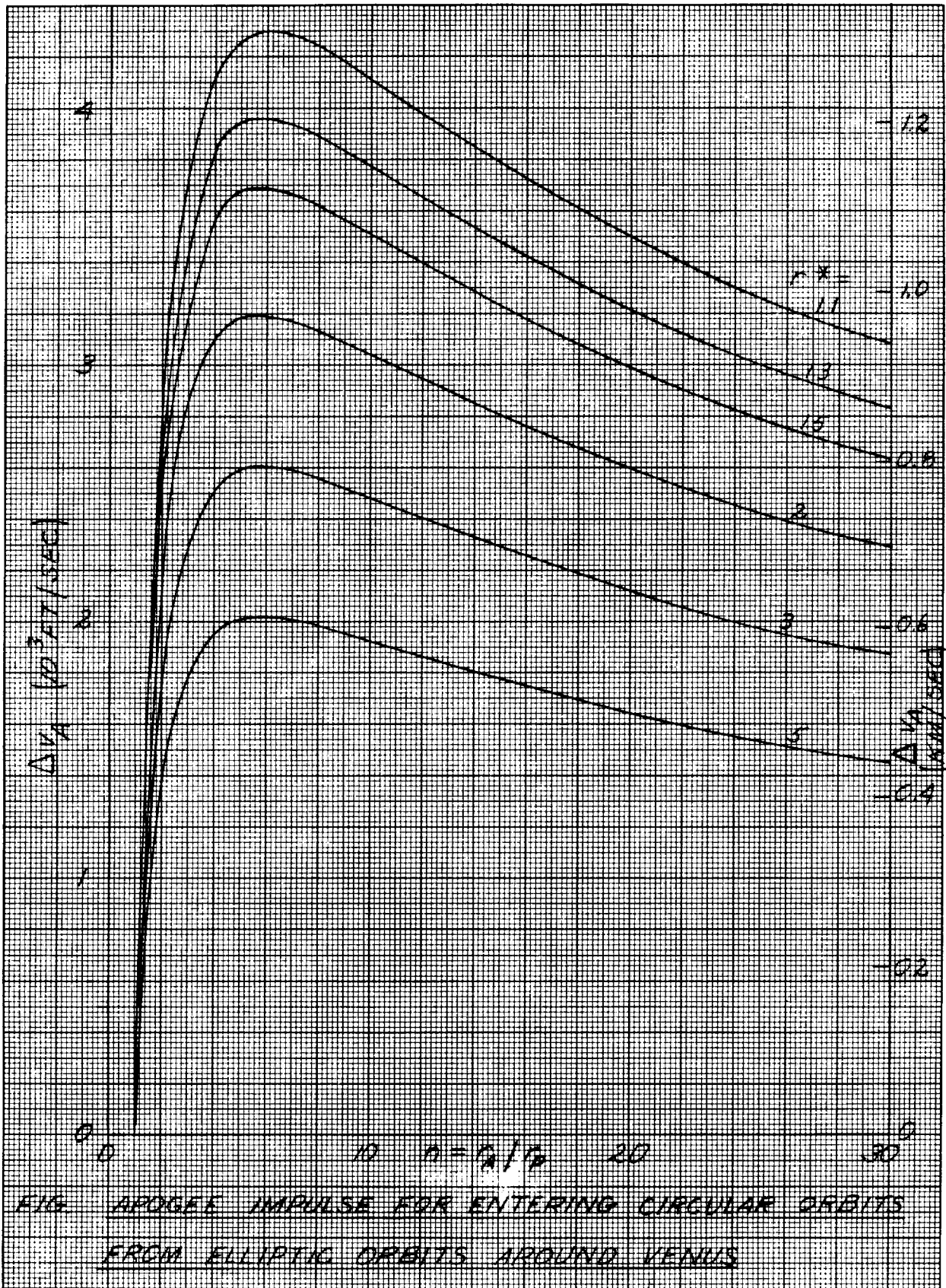
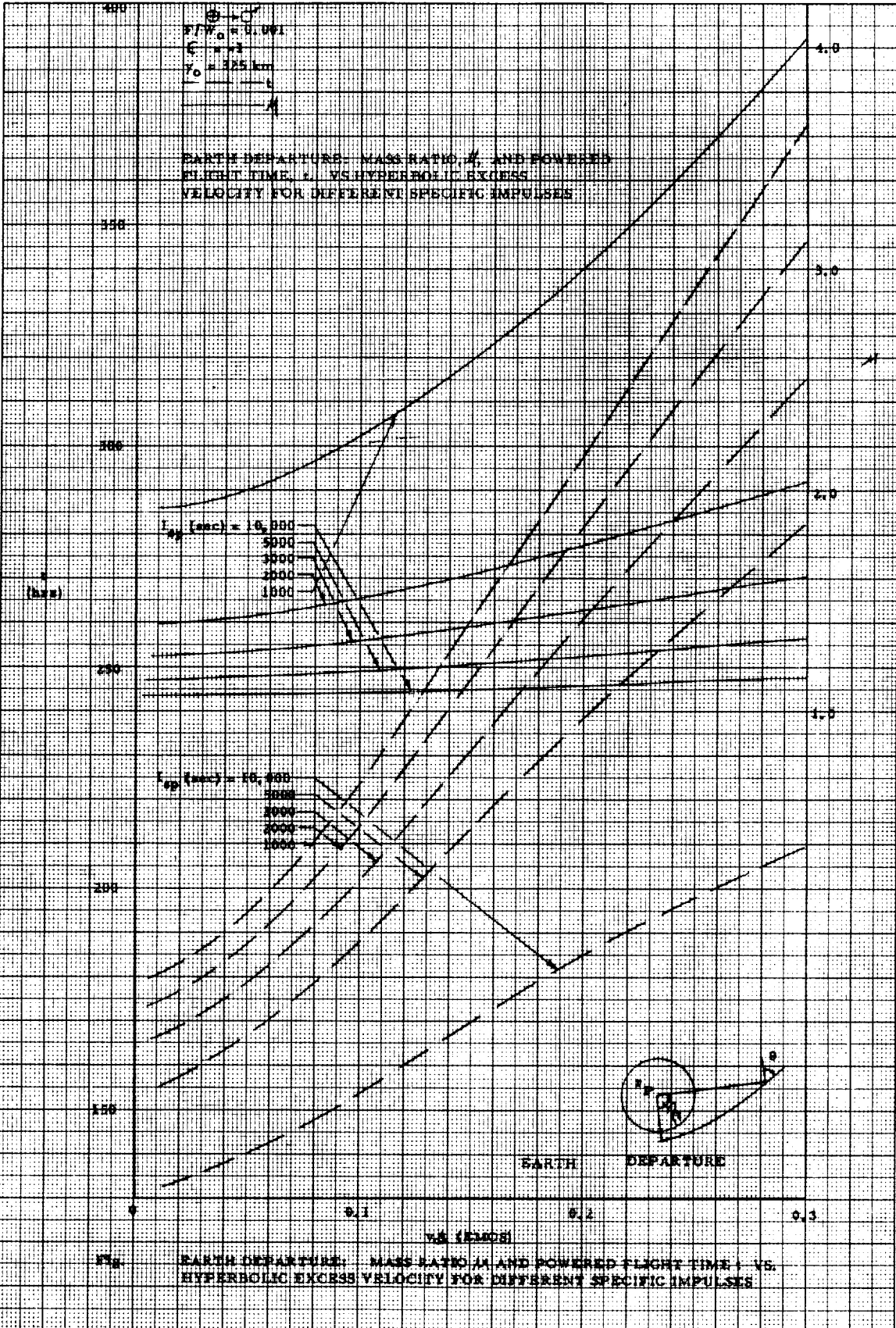


FIG. APOGEE IMPULSE FOR ENTERING CIRCULAR ORBITS FROM ELLIPTIC ORBITS AROUND VENUS

PART III EARTH



65-038

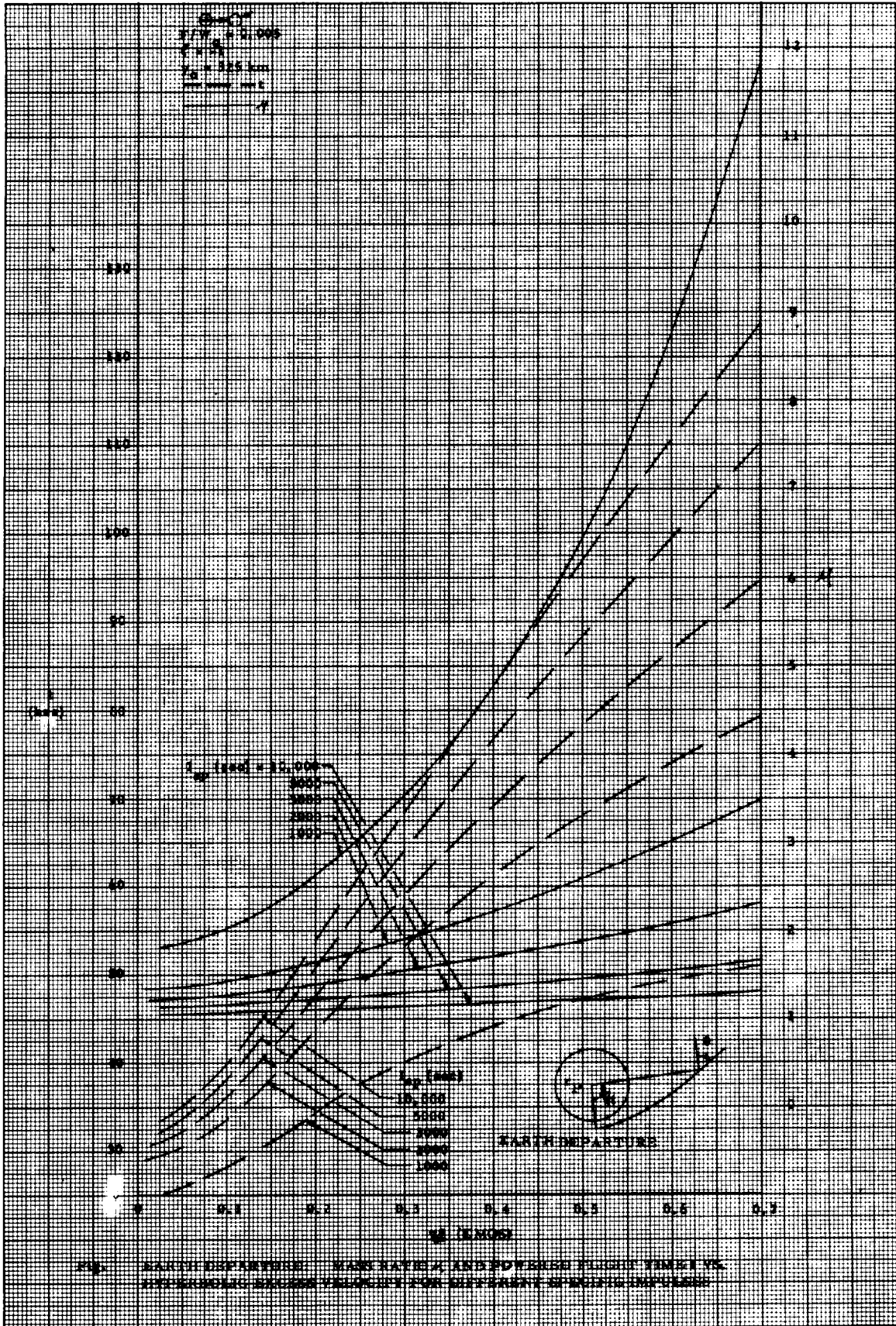
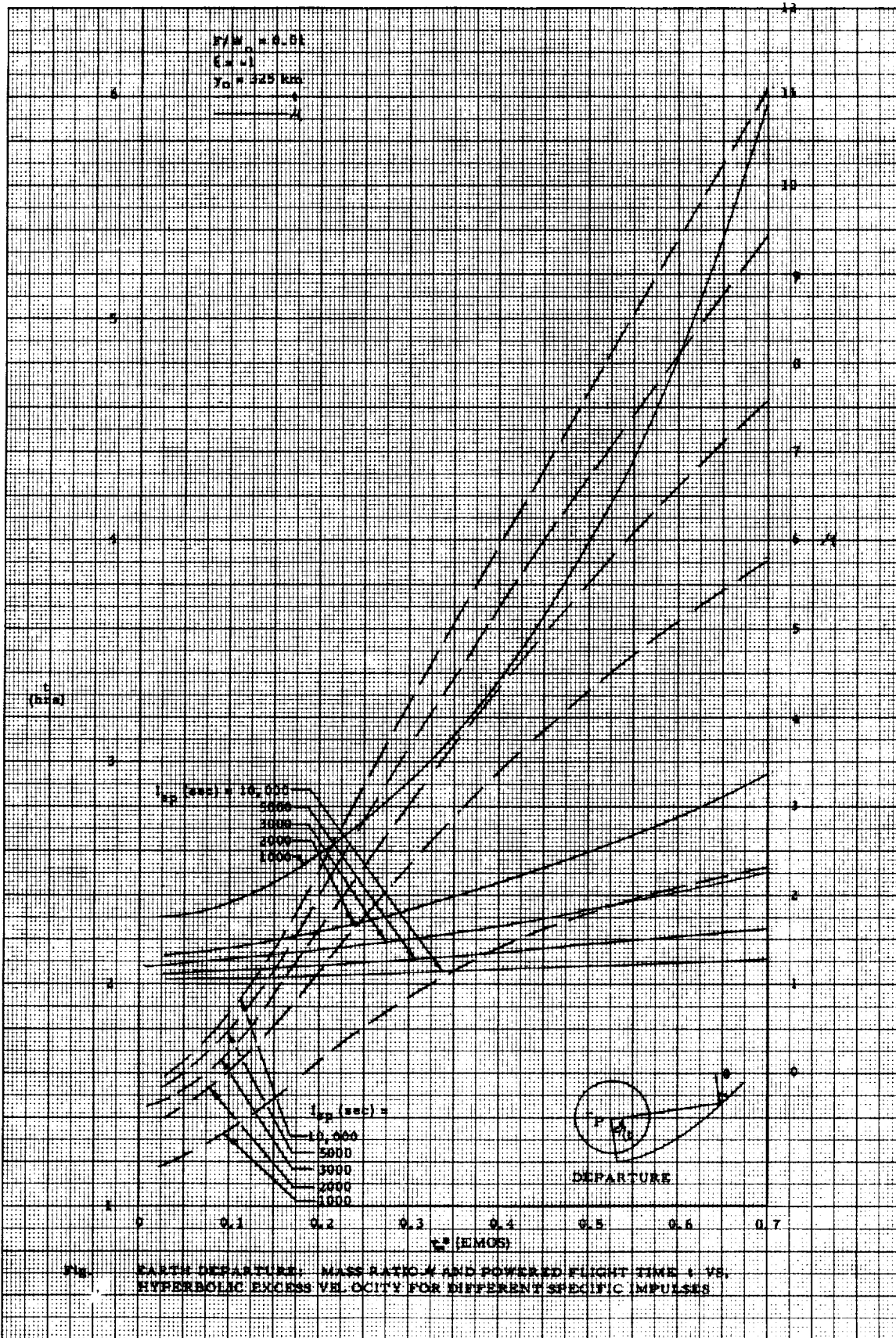
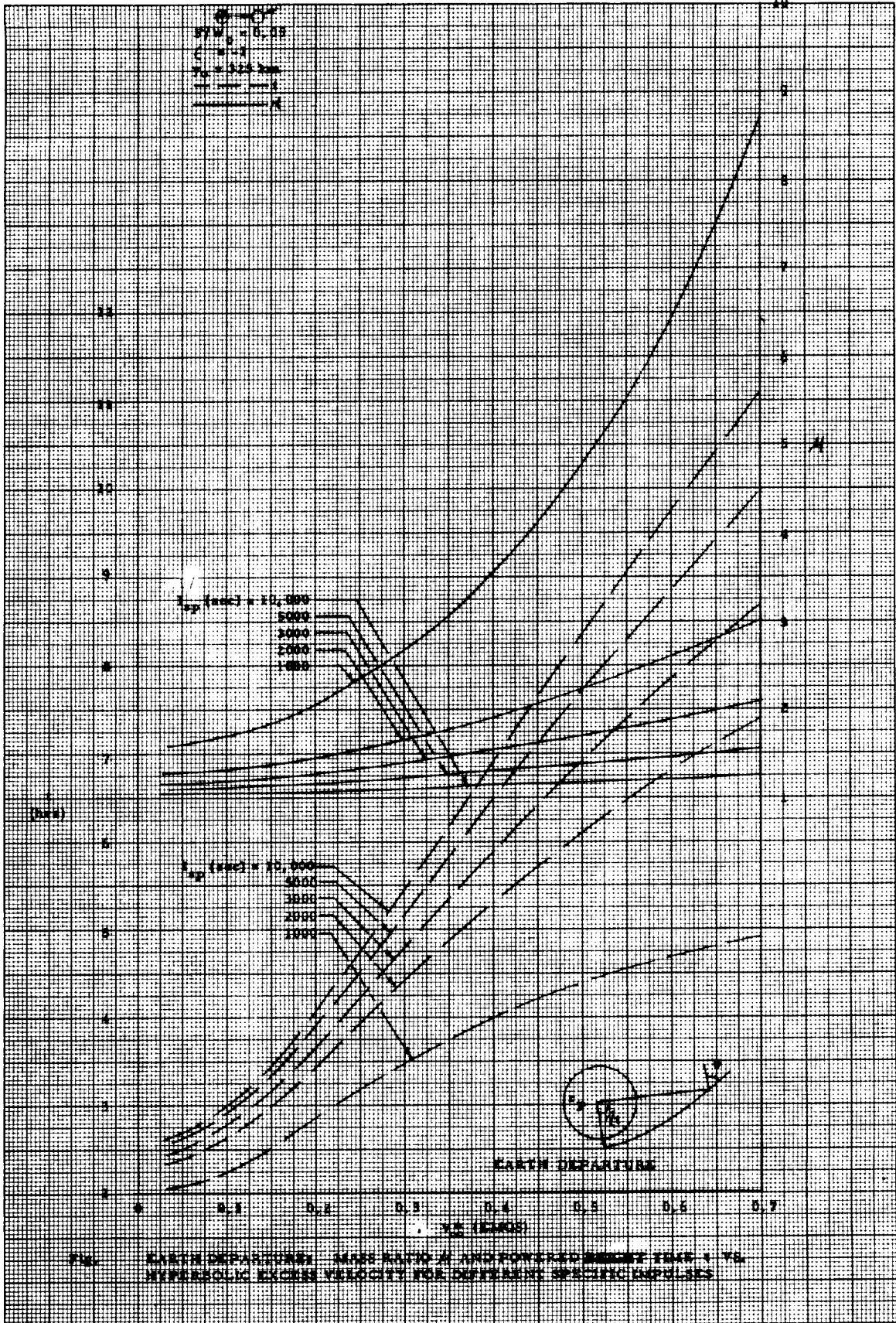


FIG. EARTH DEPARTURE: MAXIMUM ALTITUDE AND FLIGHT TIME VS. ALTITUDE FOR DIFFERENT ALTITUDES

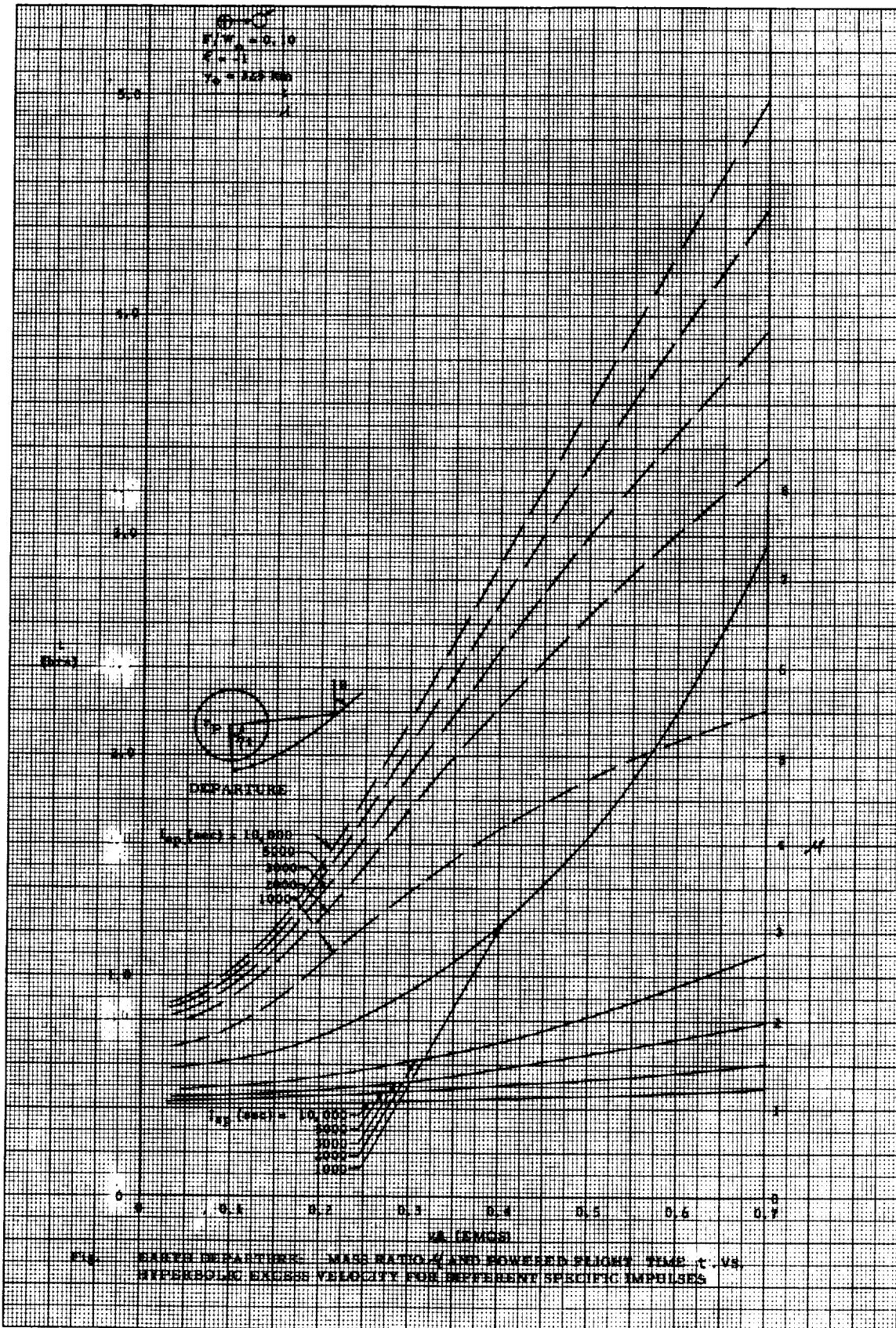
63-114
EEO-59



802-0-58



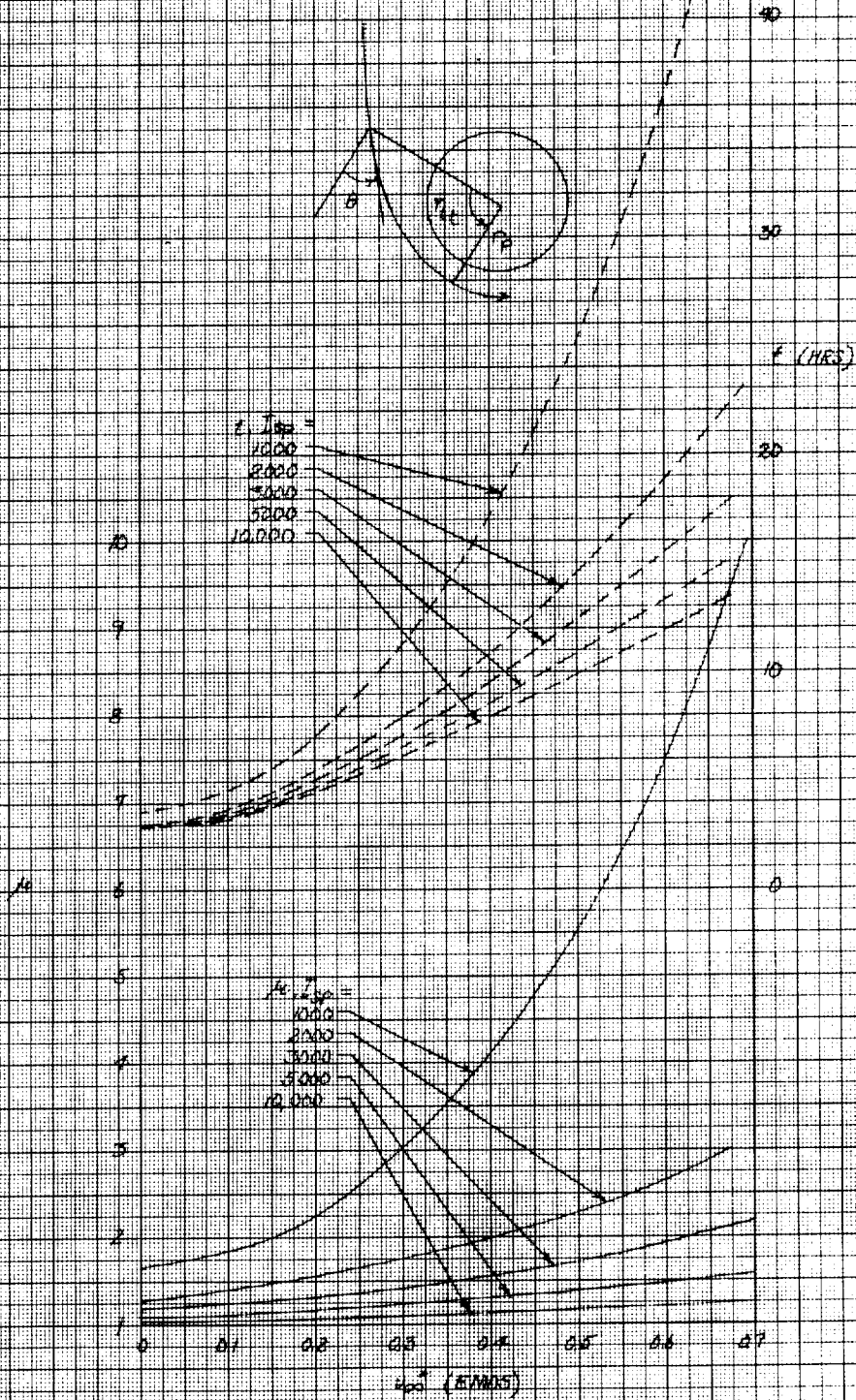
65-023



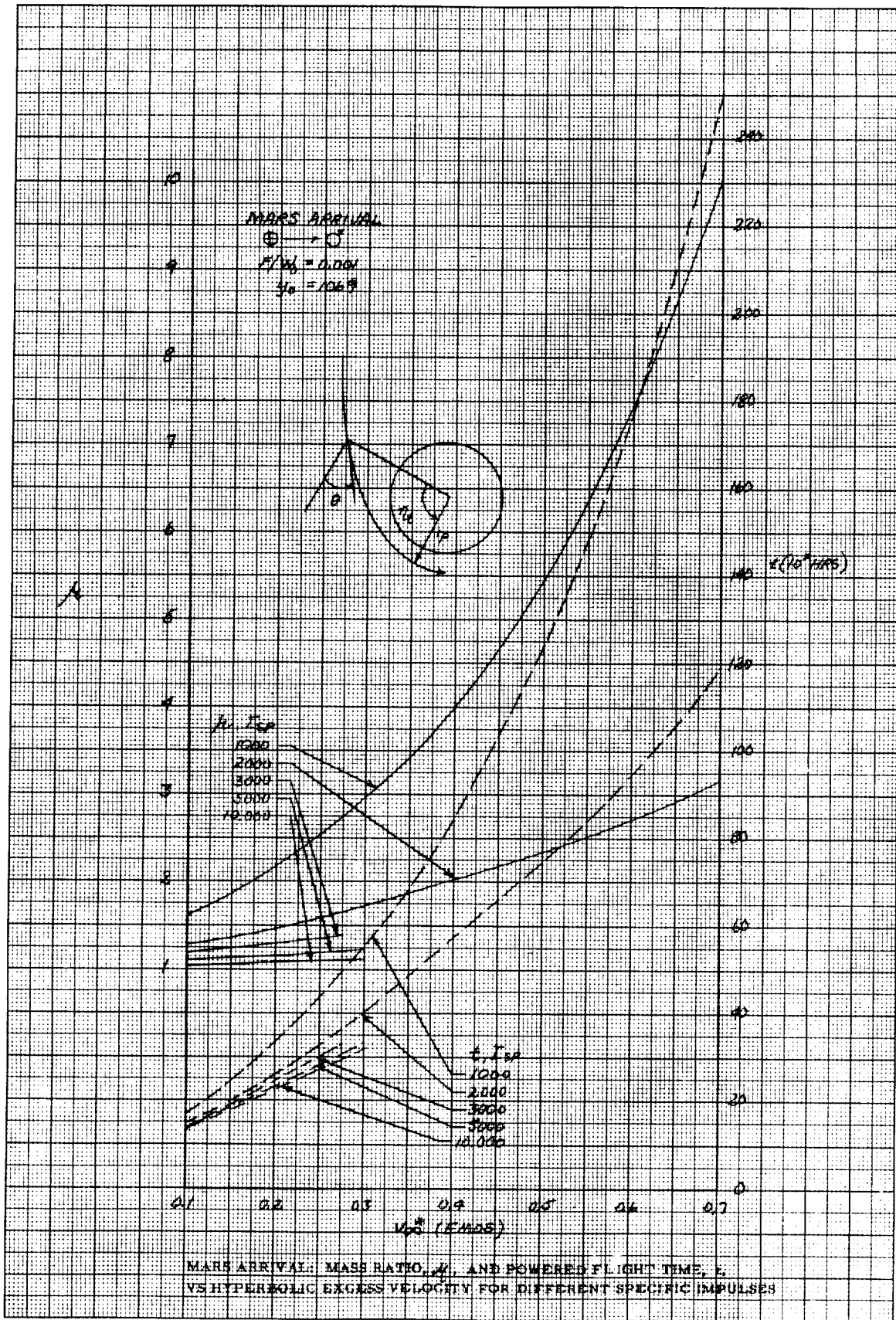
65-015

EARTH ARRIVAL: MASS RATIO, μ , AND POWERED FLIGHT TIME, t , VS HYPERBOLIC EXCESS VELOCITY FOR DIFFERENT SPECIFIC IMPULSES

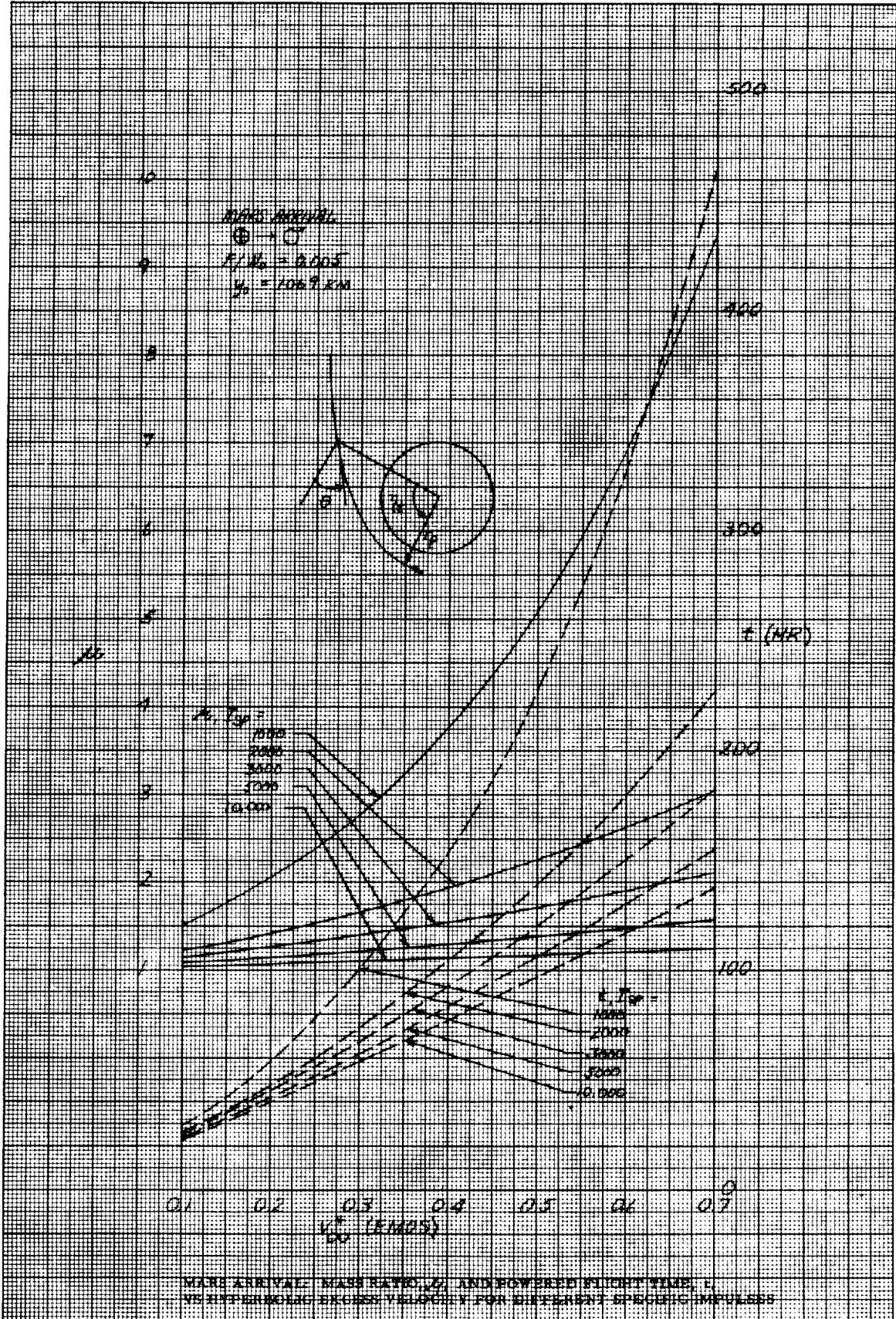
EARTH ARRIVAL
 $\odot \rightarrow \oplus$
 $R/W_0 = 0.05$
 $r_p = 3225 \text{ KM}$



PART IV MARS

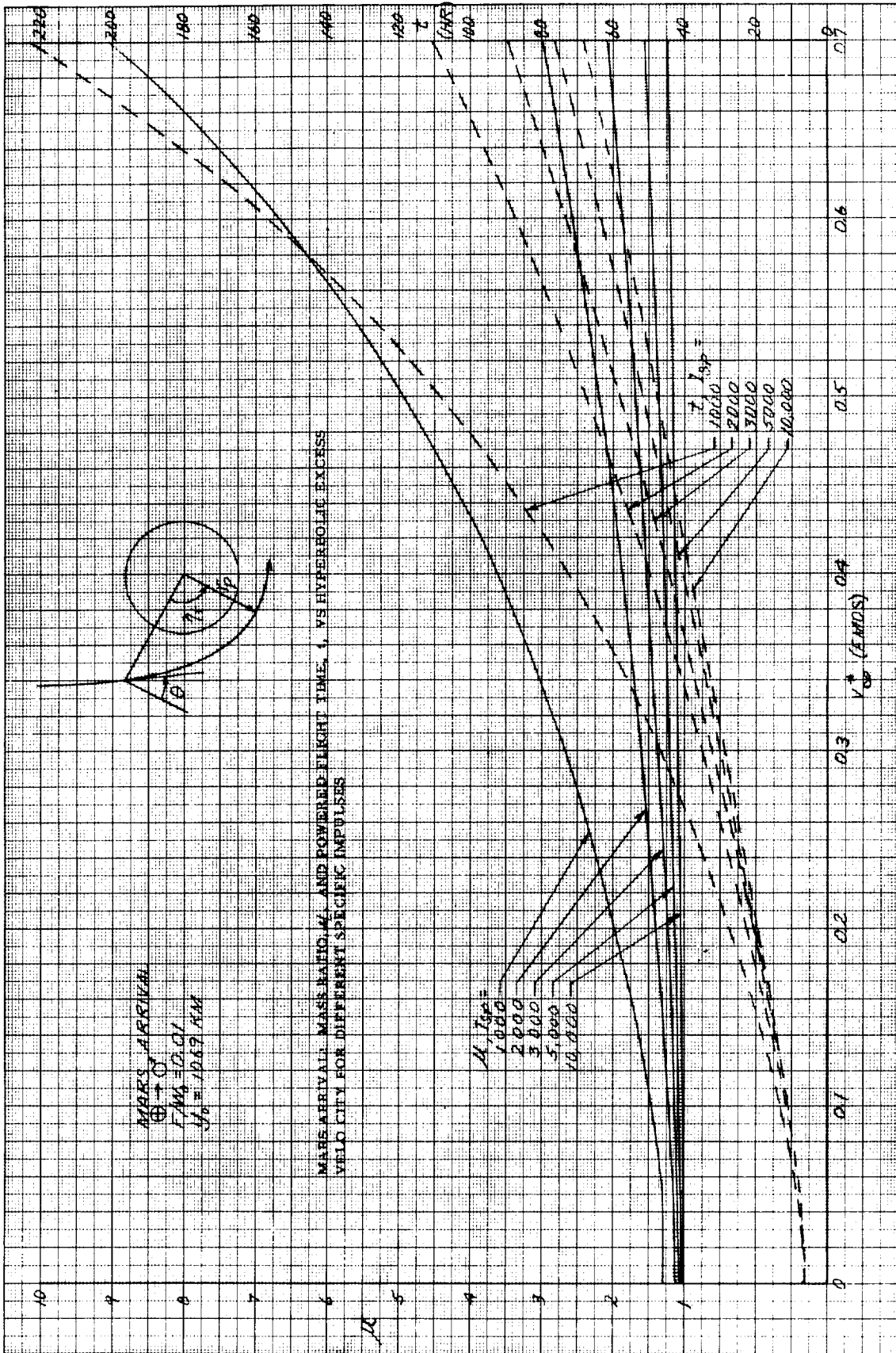


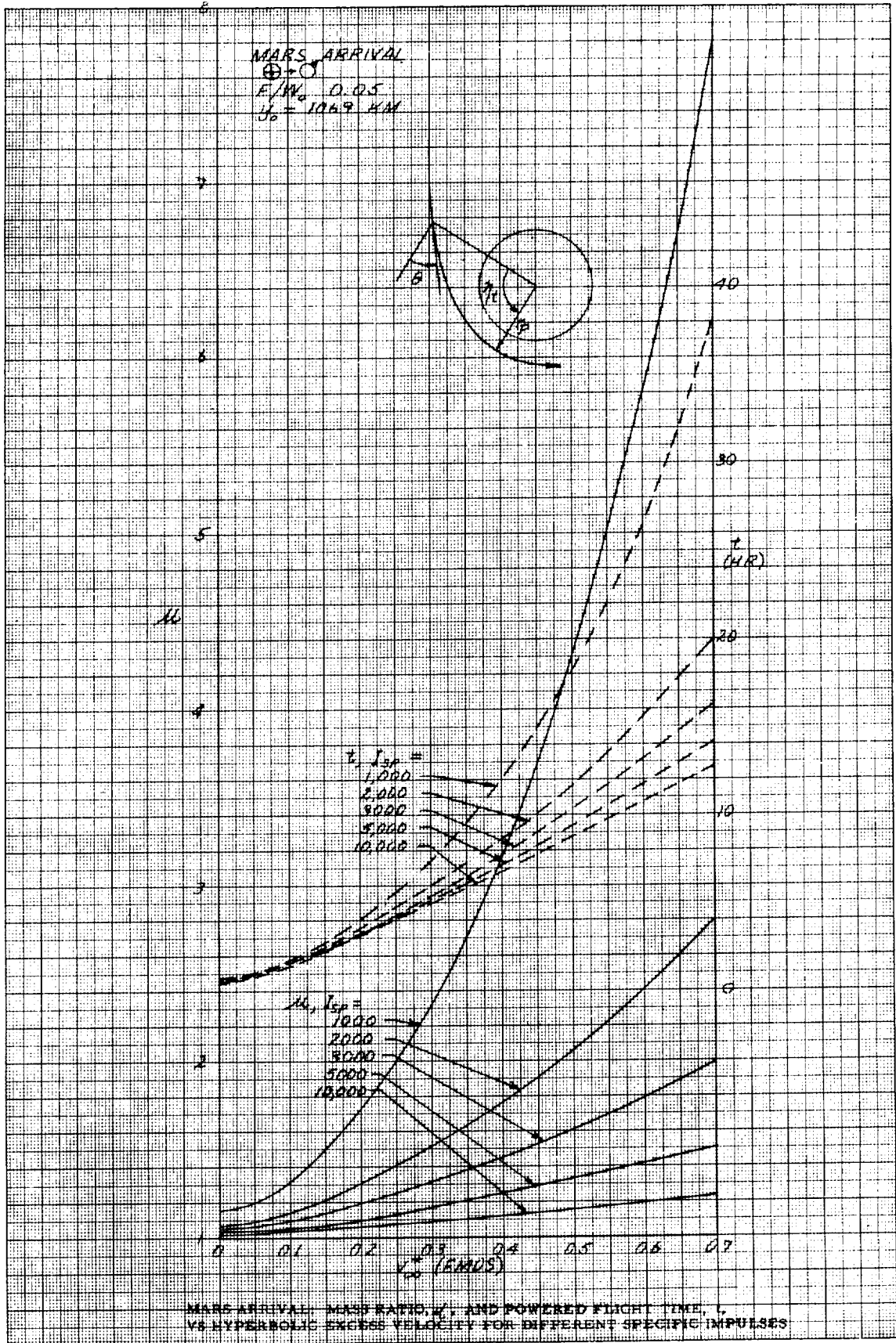
65-063



65-058

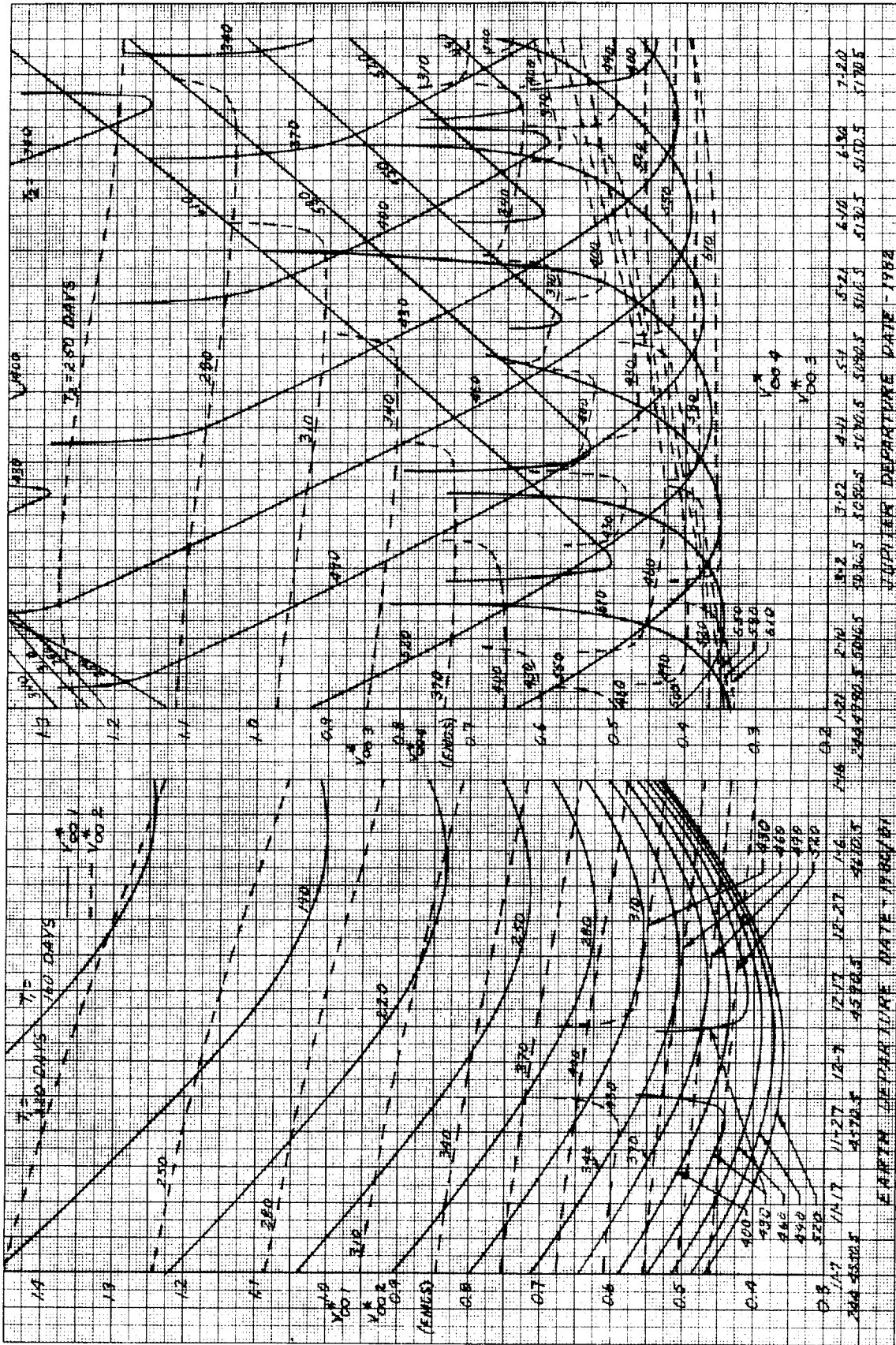
65-053





65-048

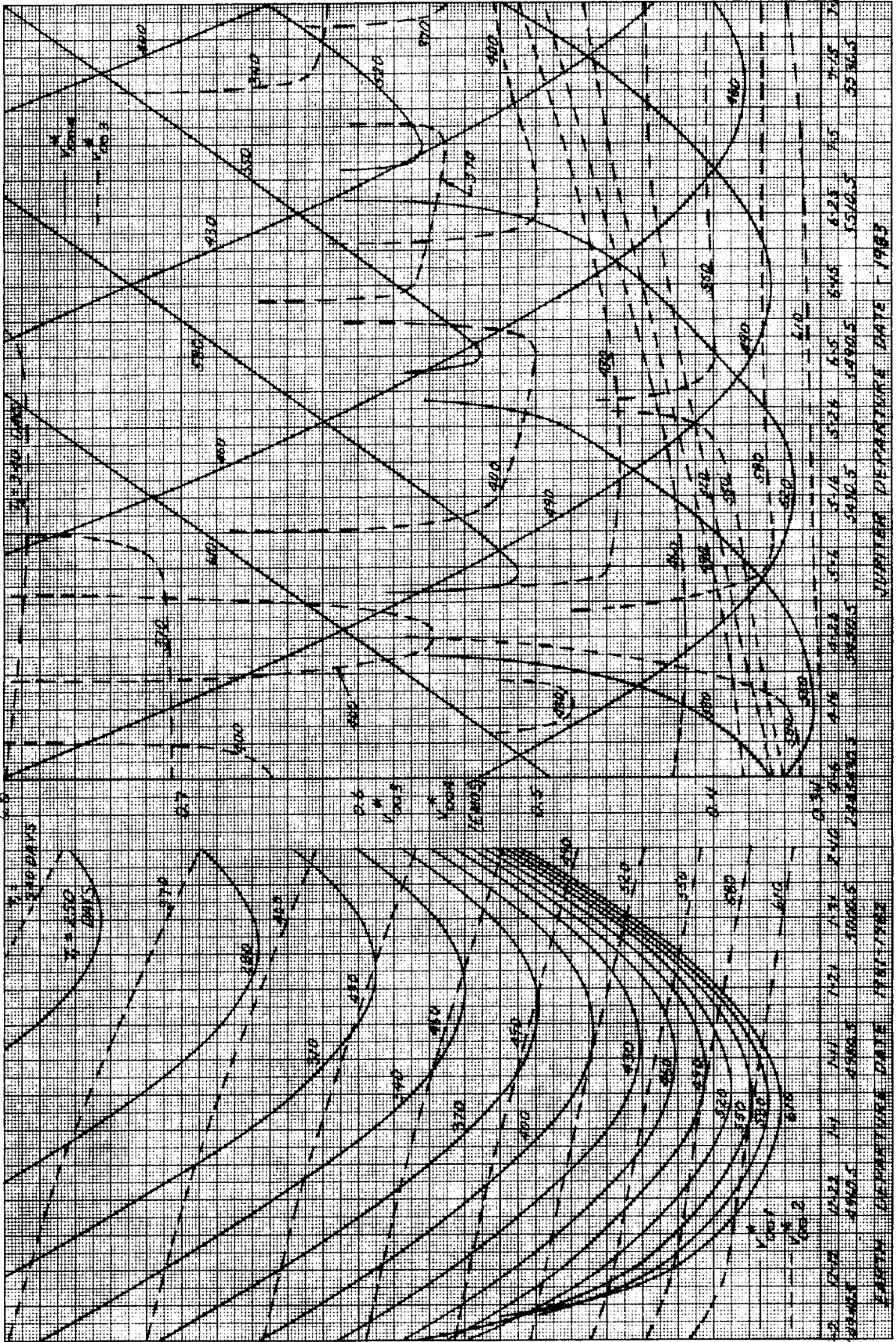
PART V JUPITER



64-099

24 → ⊕ 1983

⊕ → 24 1981/1982

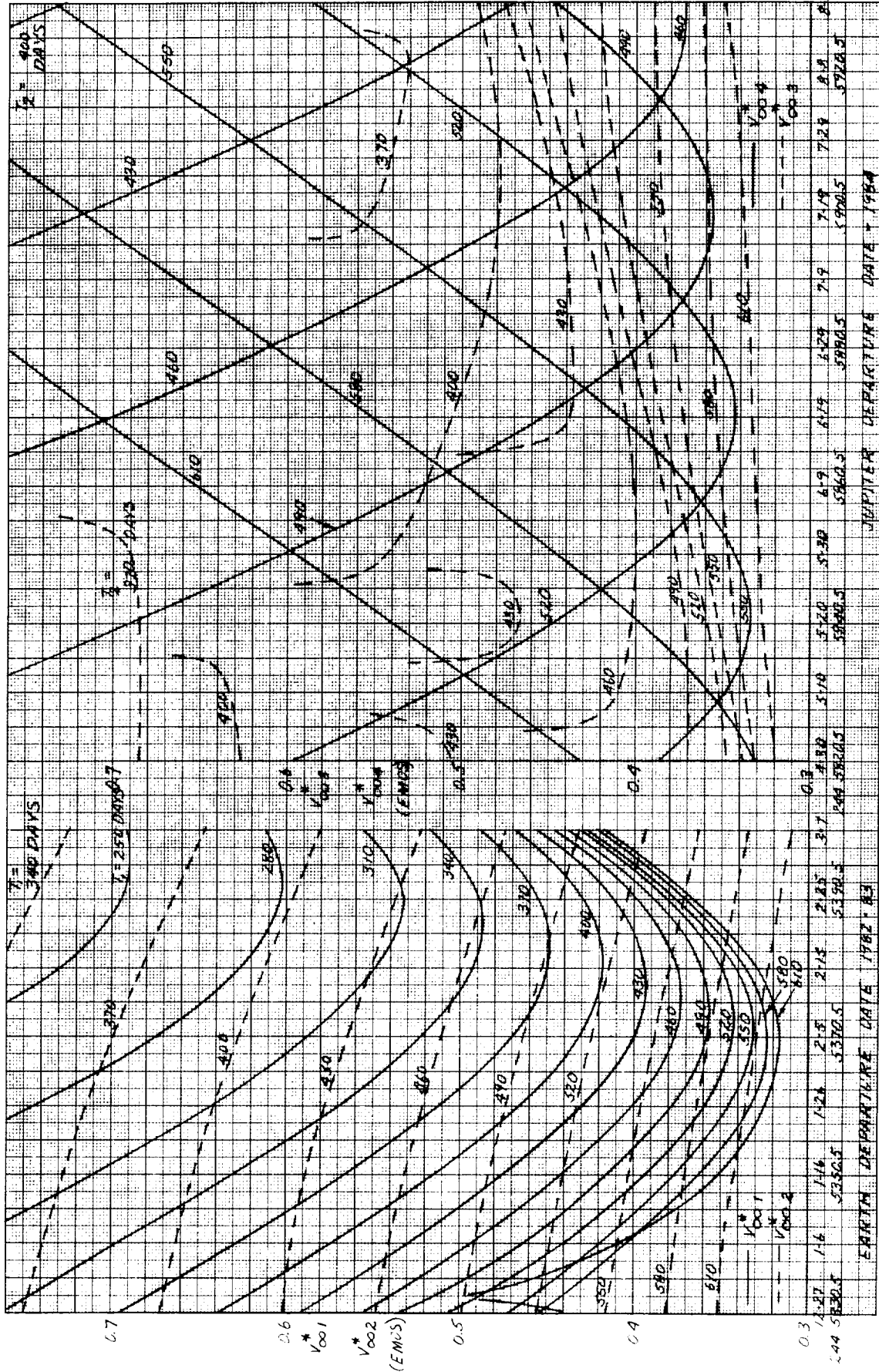


0.7
 0.6
 * V001
 * V002
 (EMCS)
 0.5
 0.4
 0.3
 244

⊕ → 24 1982/83

24 → ⊕ 1984

64-100



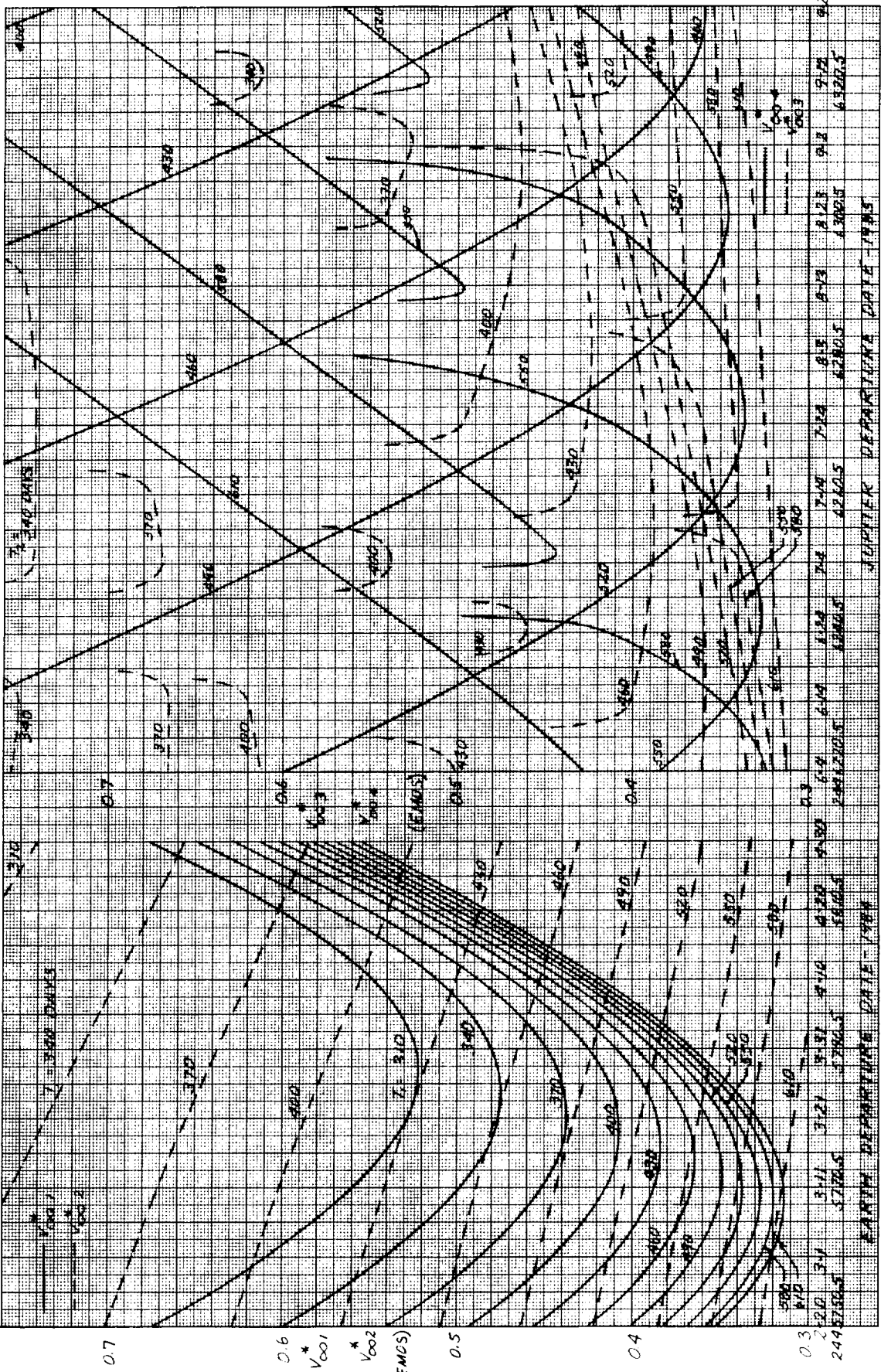
64-101

1985

4 → ⊕

1984

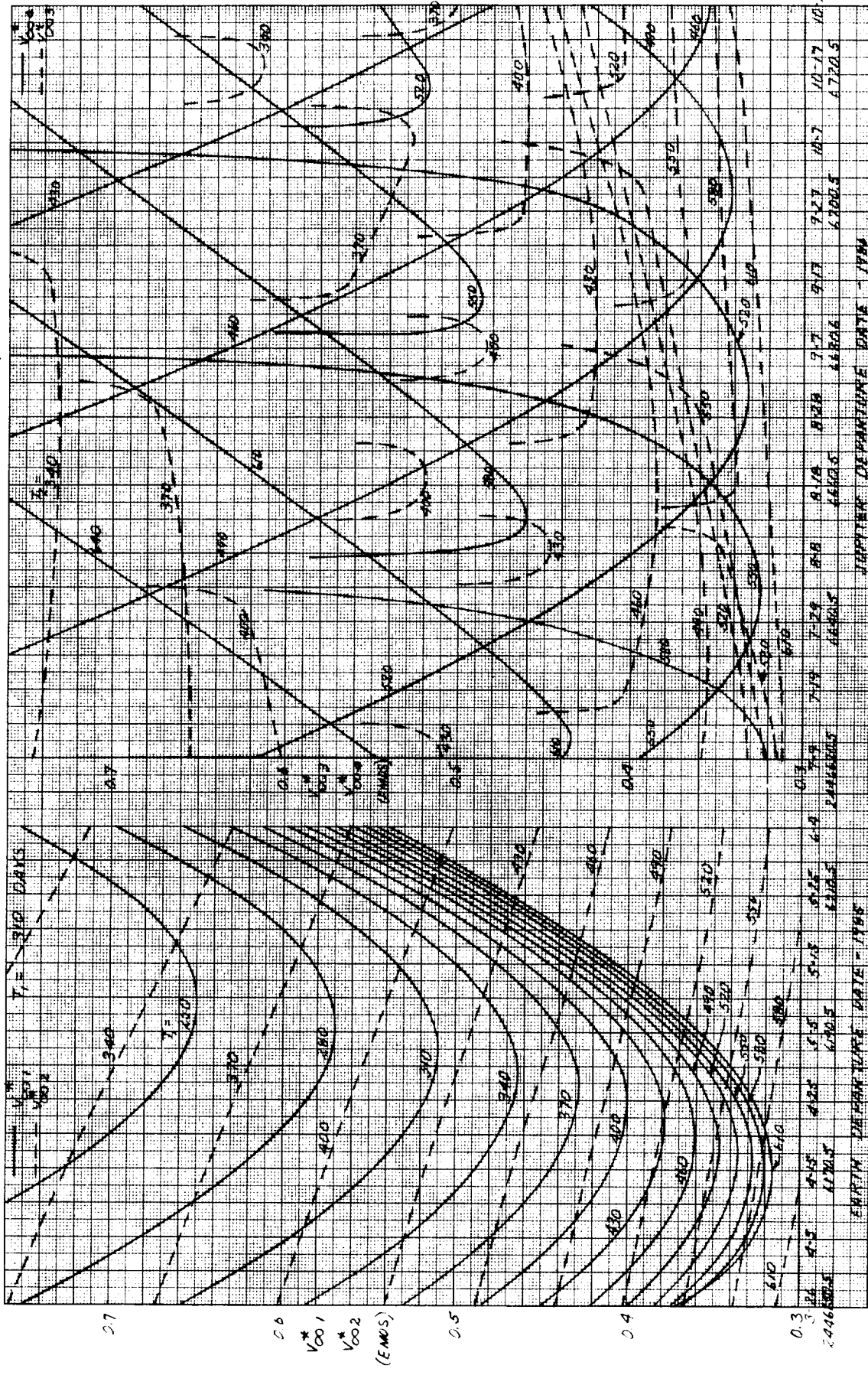
⊕ → 4

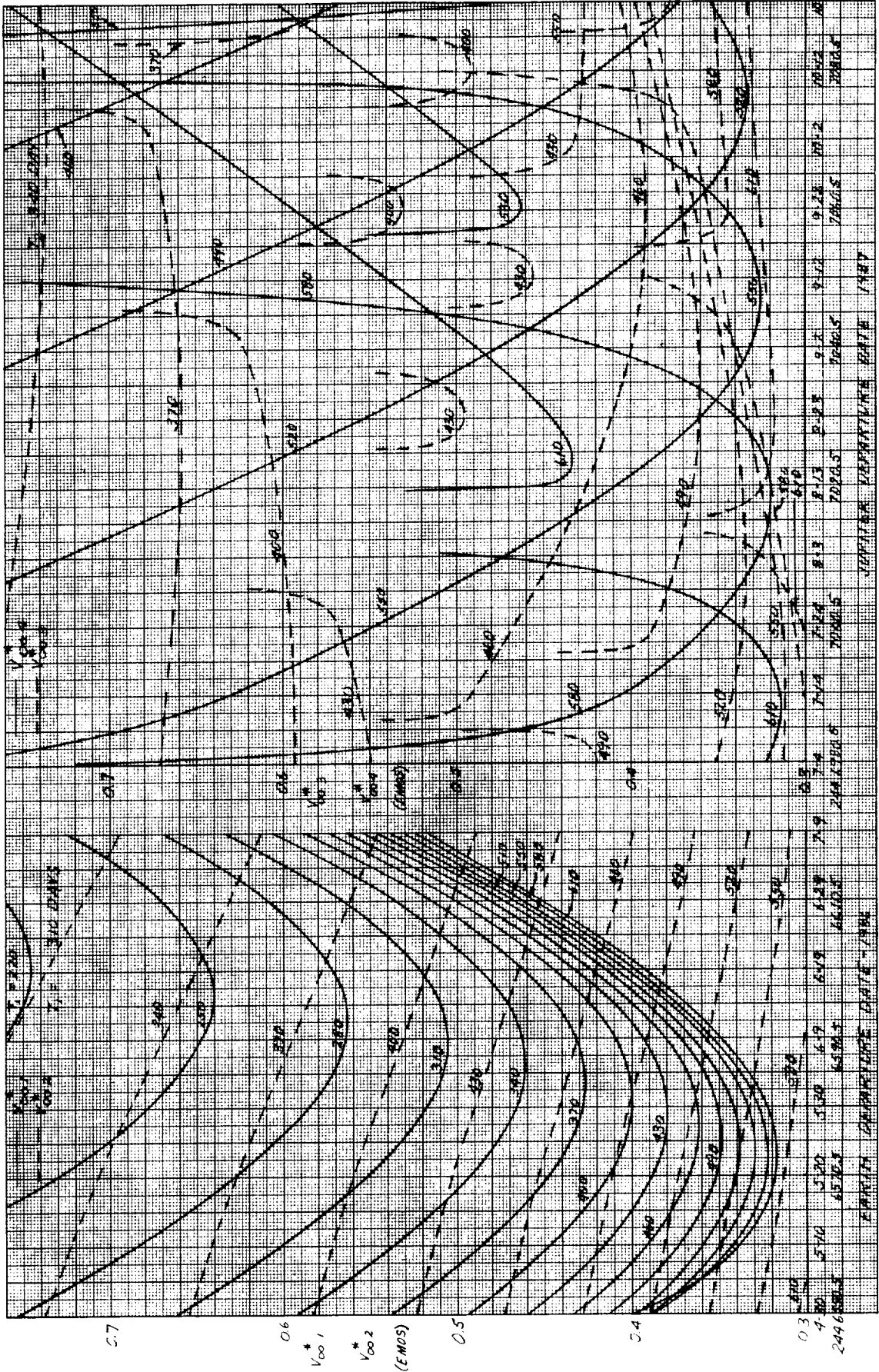


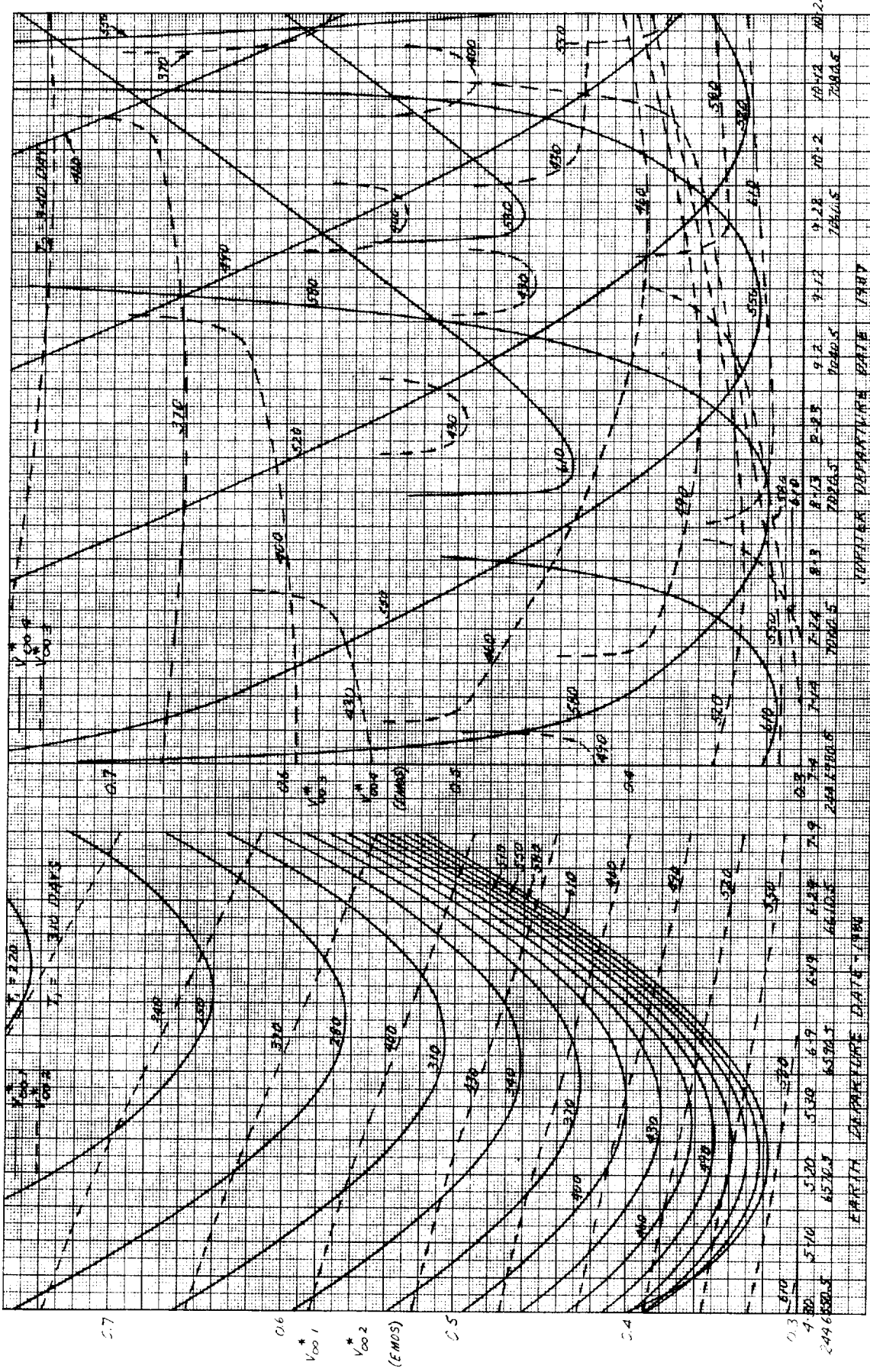
⊕ → 24 1985

24 → ⊕ 1986

64-102



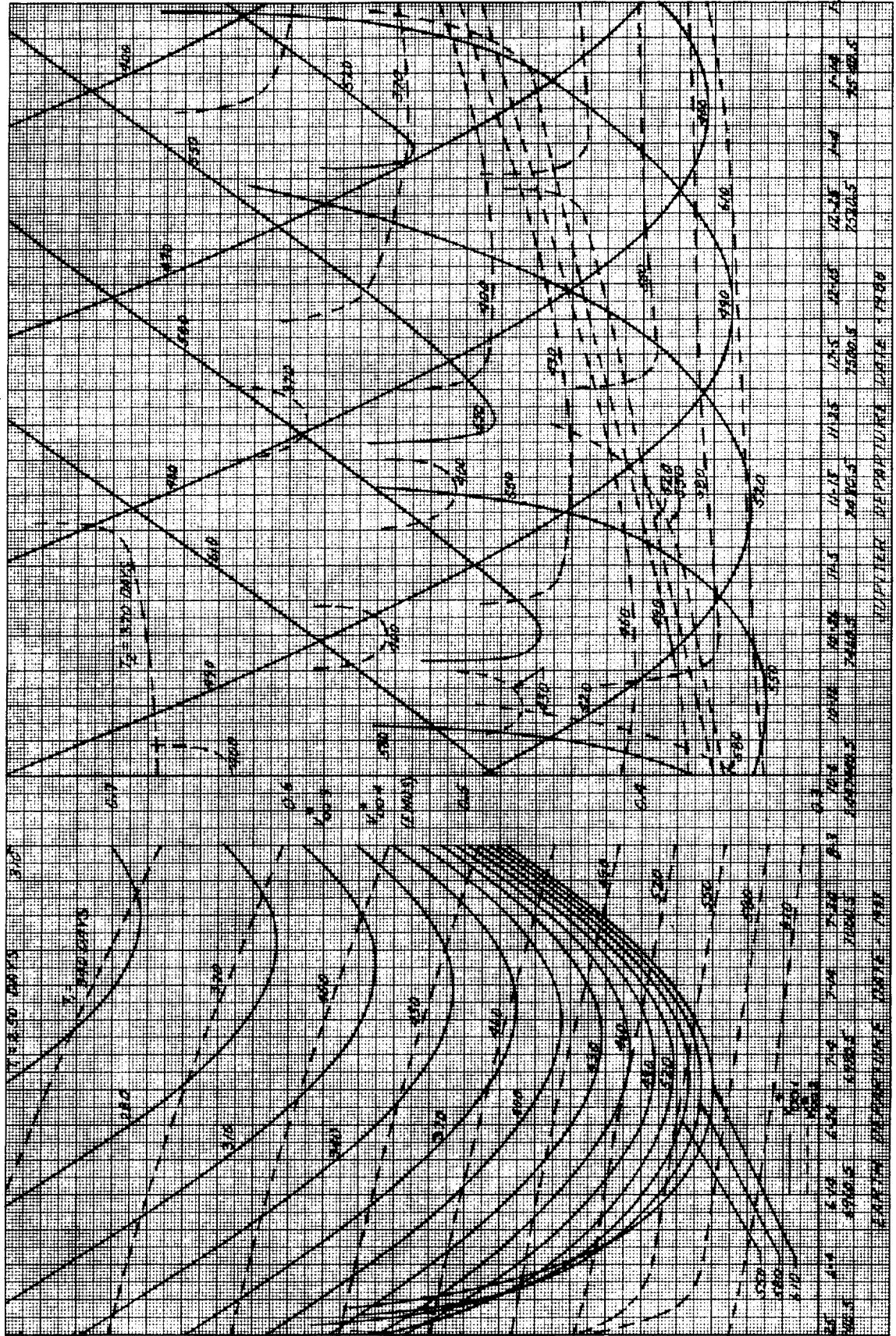




⊕ → 24 1987

24 → ⊕ 1988

64-109



0.7

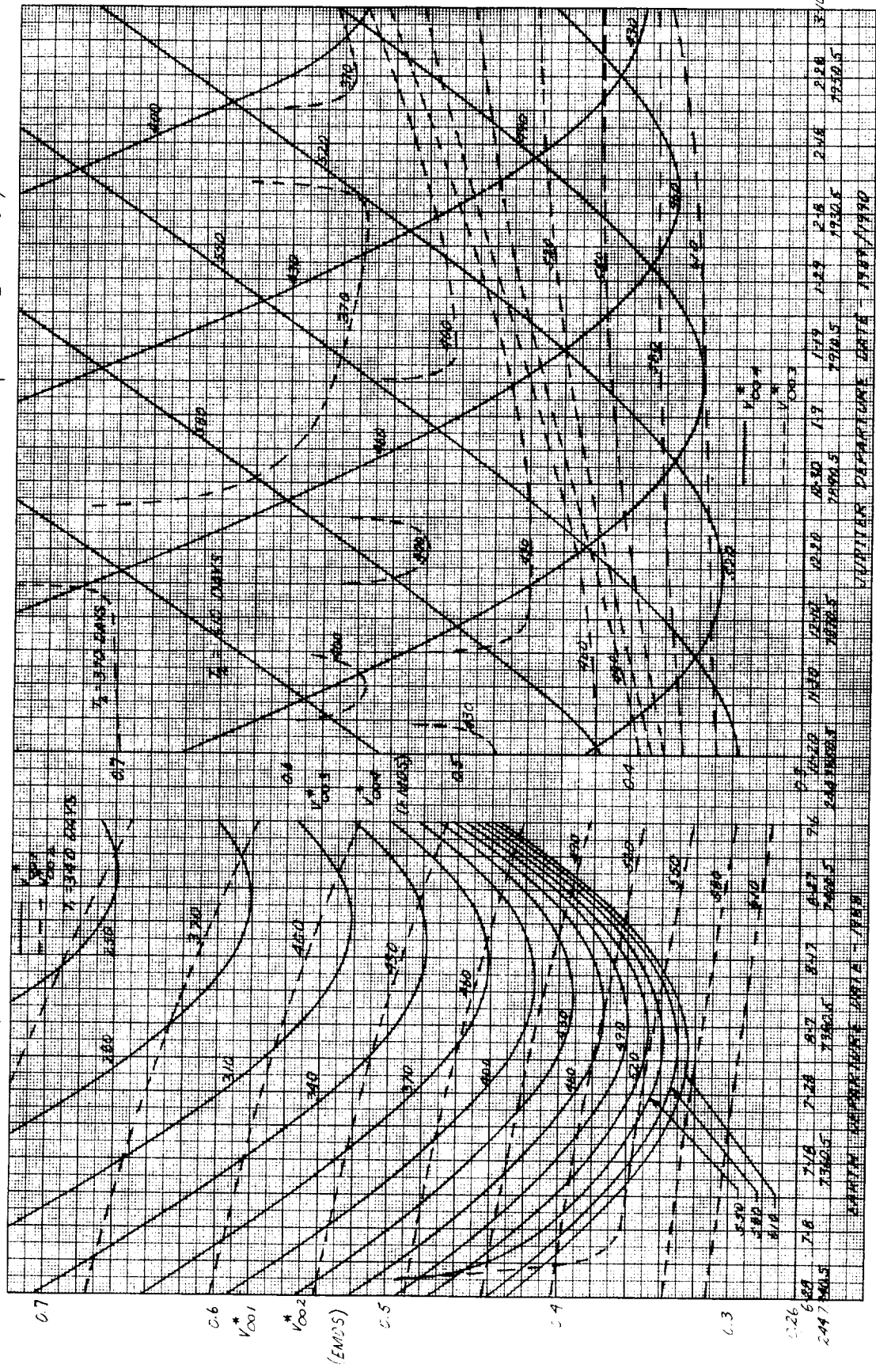
0.6
*
 $V_{\infty 1}$
*
 $V_{\infty 2}$
(EMOS)

0.5

0.4

0.3

2.65
2.44
2.15
2.00
1.85
1.70
1.55
1.40
1.25
1.10
0.95
0.80
0.65
0.50
0.35
0.20
0.05

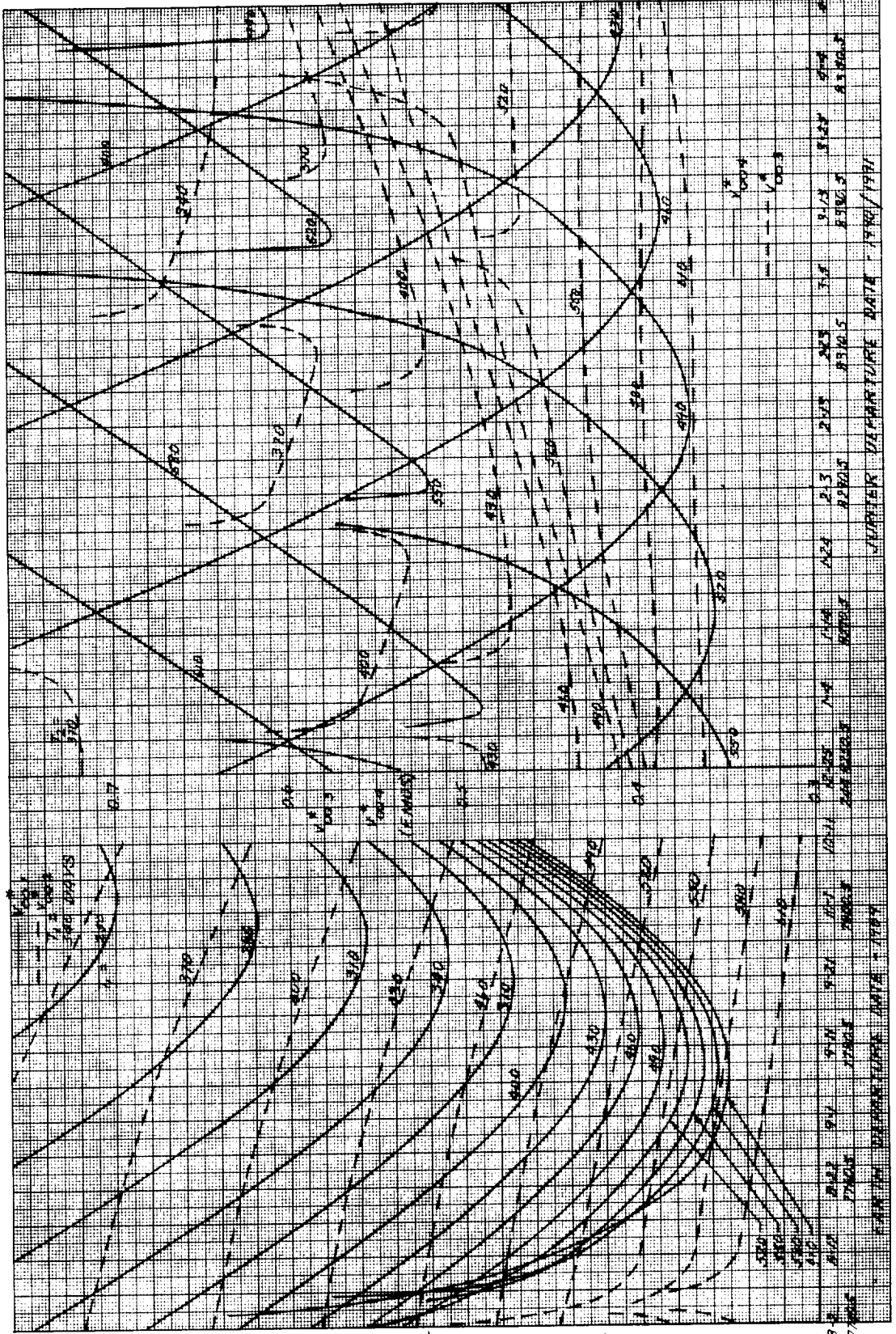


69-106

1990/1991

24 → ⊕

⊕ → 24 1989



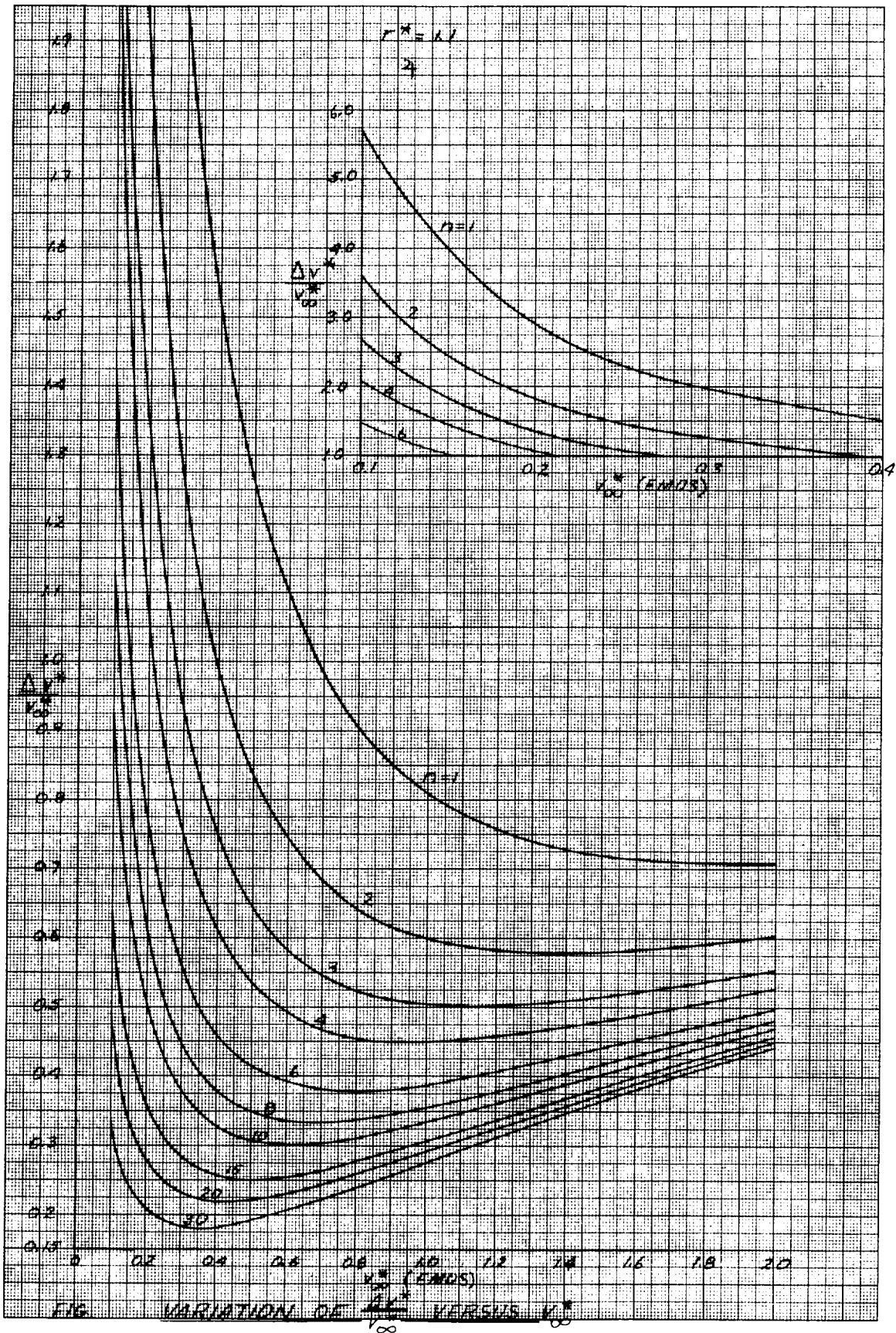


FIG. VARIATION OF $\frac{\Delta V}{V_{\infty}^*}$ VERSUS V_{∞}^*

040-49

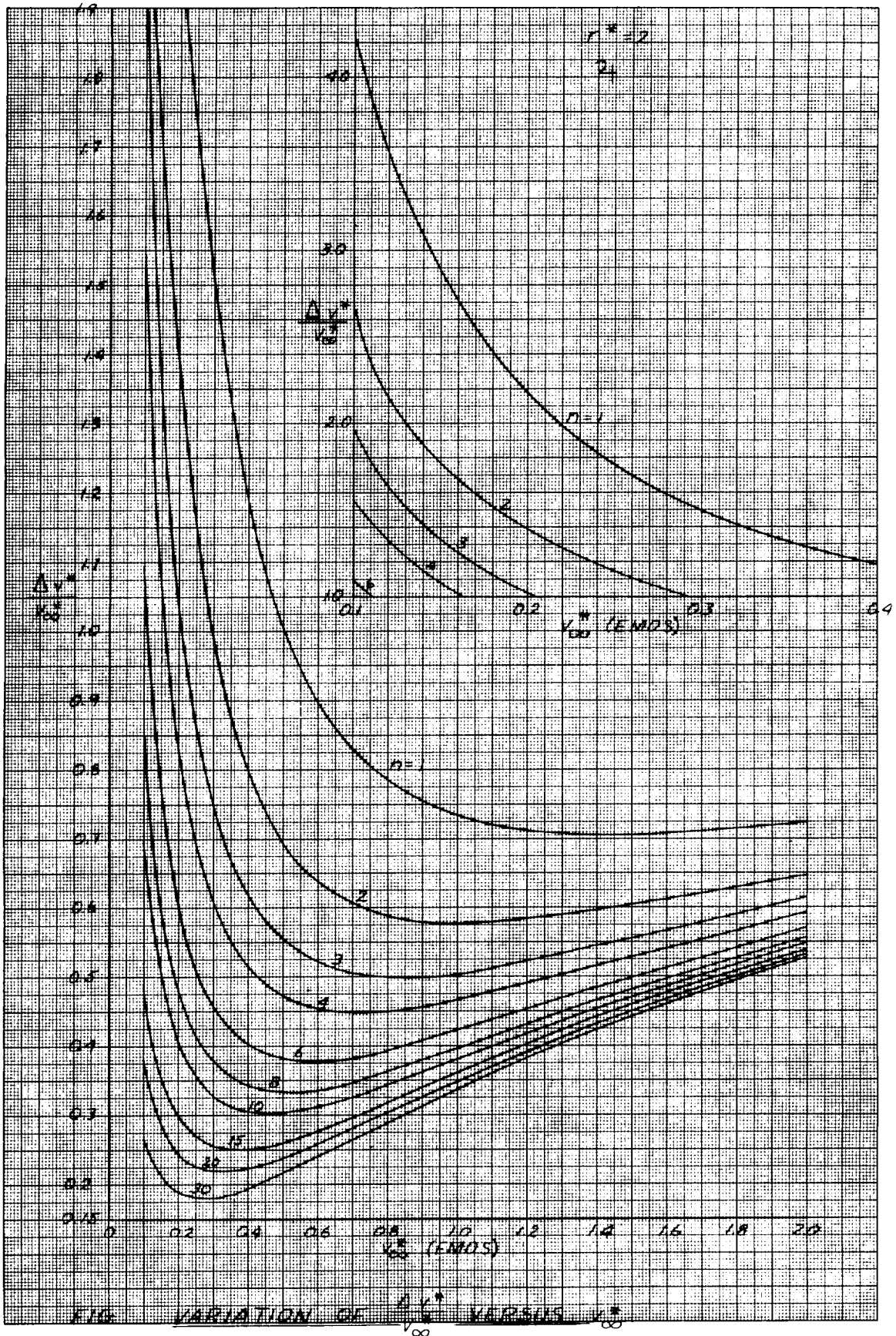


FIG. VARIATION OF $\frac{\Delta V_\infty}{V_\infty}$ VERSUS V_∞

170-17

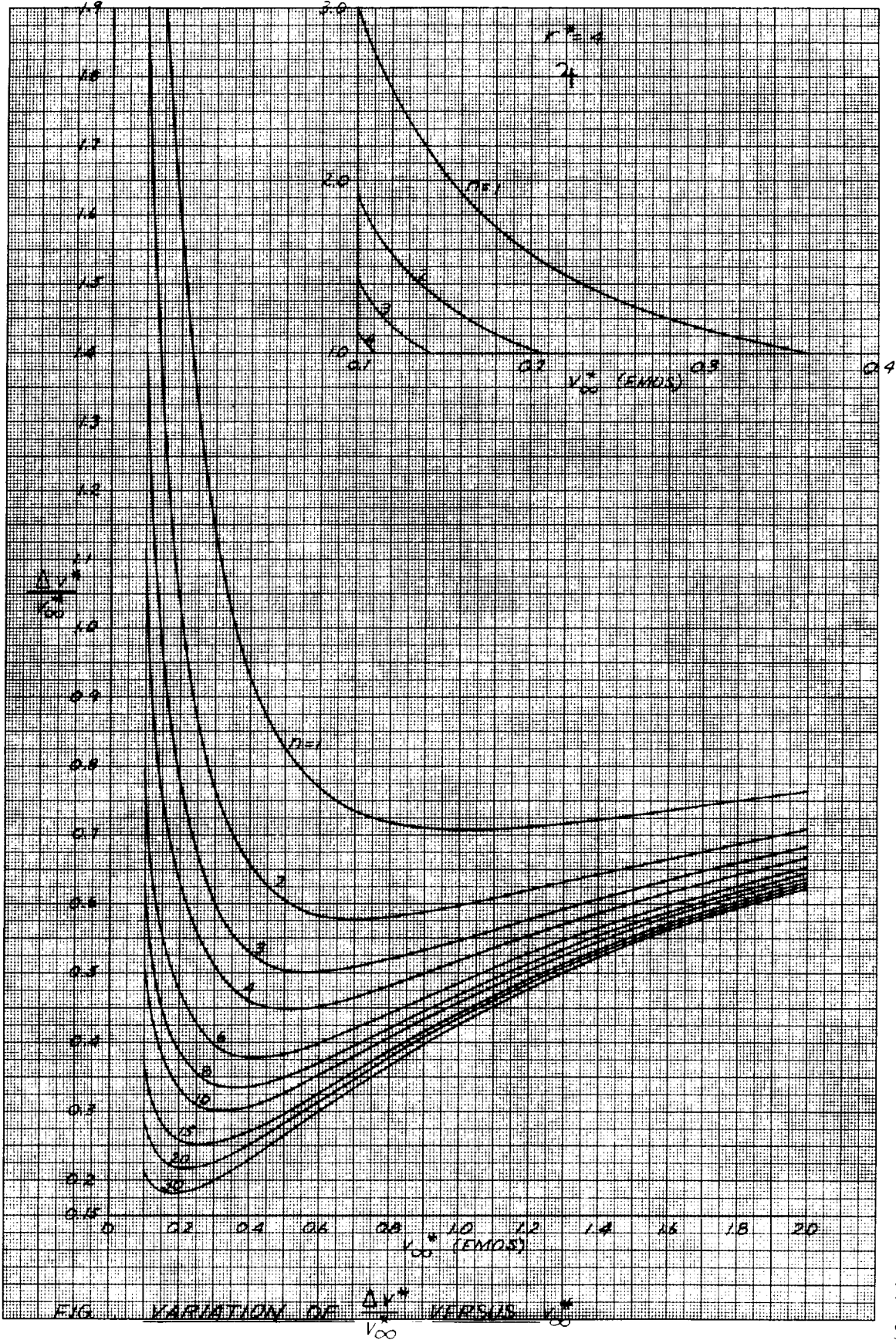
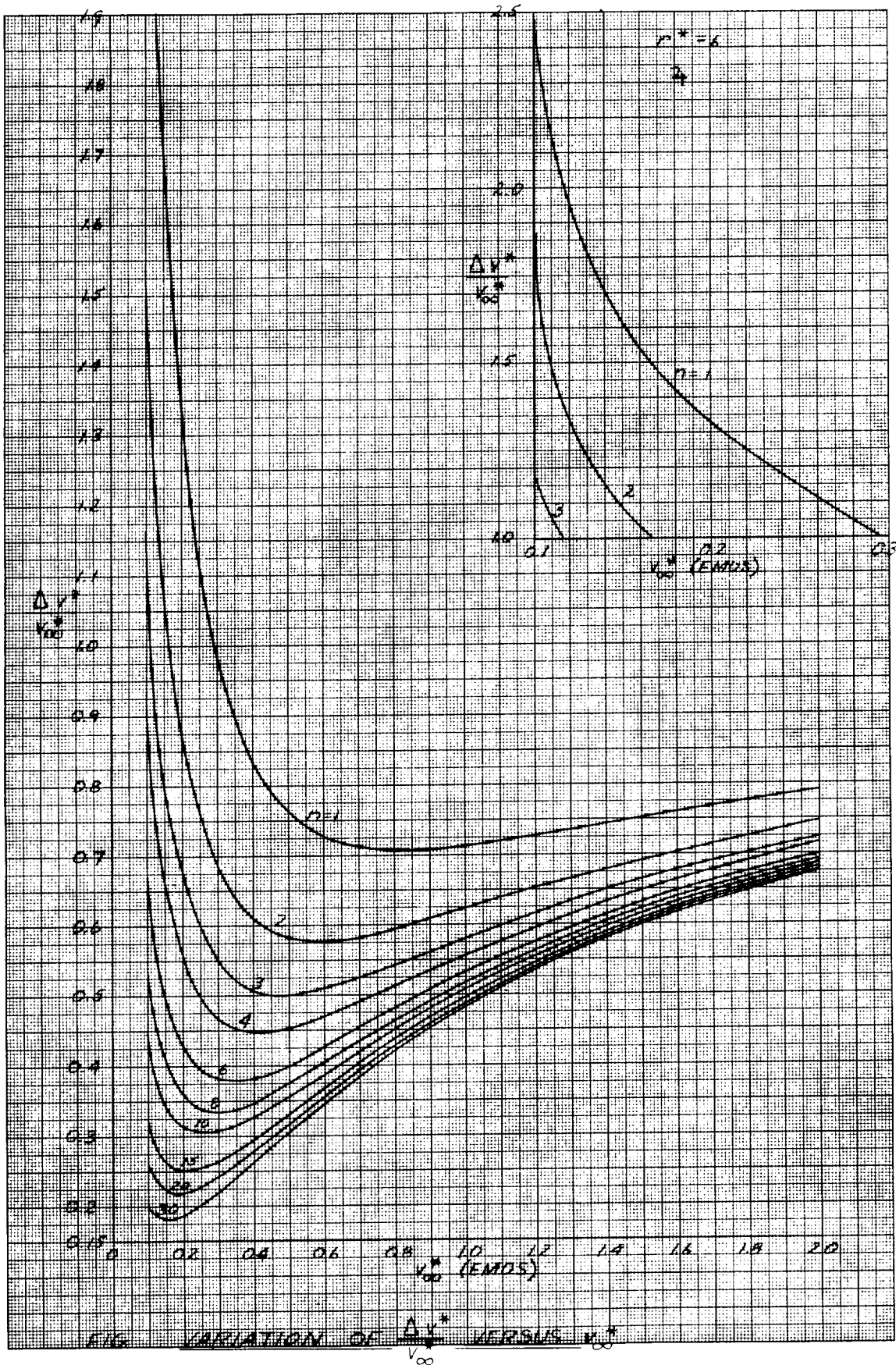


FIG. VARIATION OF $\frac{\Delta V^*}{V_\infty}$ VERSUS V_∞^*

740-12



64-443

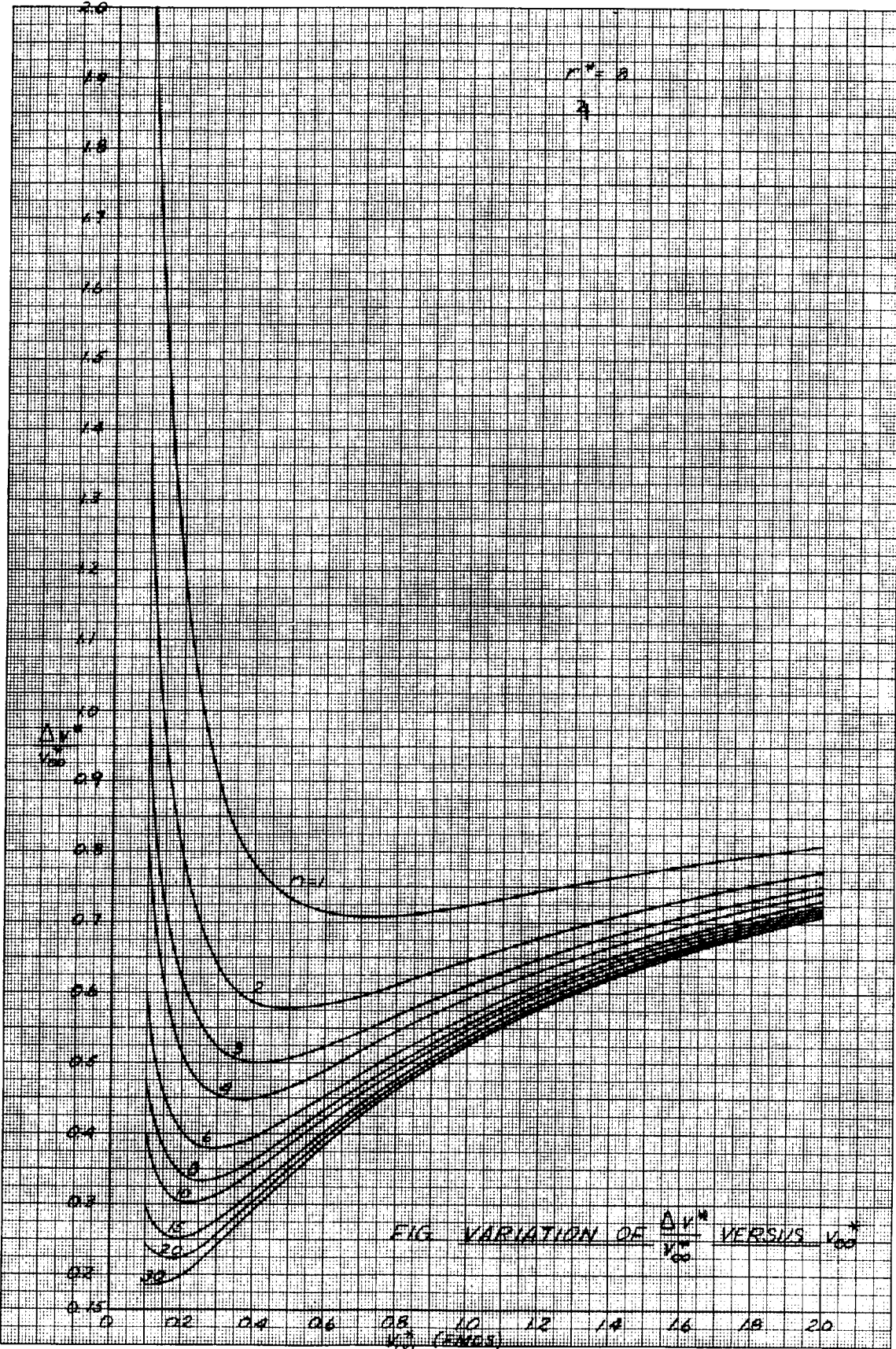
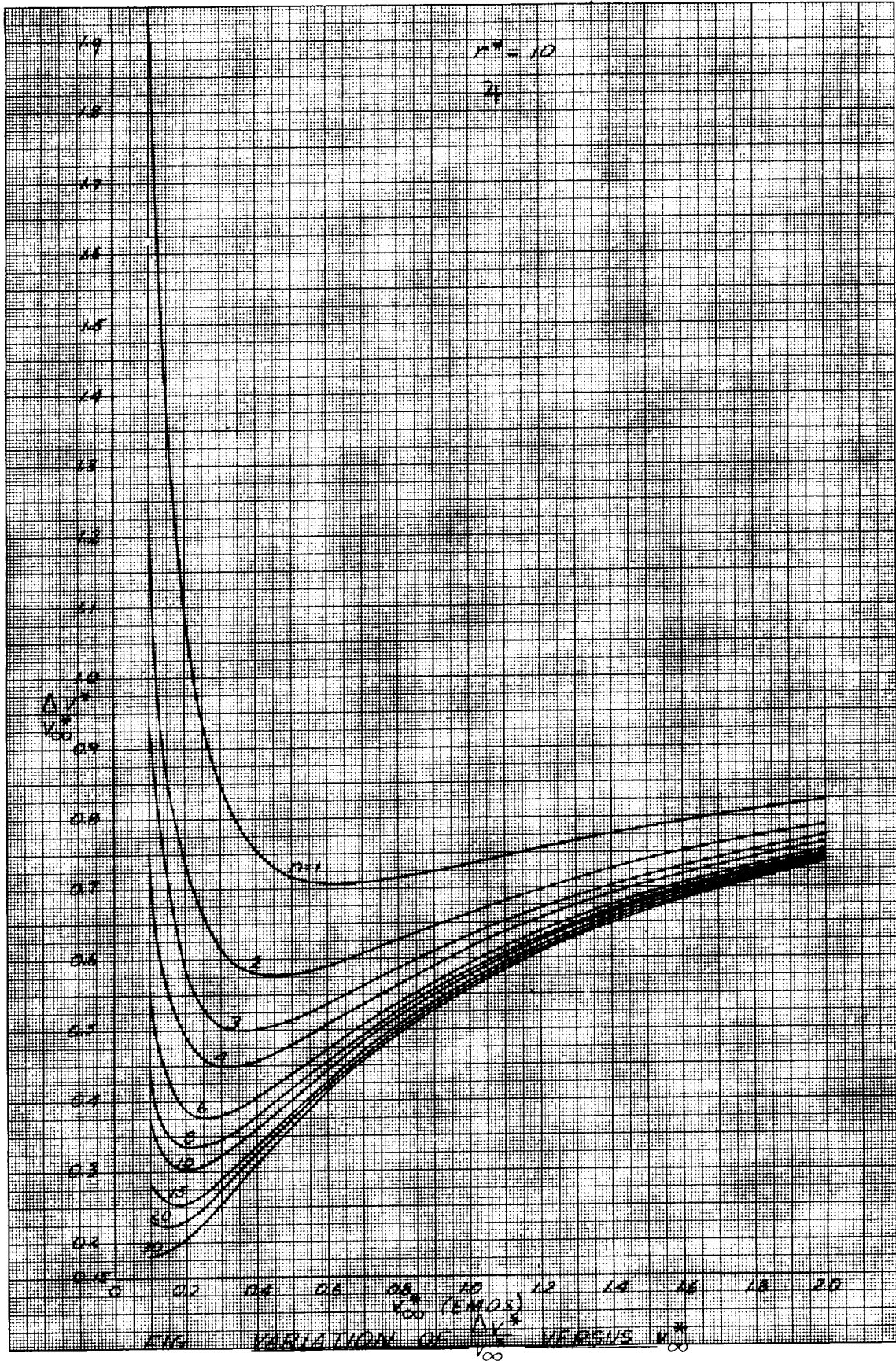
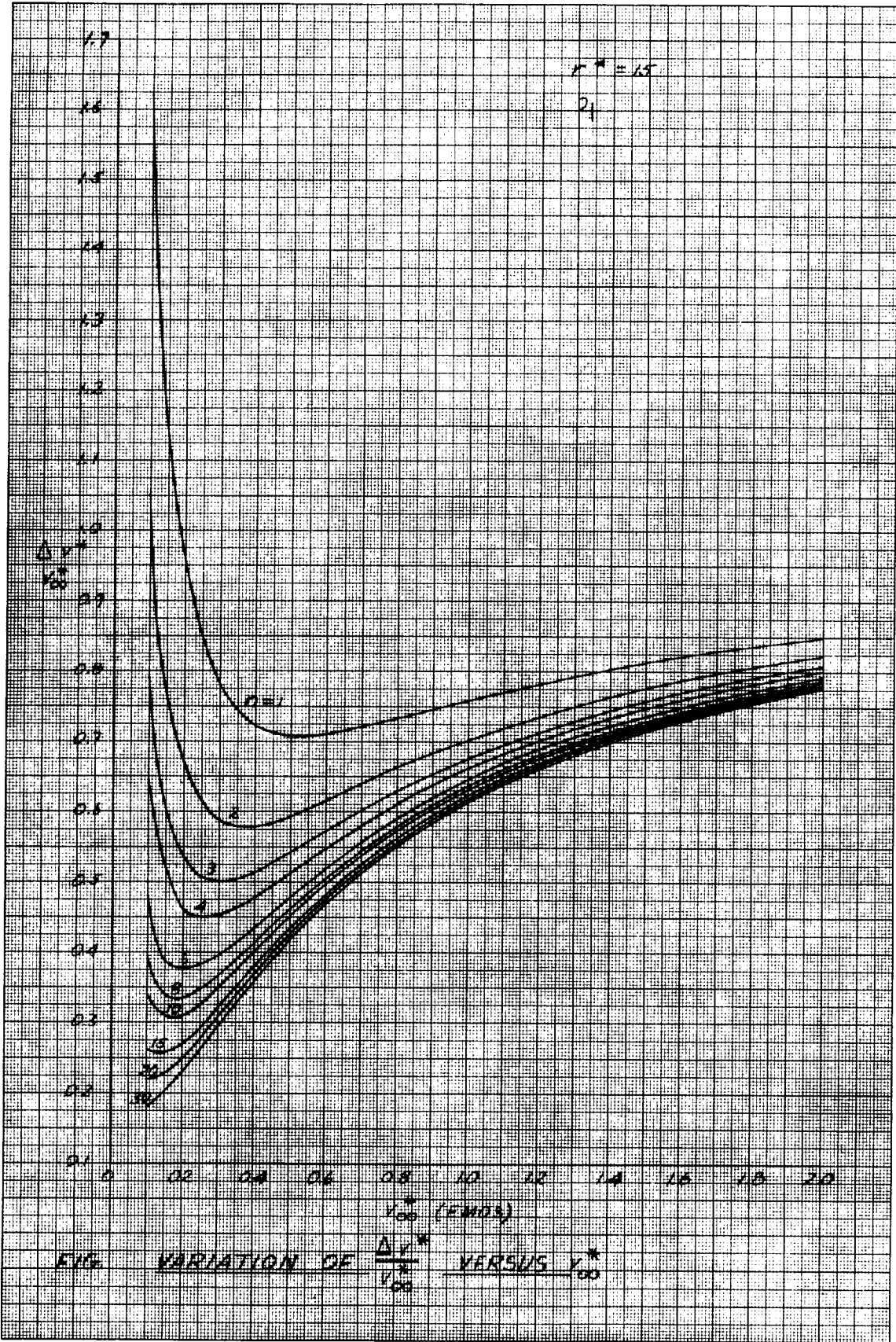


FIG VARIATION OF $\frac{\Delta V}{V_0}$ VERSUS V_0

440-49



64-005



64-0-49

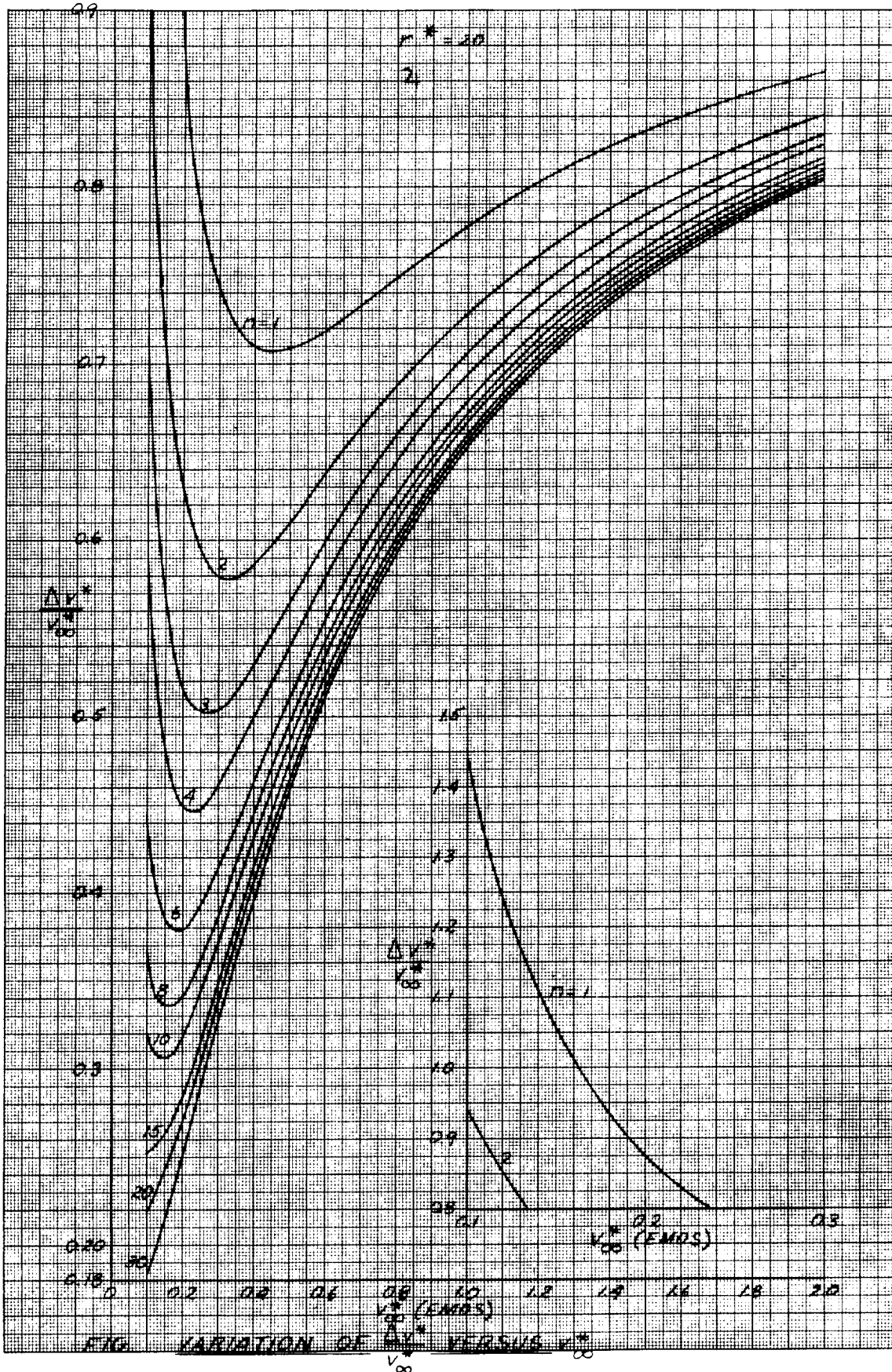
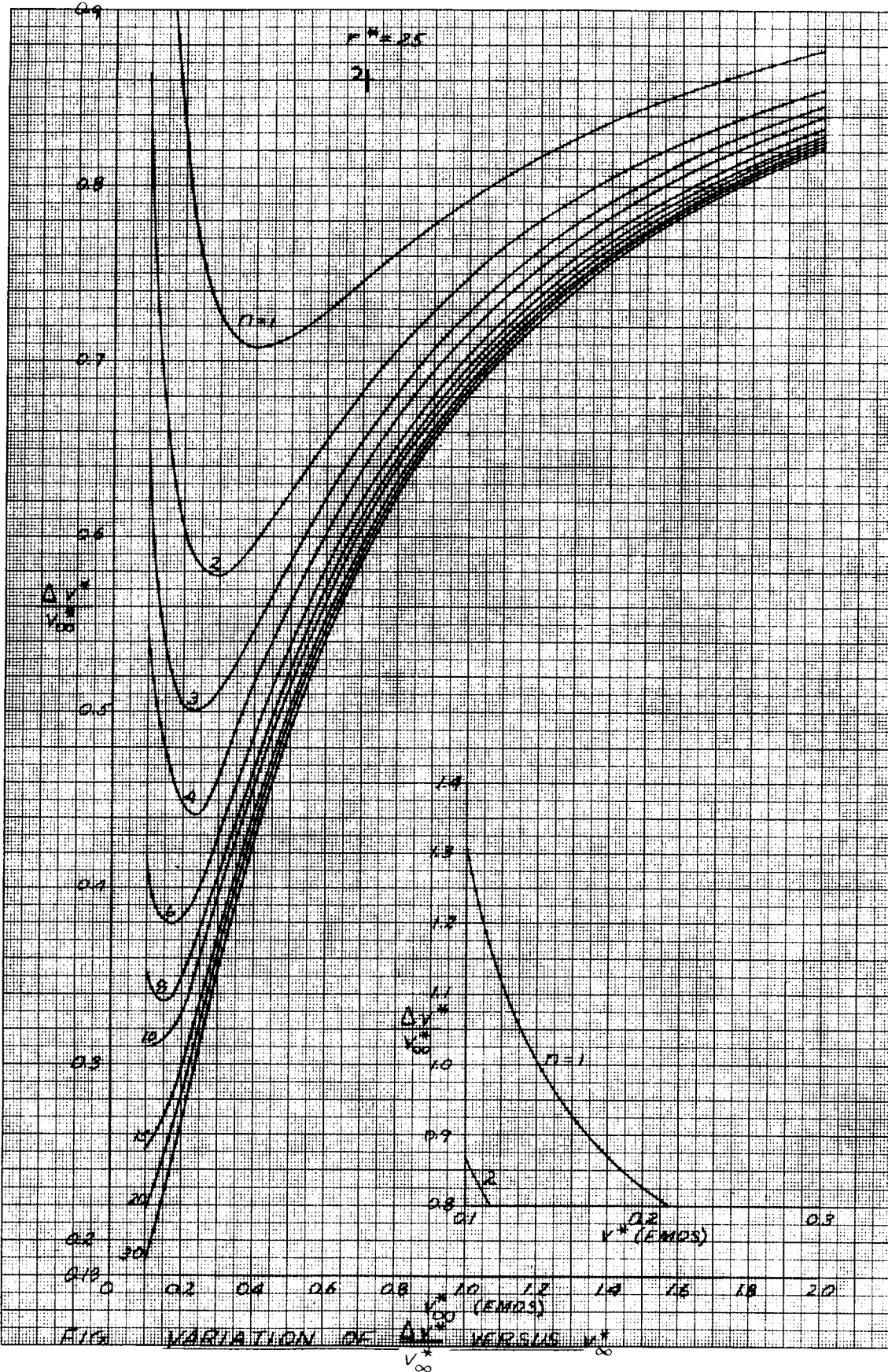


FIG. VARIATION OF $\frac{\Delta V^*}{V_\infty^*}$ VERSUS V_∞^*

64-647



847-19

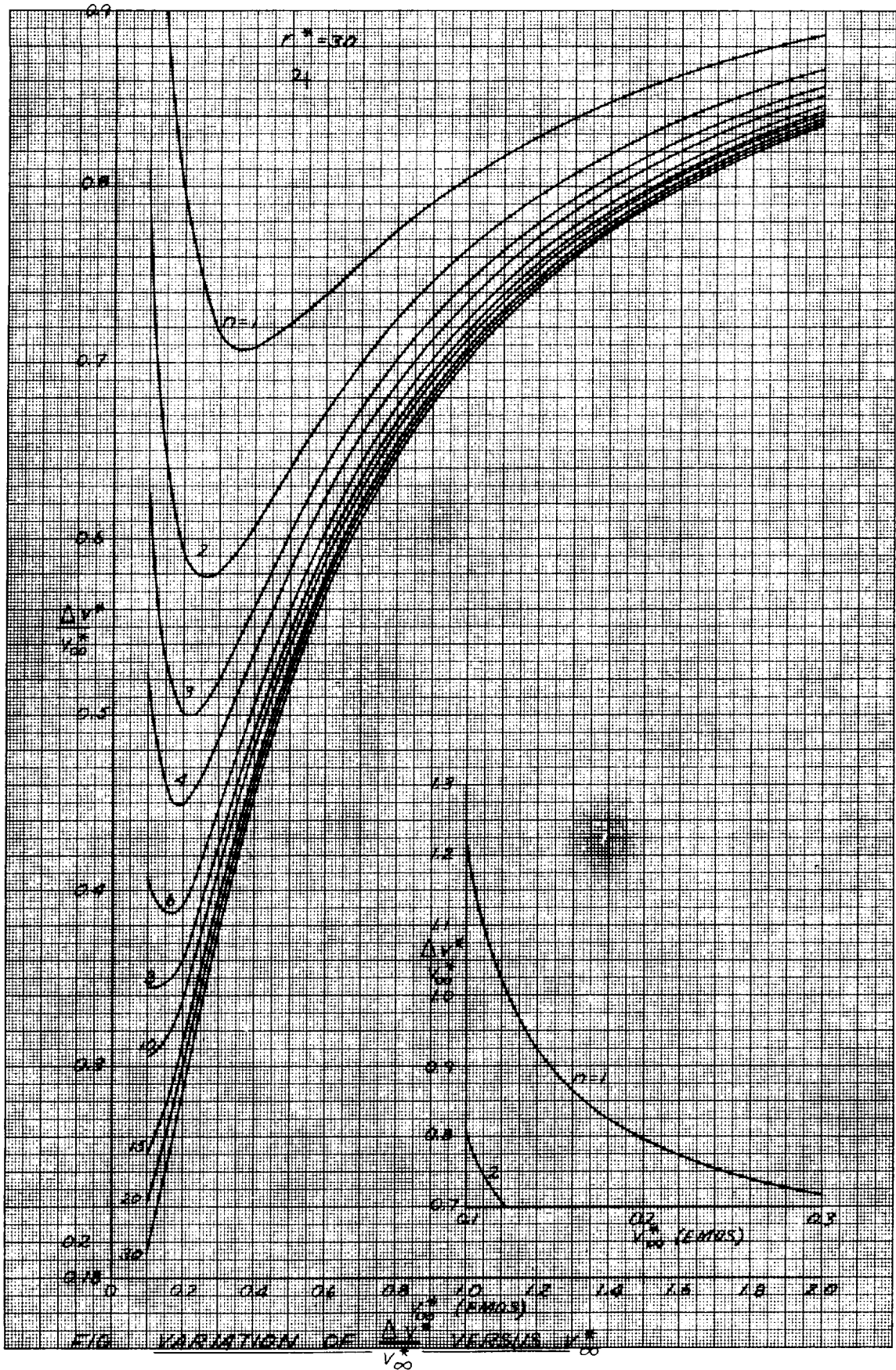
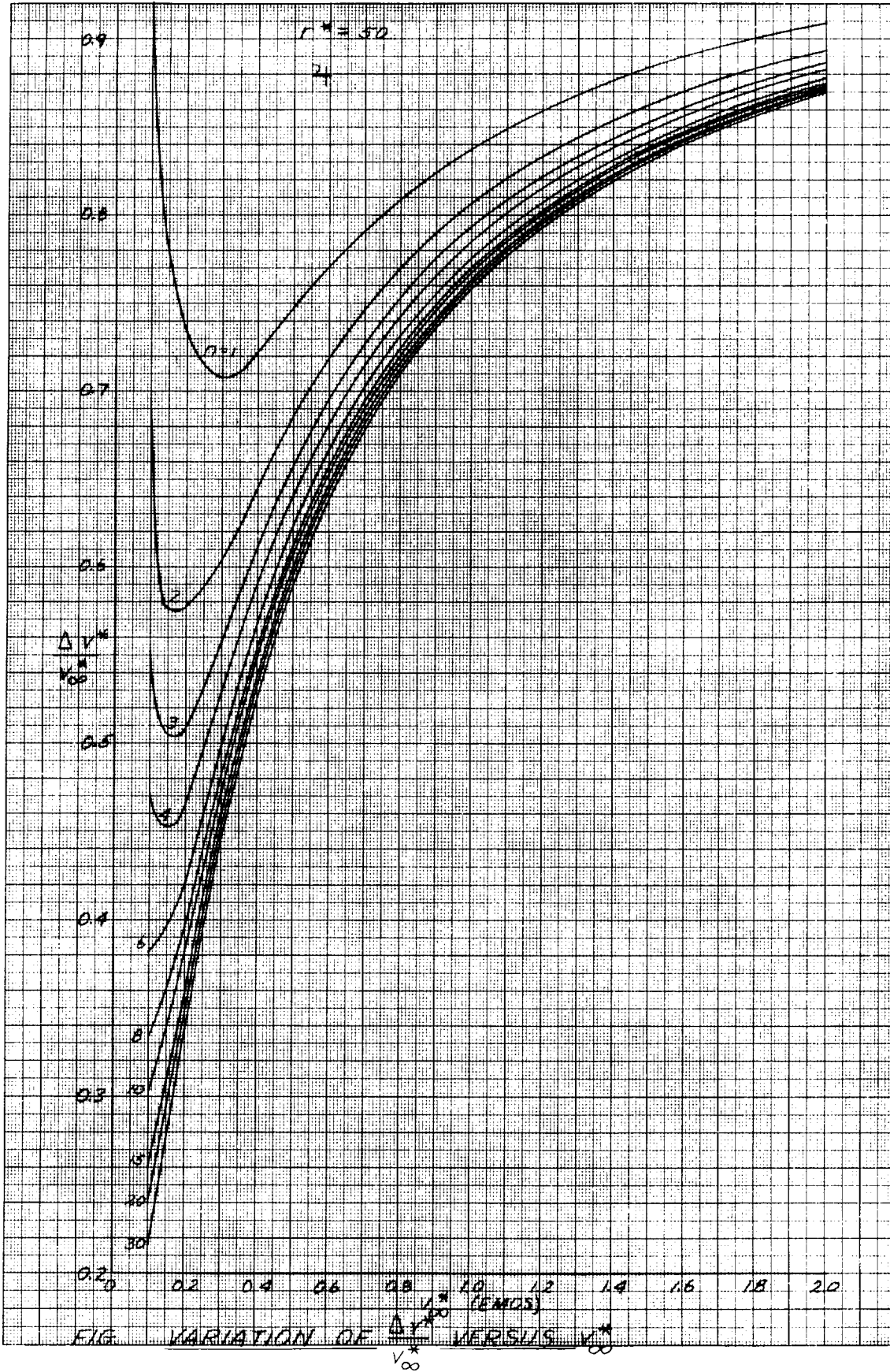
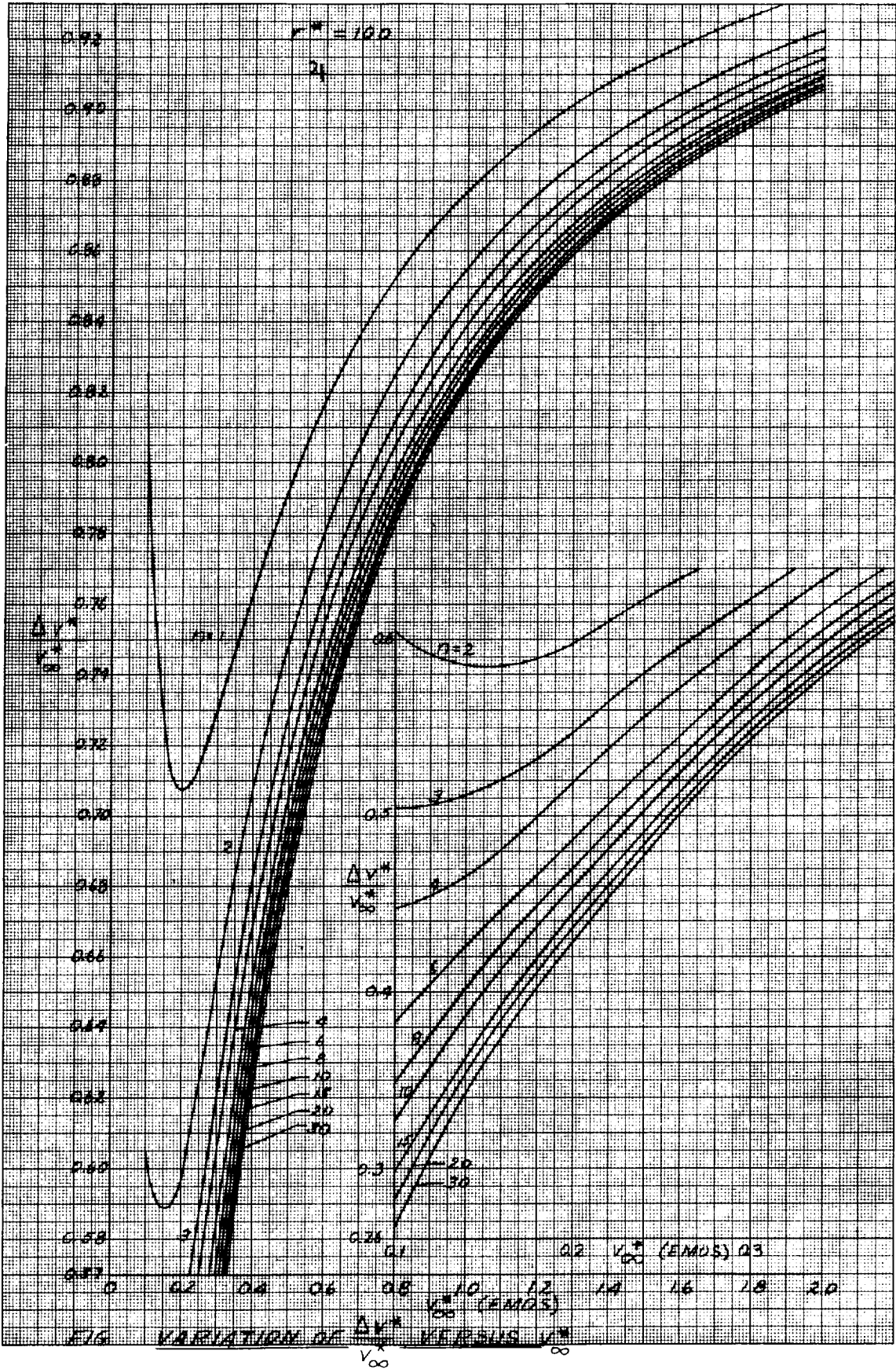


FIG. VARIATION OF $\frac{\Delta V^*}{V_{\infty}^*}$ VERSUS V_{∞}^*



14-650-47



64-51

64-065

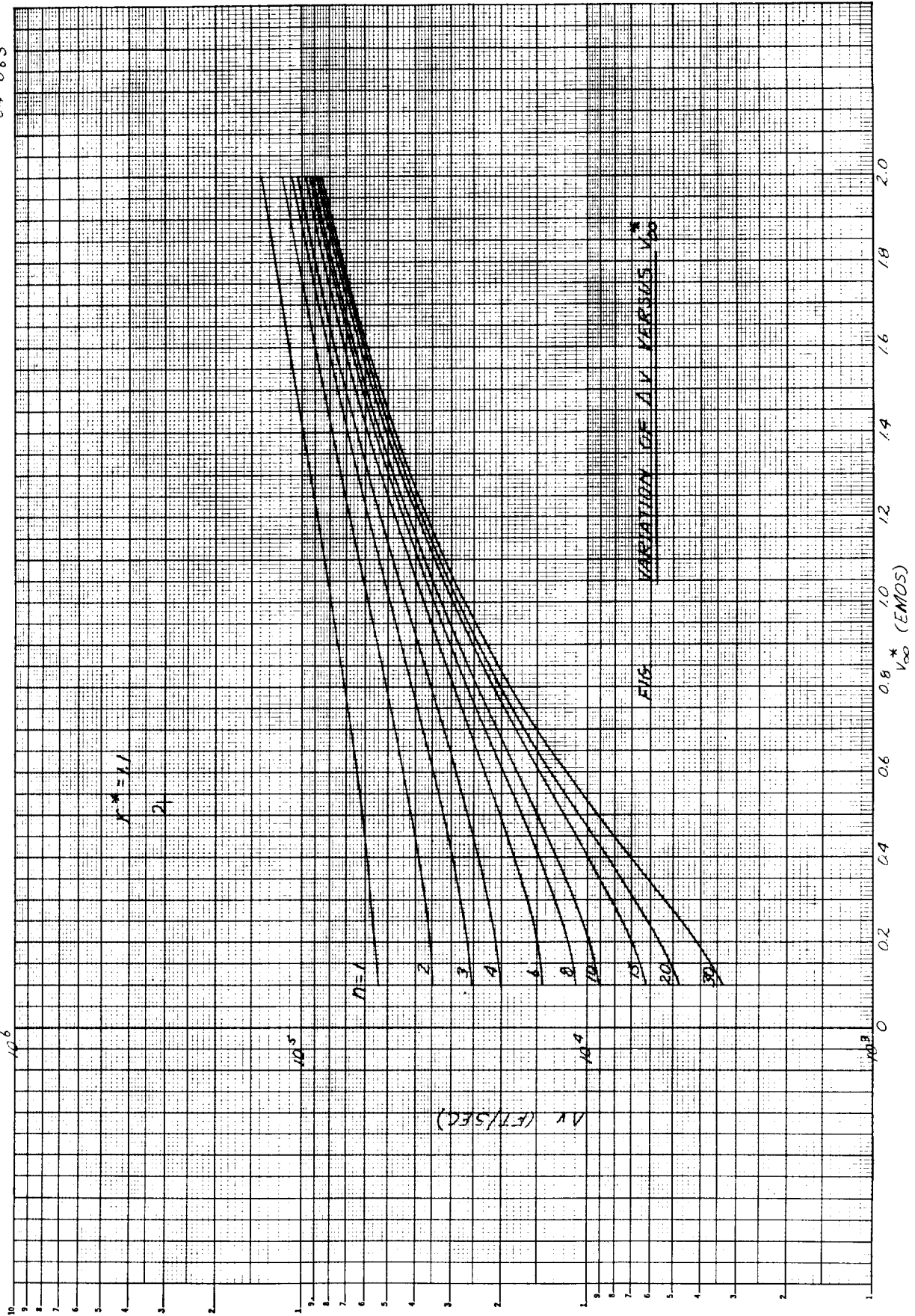
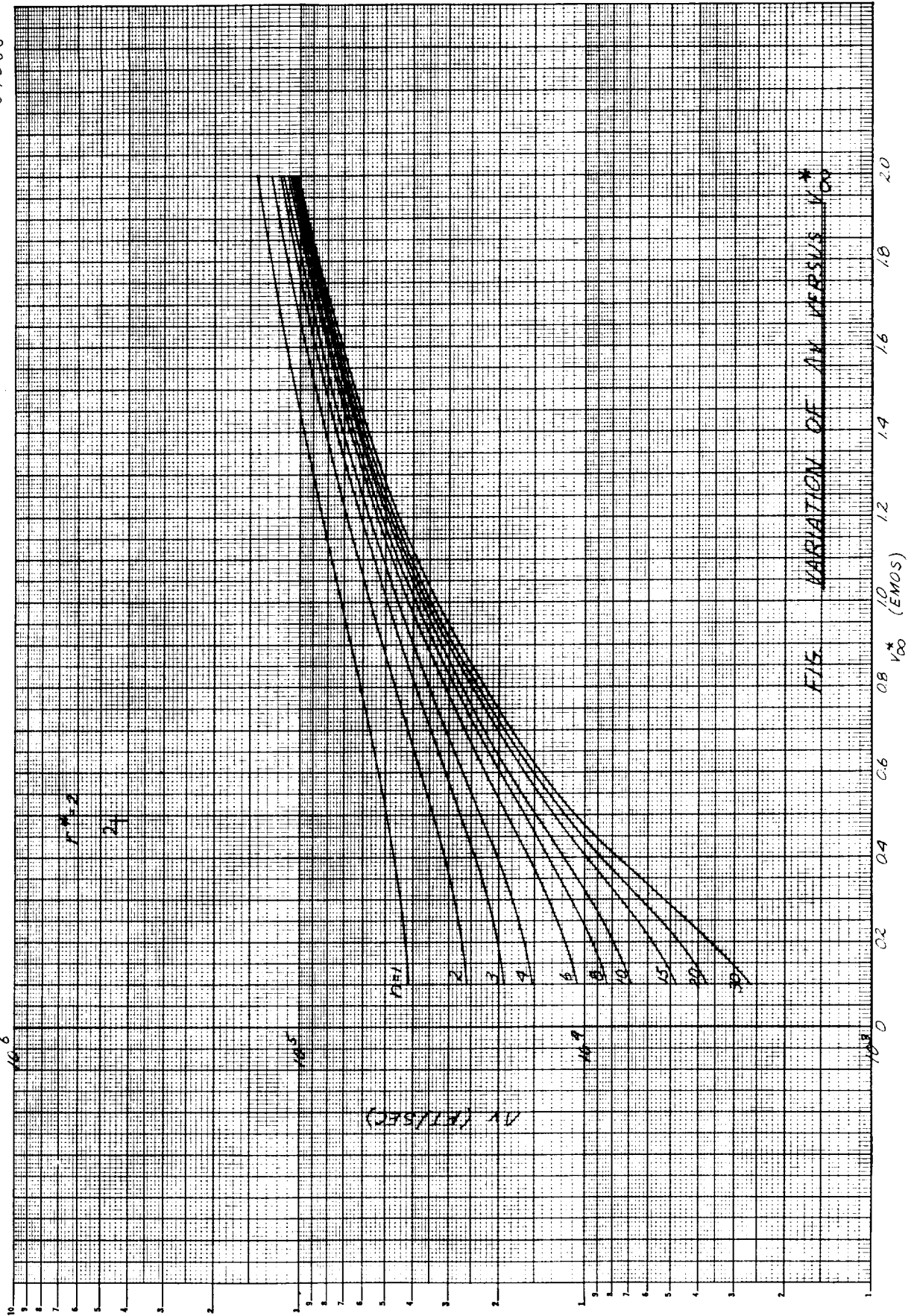
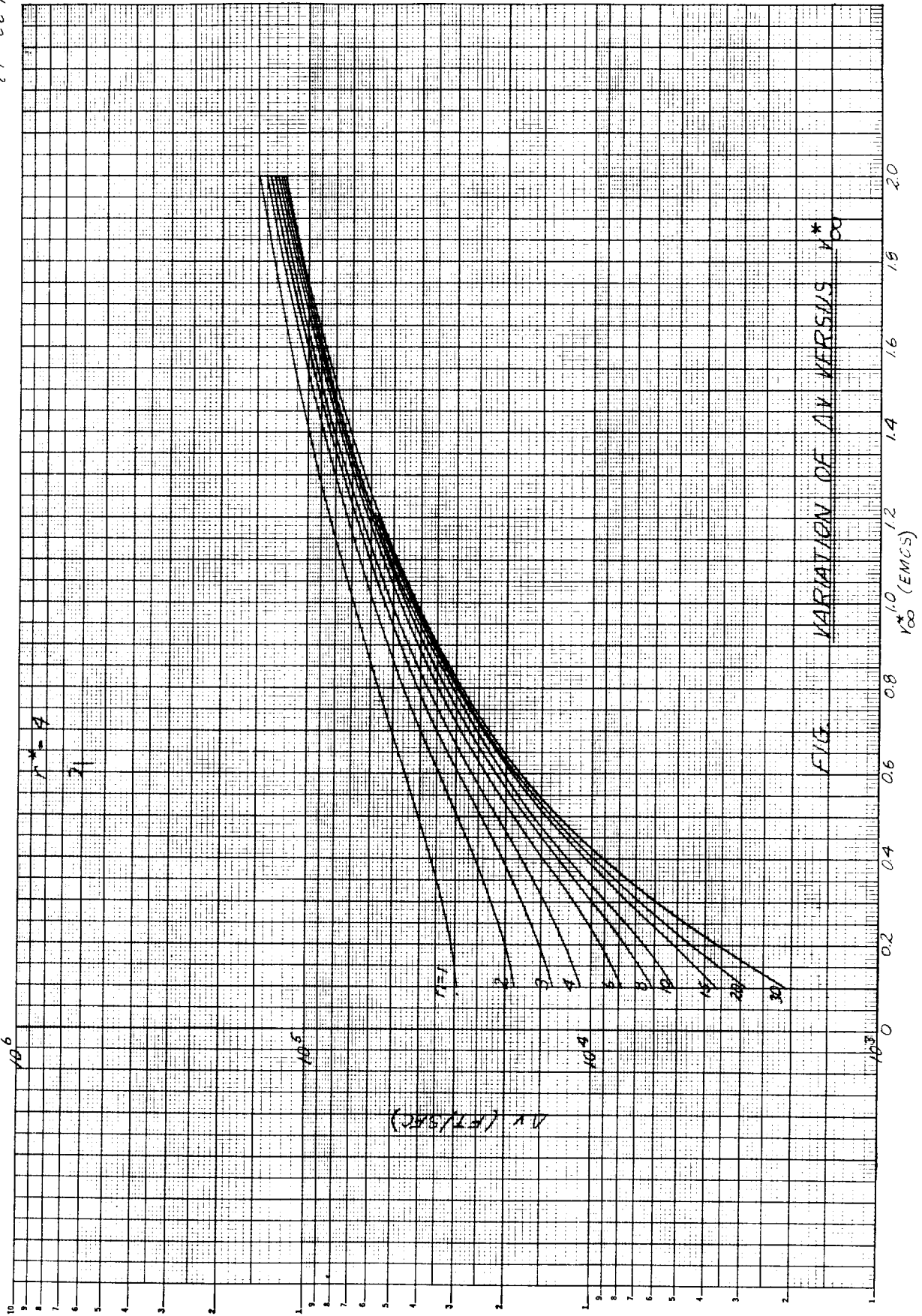


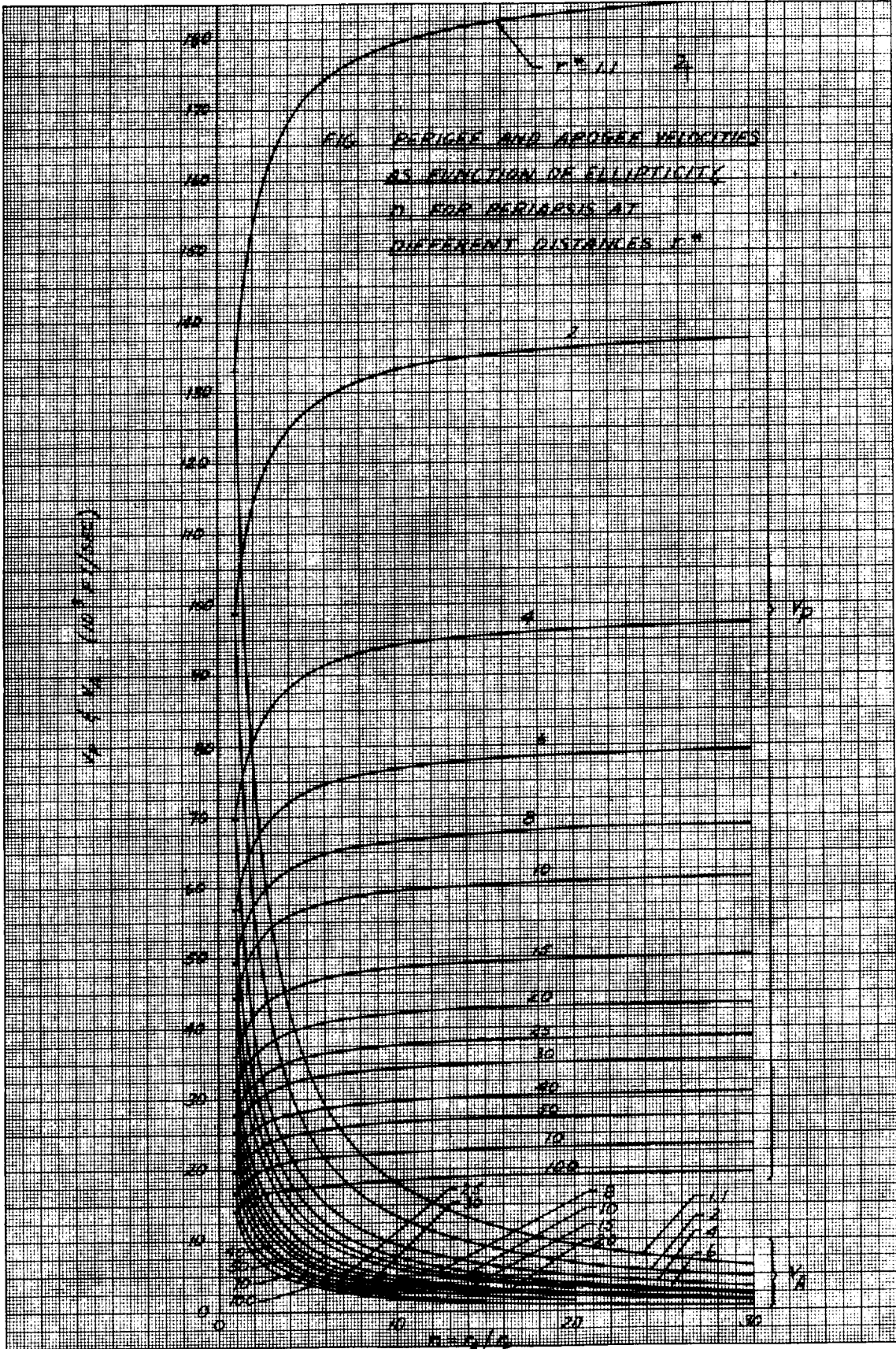
FIG. VARIATION OF AV VERSUS V_{∞}^*

64066



14-667





64-039

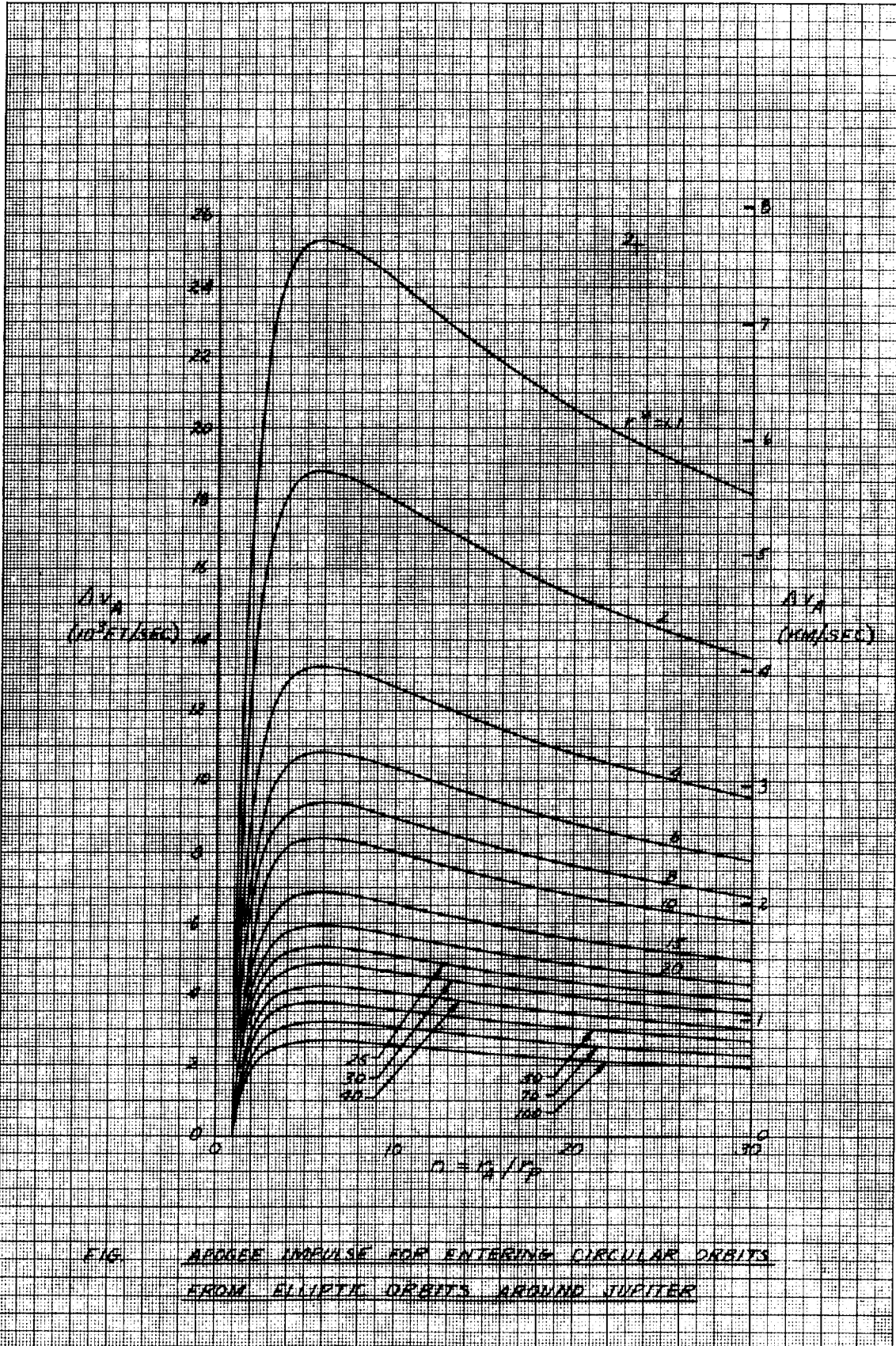
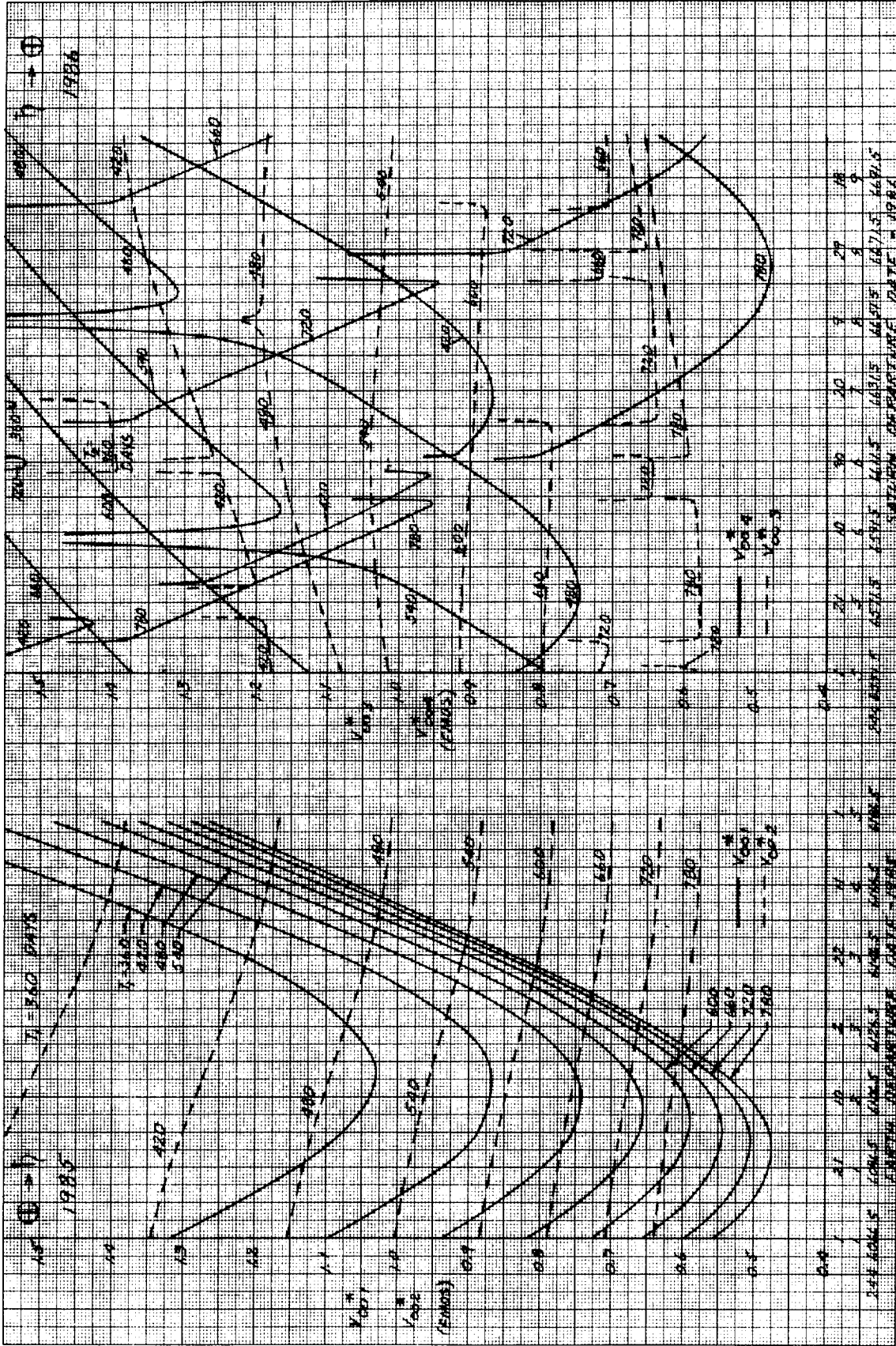


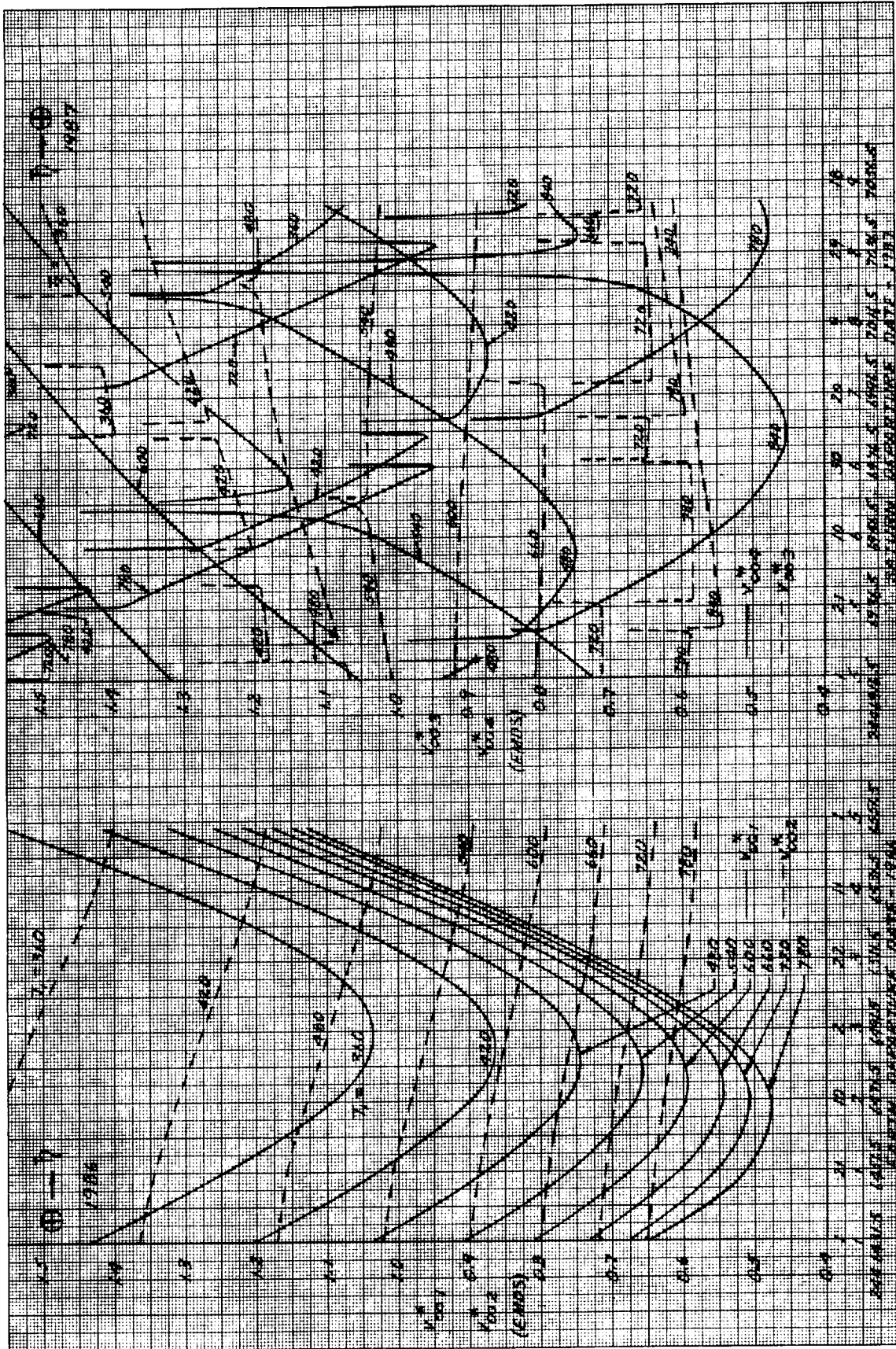
FIG. ABOGEE IMPULSE FOR ENTERING CIRCULAR ORBITS
FROM ELLIPTIC ORBITS AROUND JUPITER

64-03X

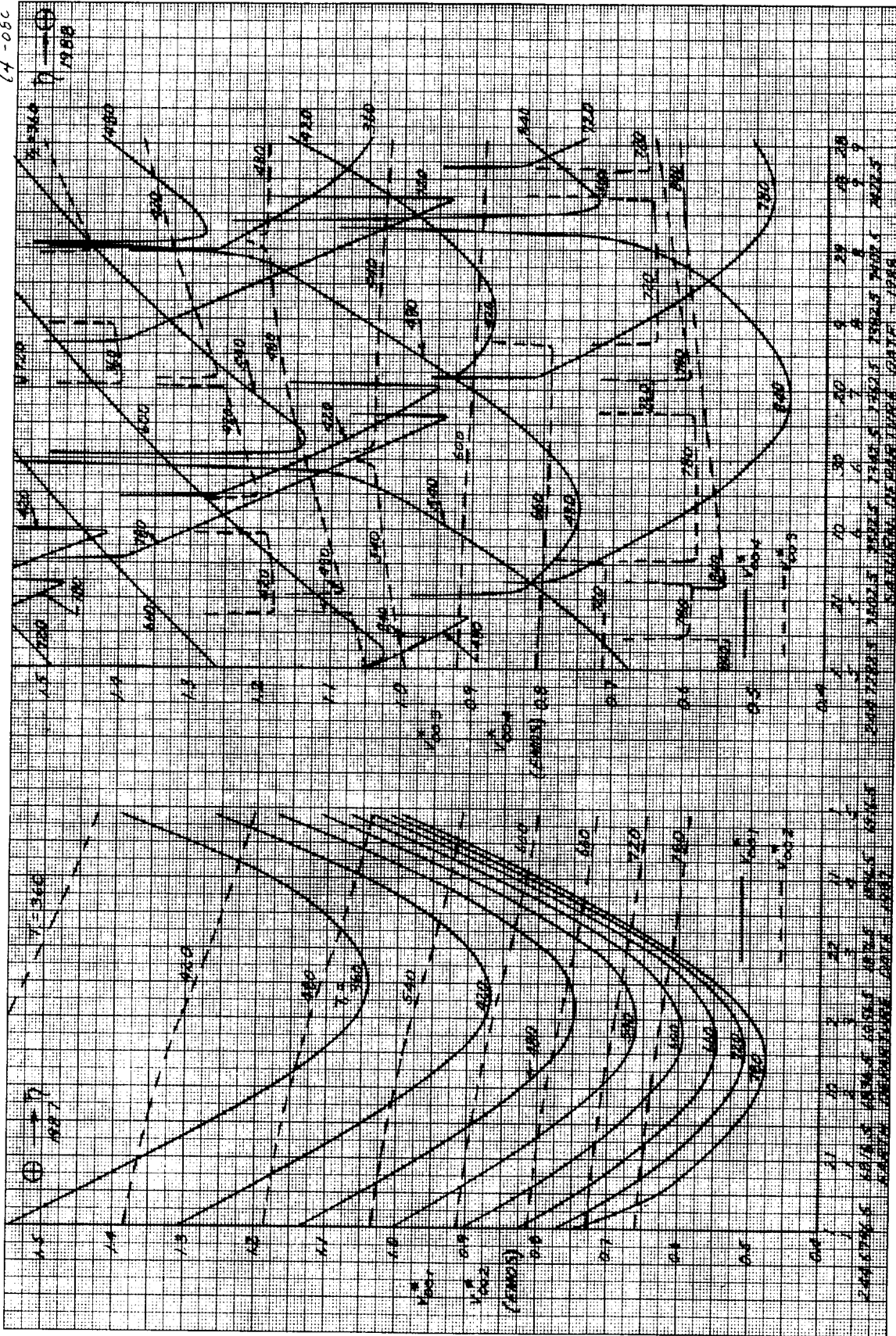
PART VI SATURN

14-078

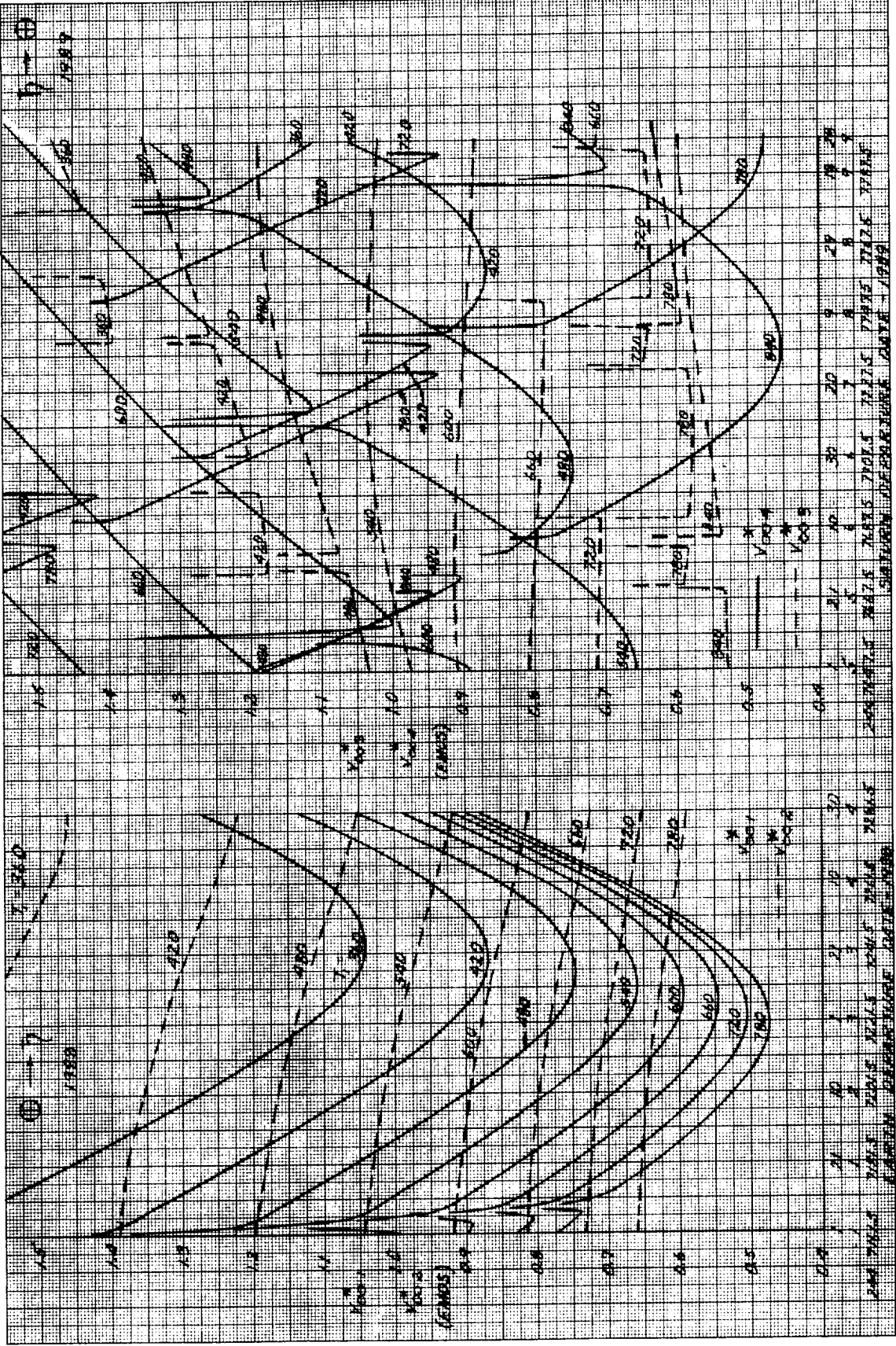




64-05c



187-13



62-683

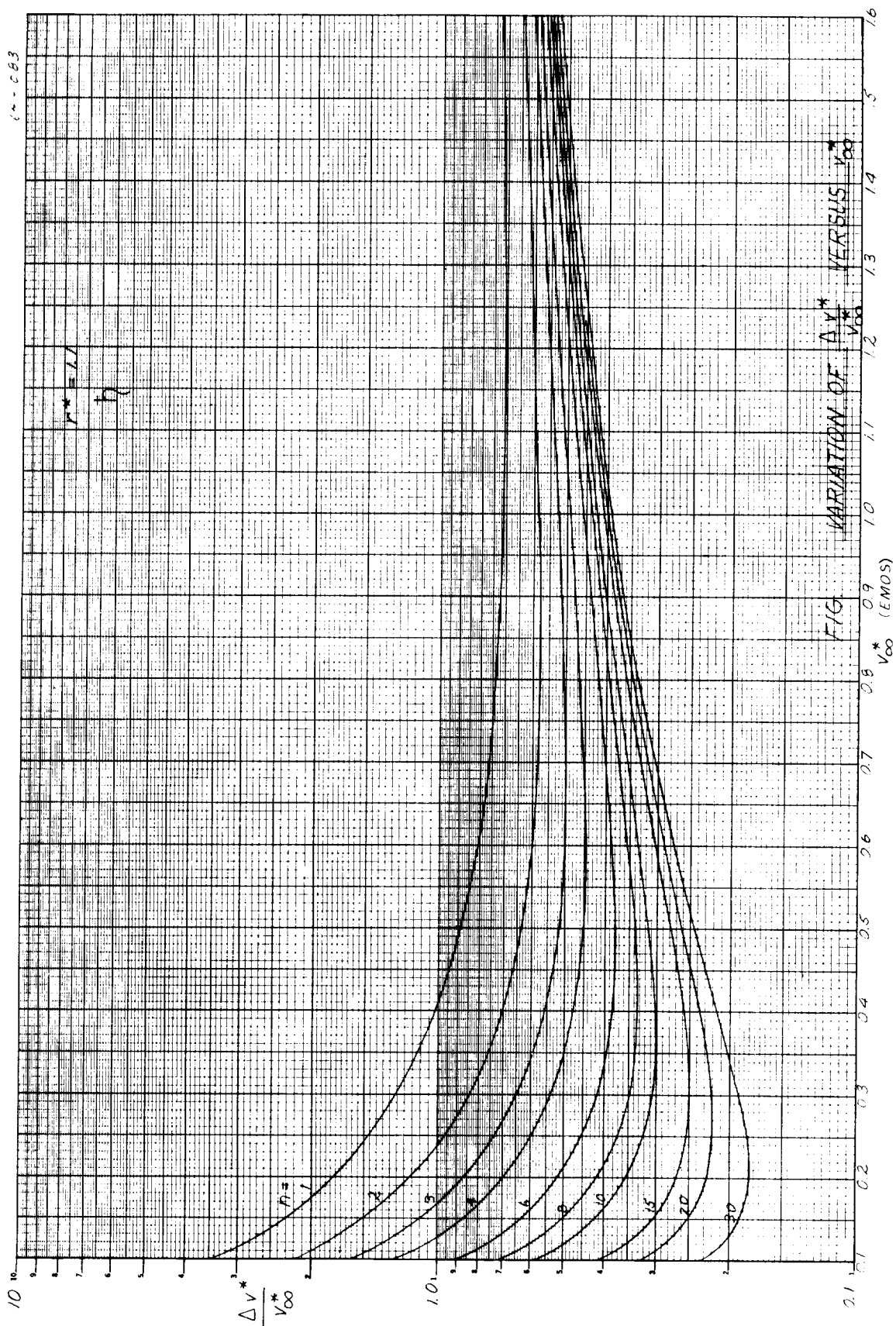
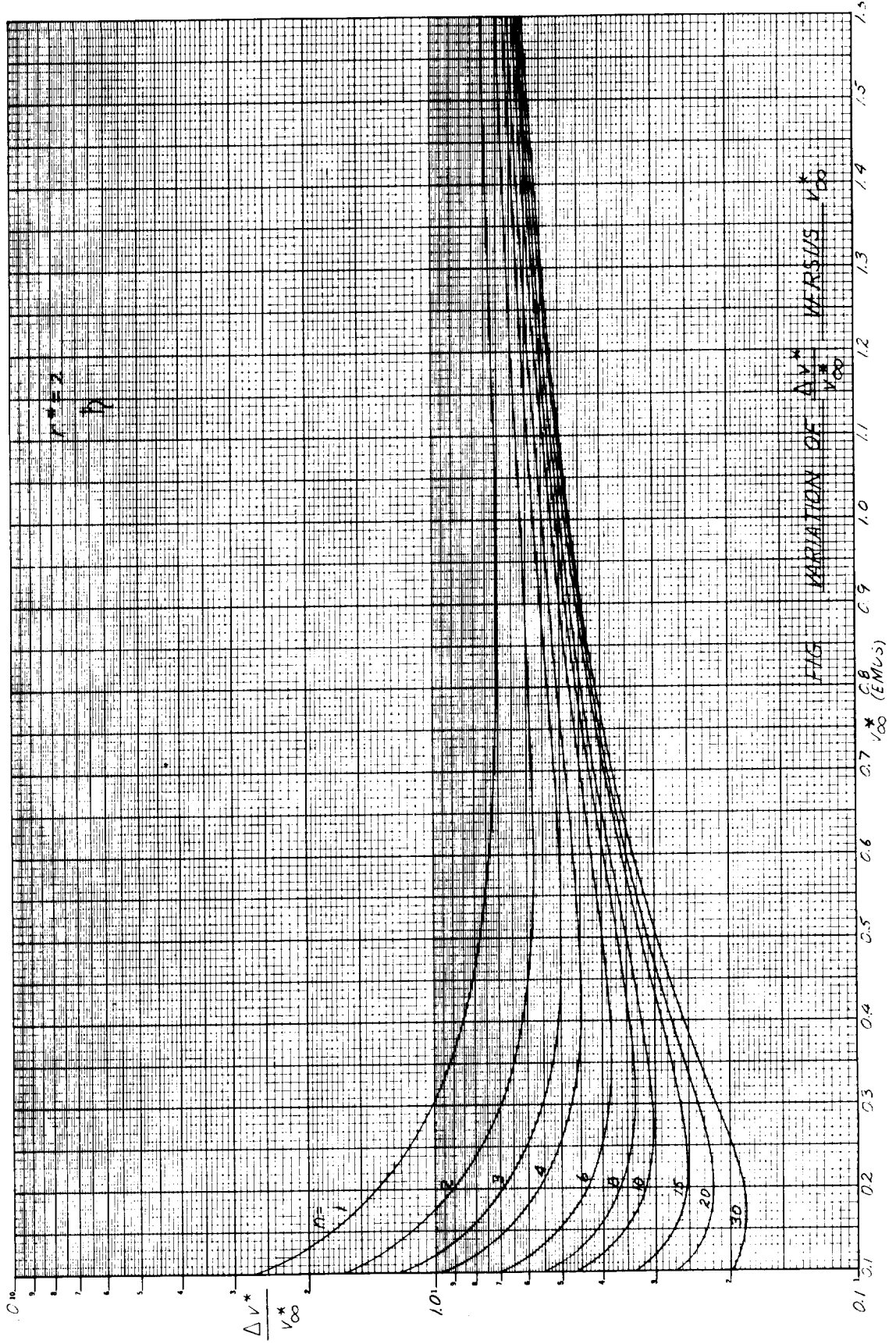


FIG.

VARIATION OF $\frac{\Delta V^*}{V_{\infty}^*}$ VERSUS V_{∞}^*

(EMOS)

64-084



64-085

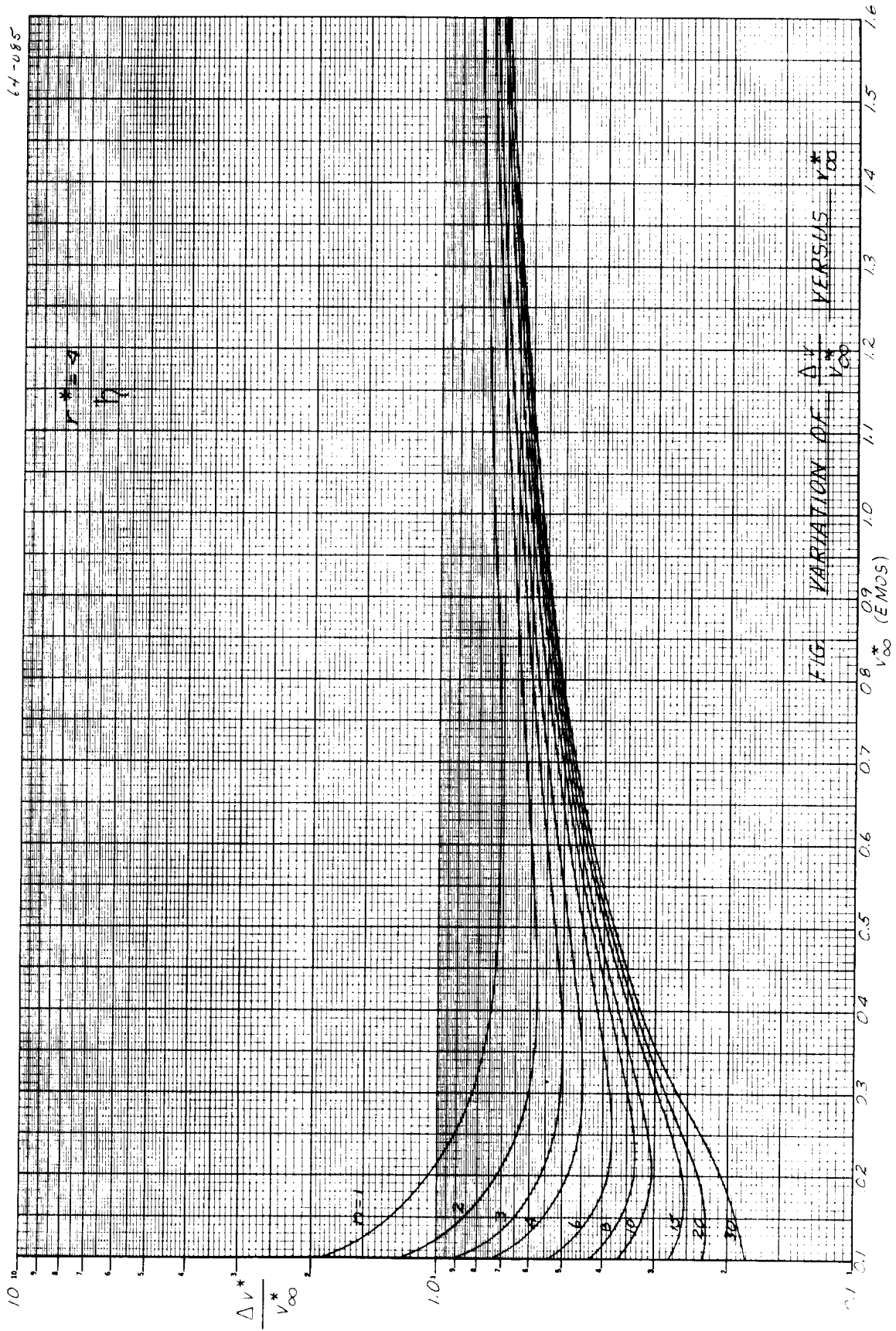


FIG. VARIATION OF $\frac{\Delta V^*}{V_{\infty}^*}$ VERSUS V_{∞}^*

64-086

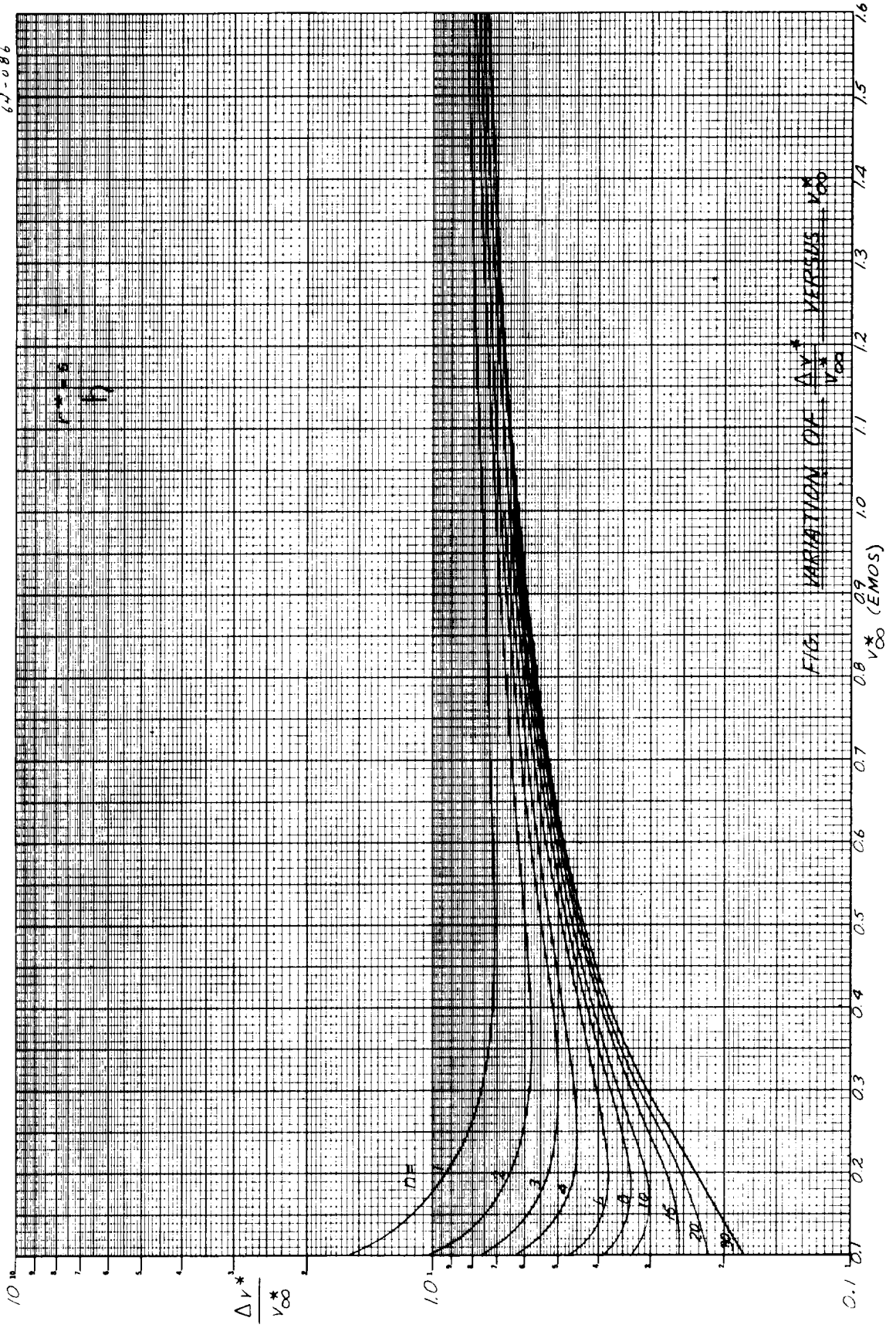


FIG. 10 VARIATION OF $\frac{\Delta V^*}{V_{\infty}^*}$ VERSUS V_{∞}^* (EMOS)

64-027

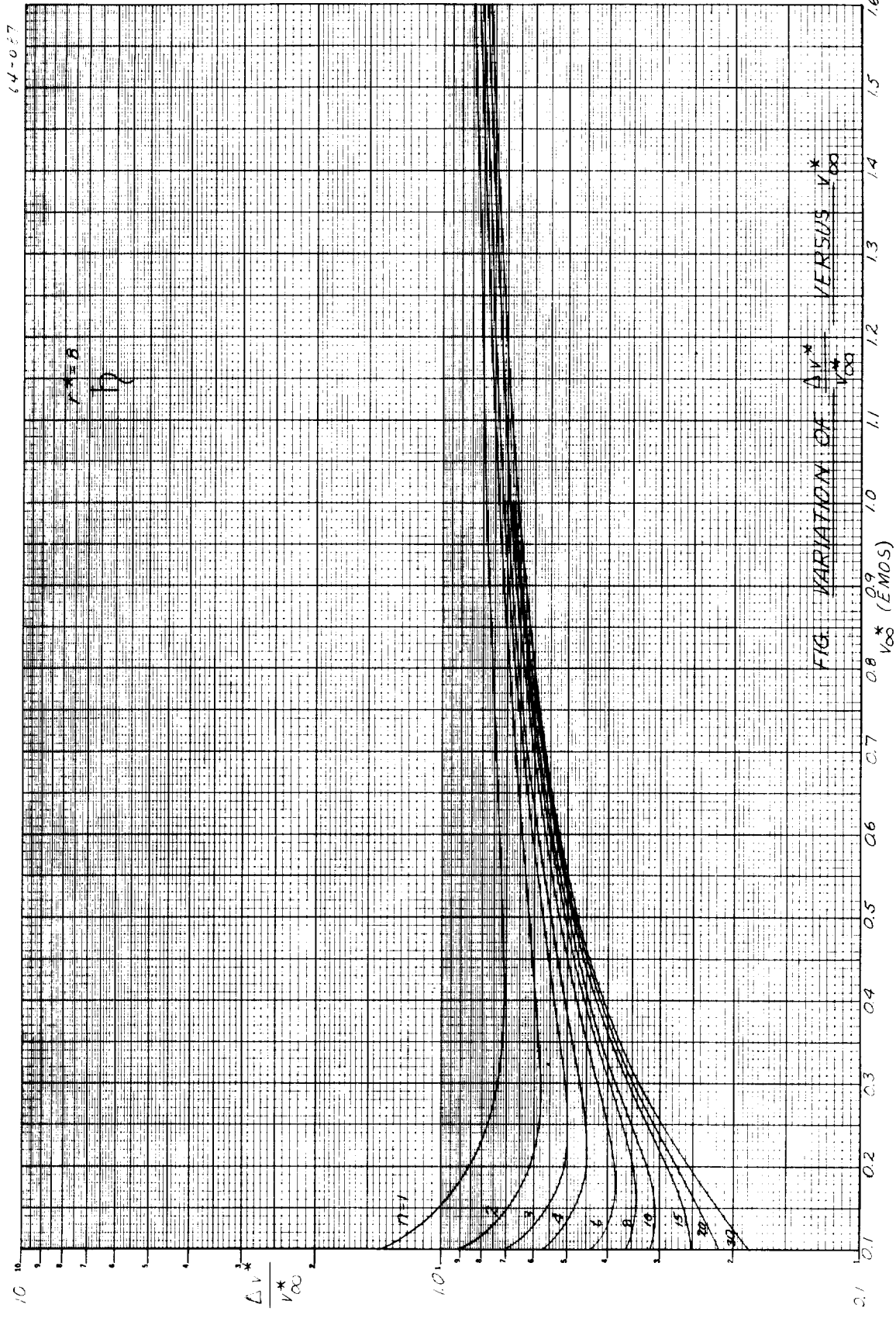
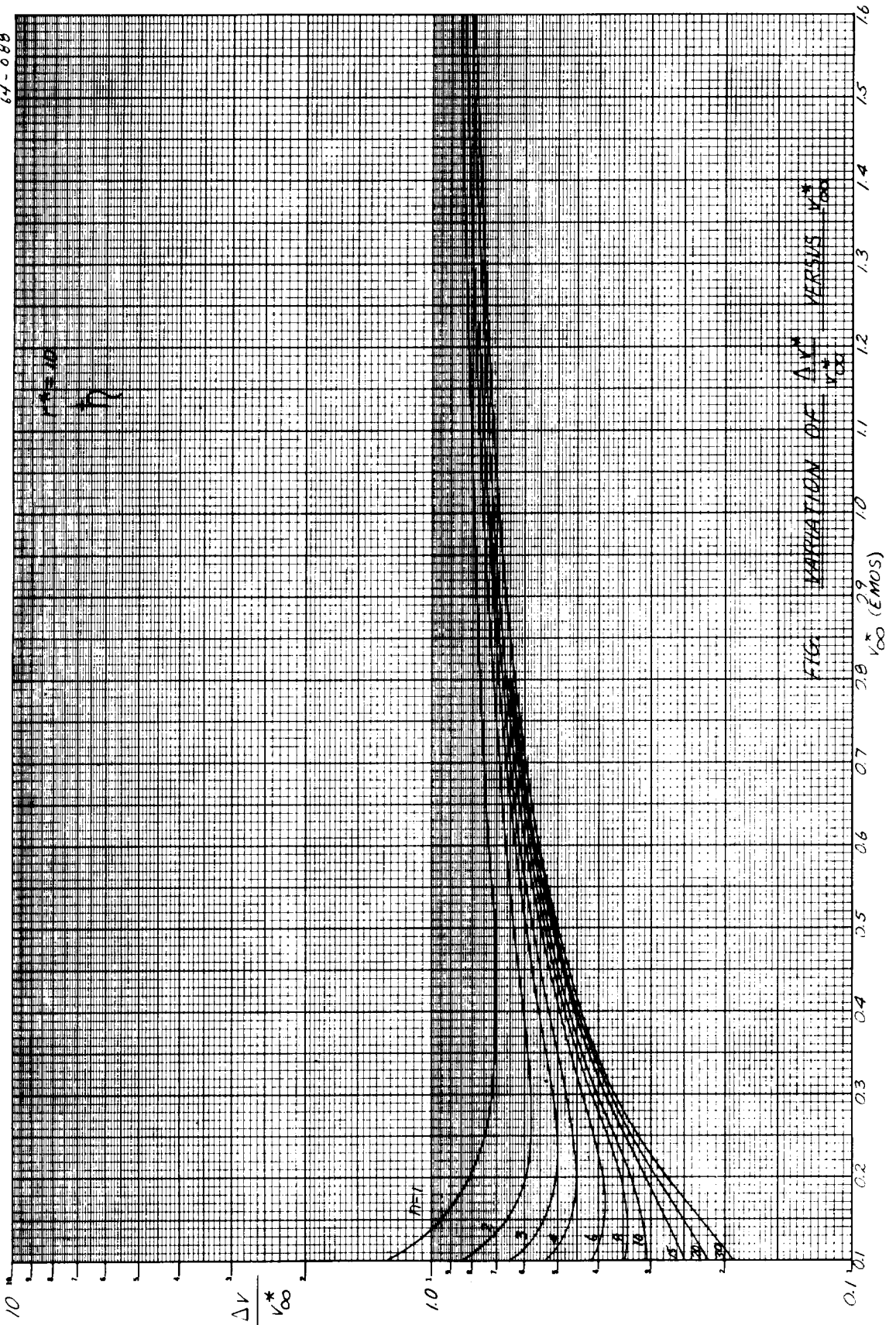
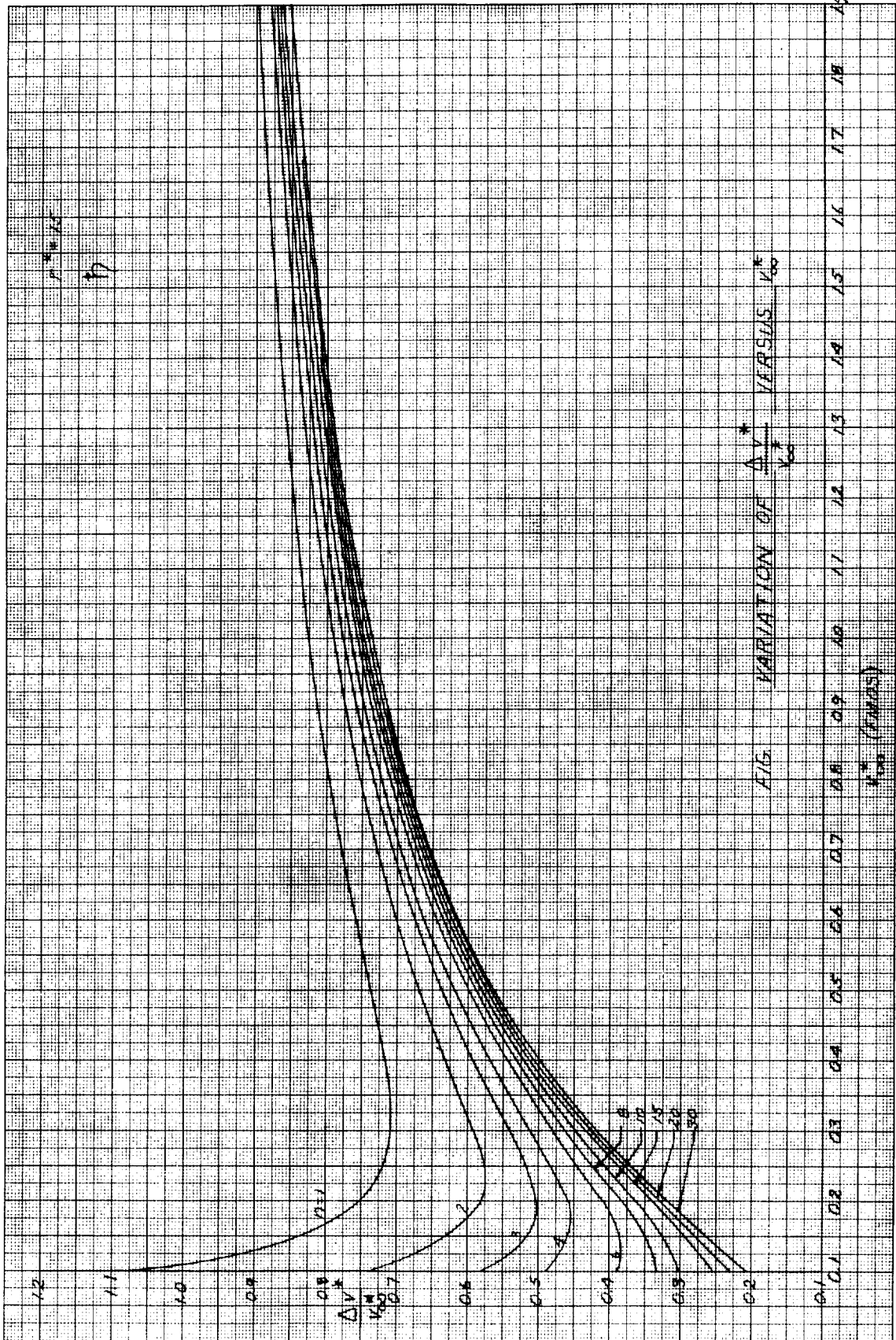


FIG. VARIATION OF $\frac{\Delta V^*}{V_{\infty}^*}$ VERSUS V_{∞}^* (EMOS)

64-088



62-117



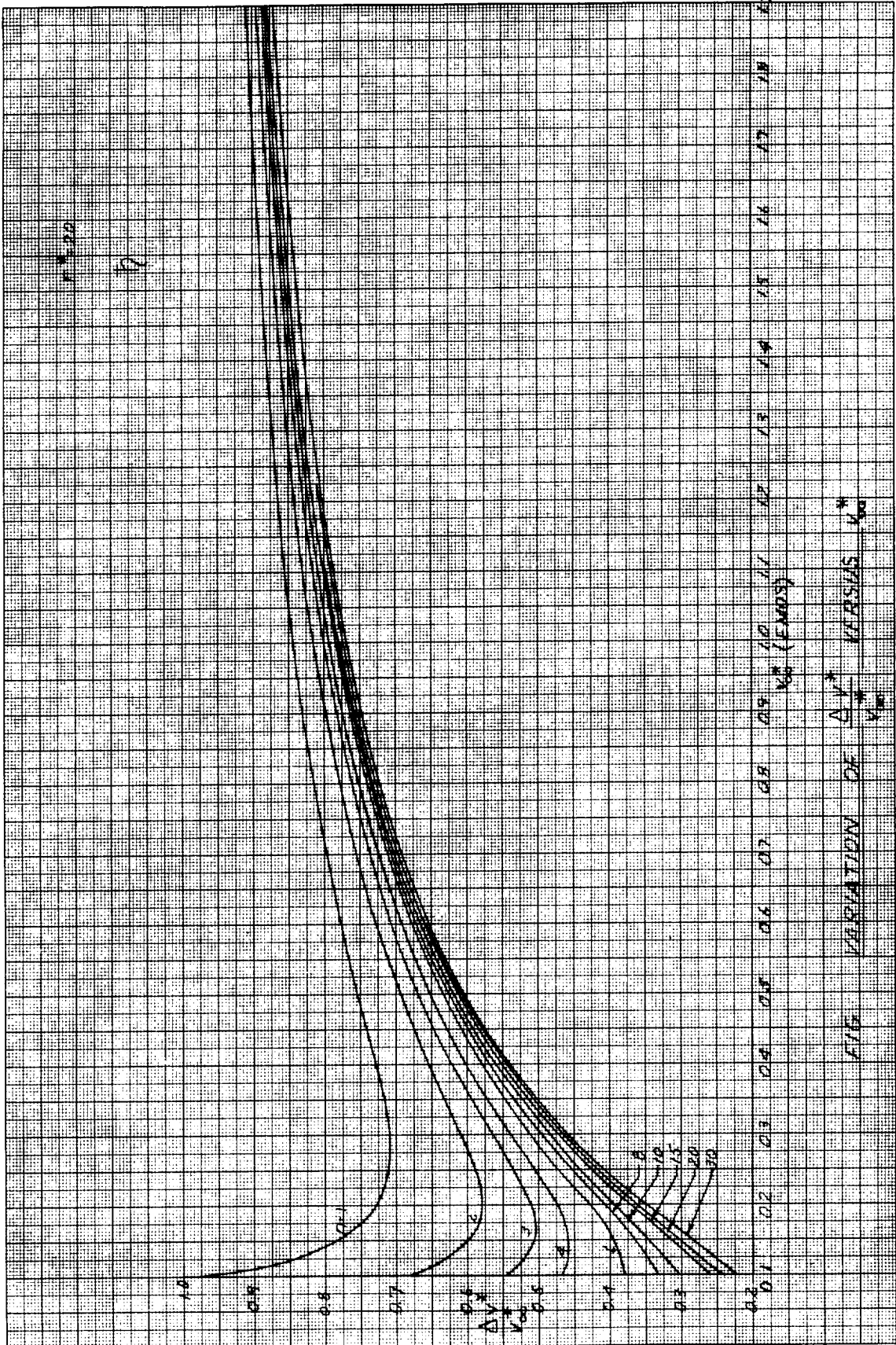


FIG. VARIATION OF $\frac{\Delta V}{V_0}$ VERSUS $\frac{V}{V_0}$

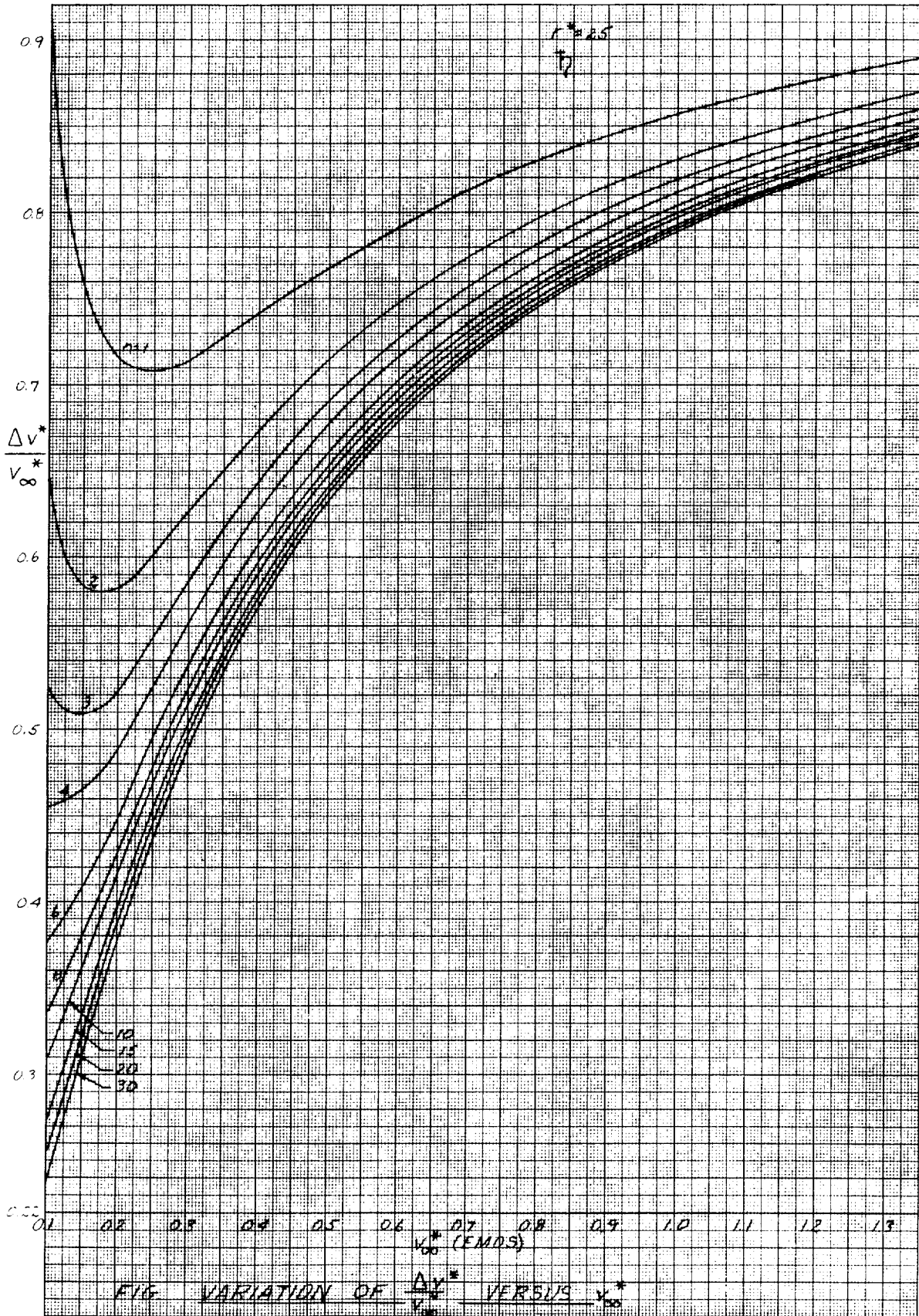


FIG VARIATION OF $\frac{\Delta V^*}{V_\infty^*}$ VERSUS V_∞^*

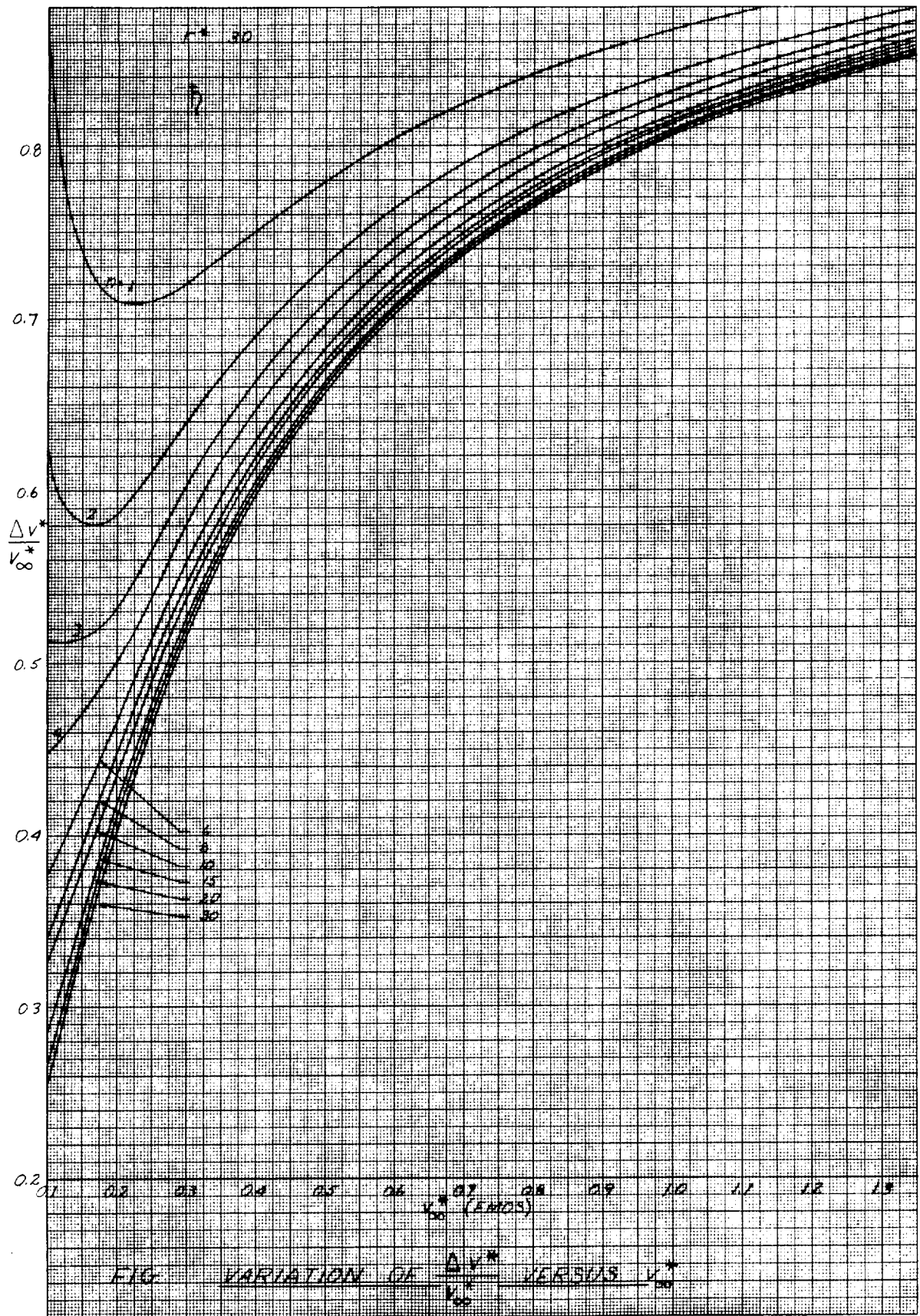
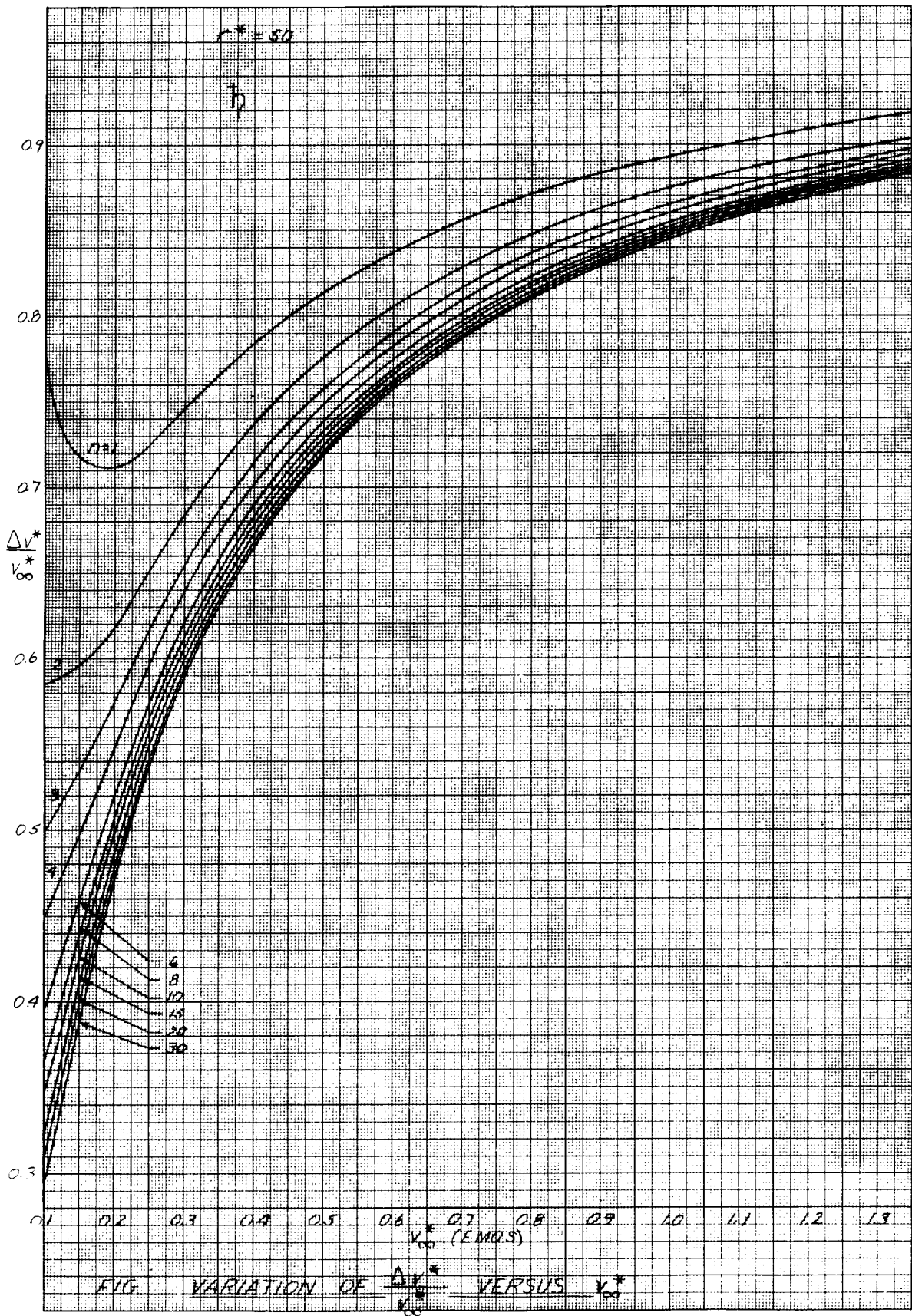


FIG VARIATION OF $\frac{\Delta V^*}{V_\infty^*}$ VERSUS V_∞^*



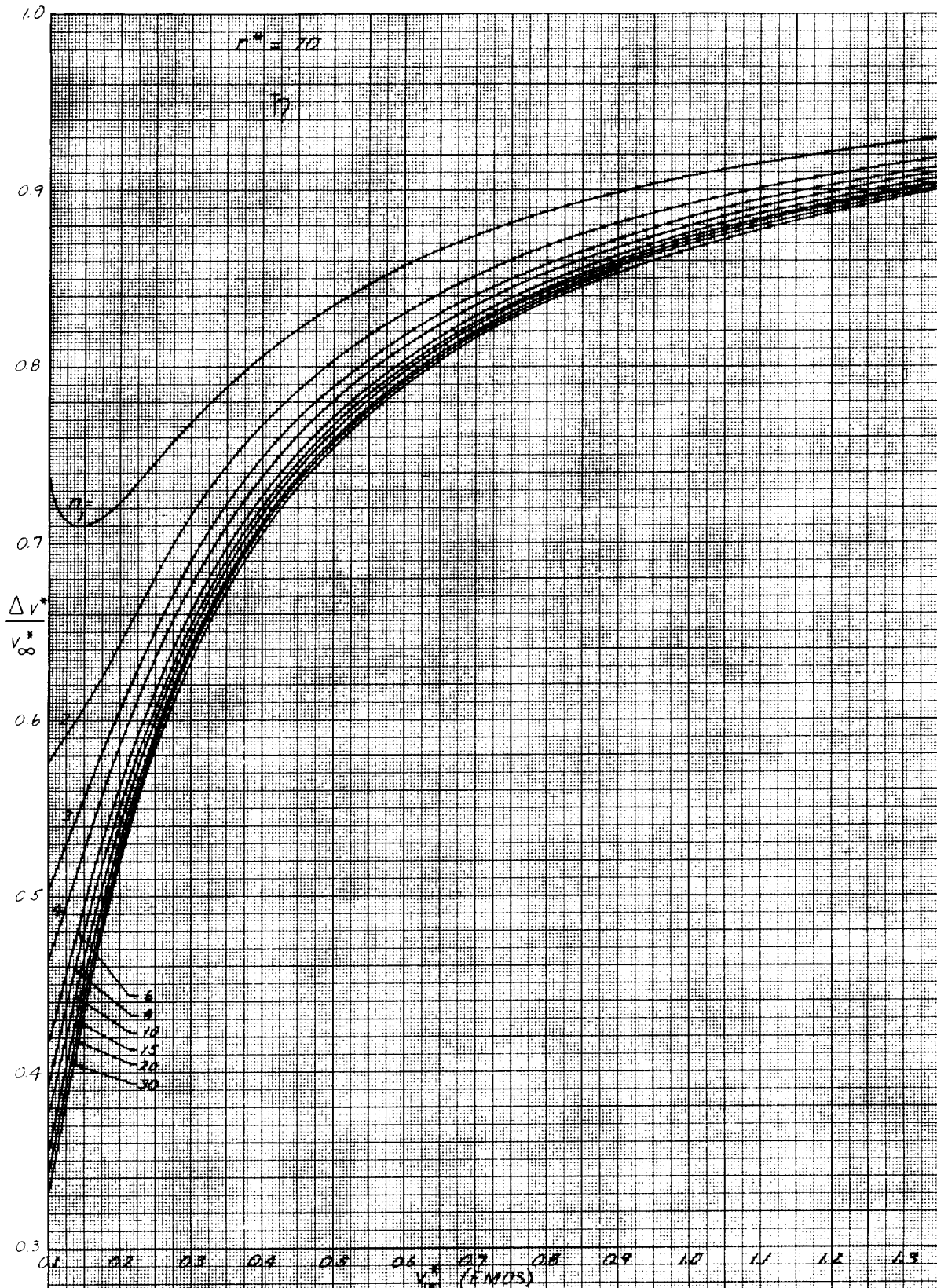
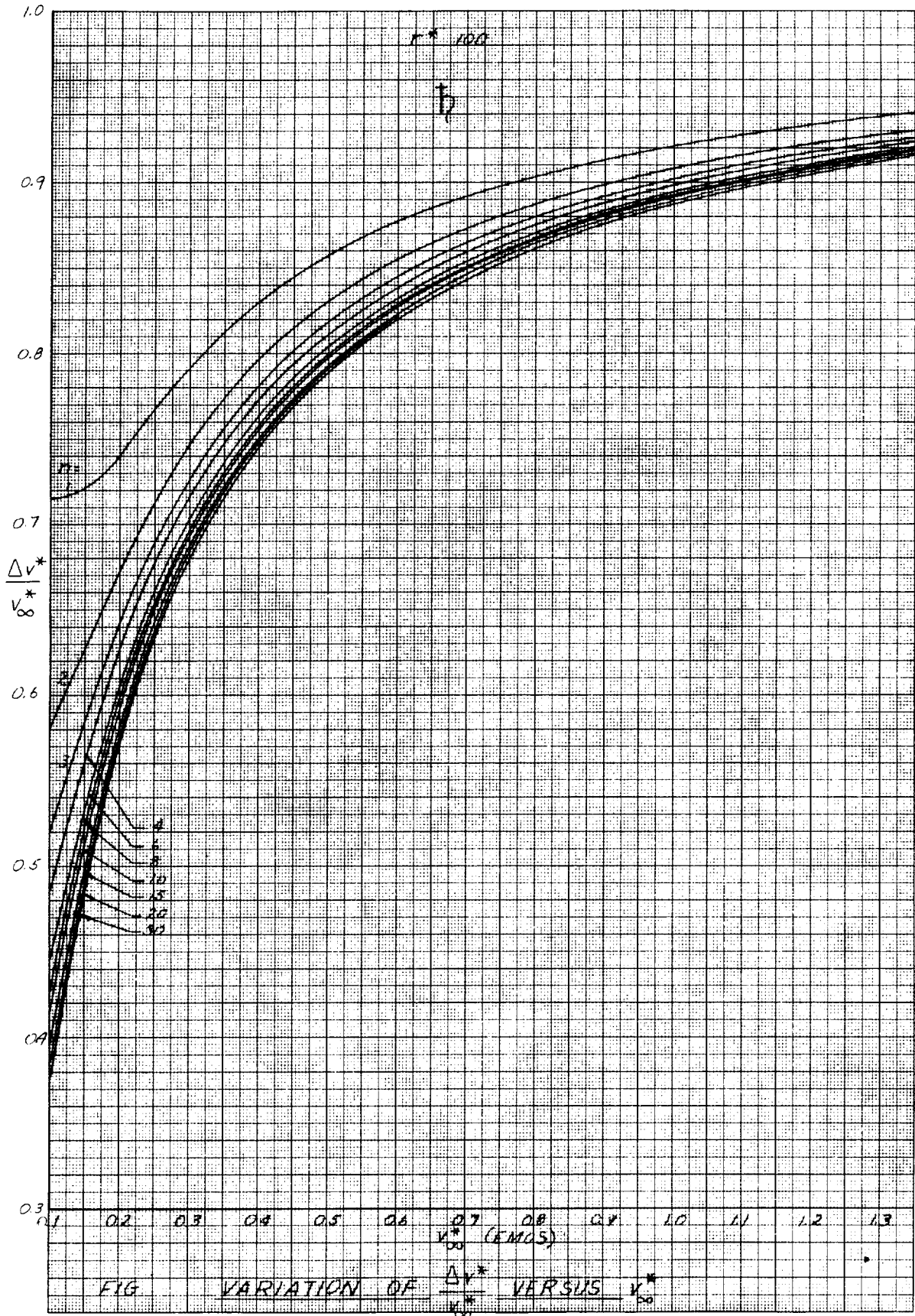
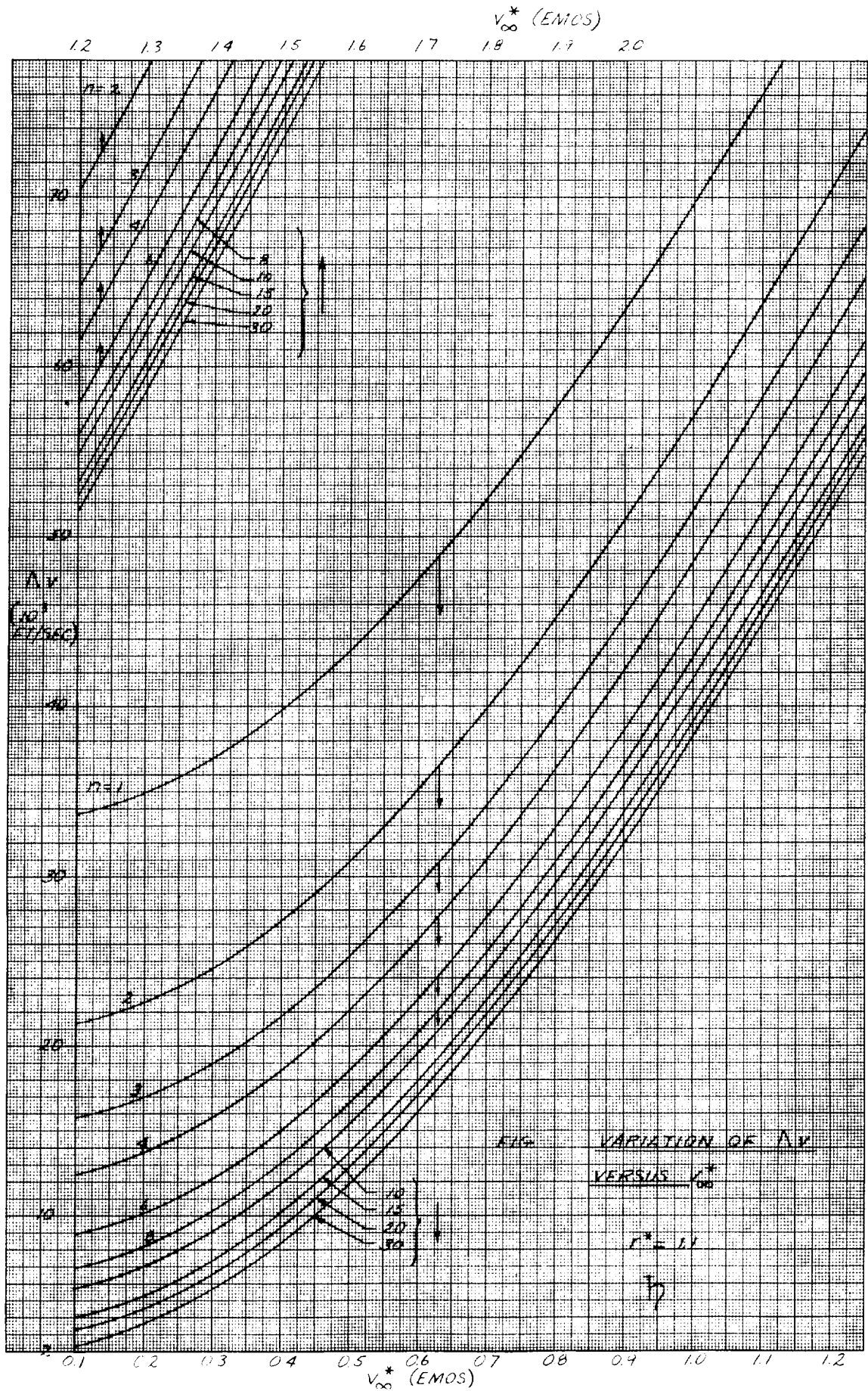
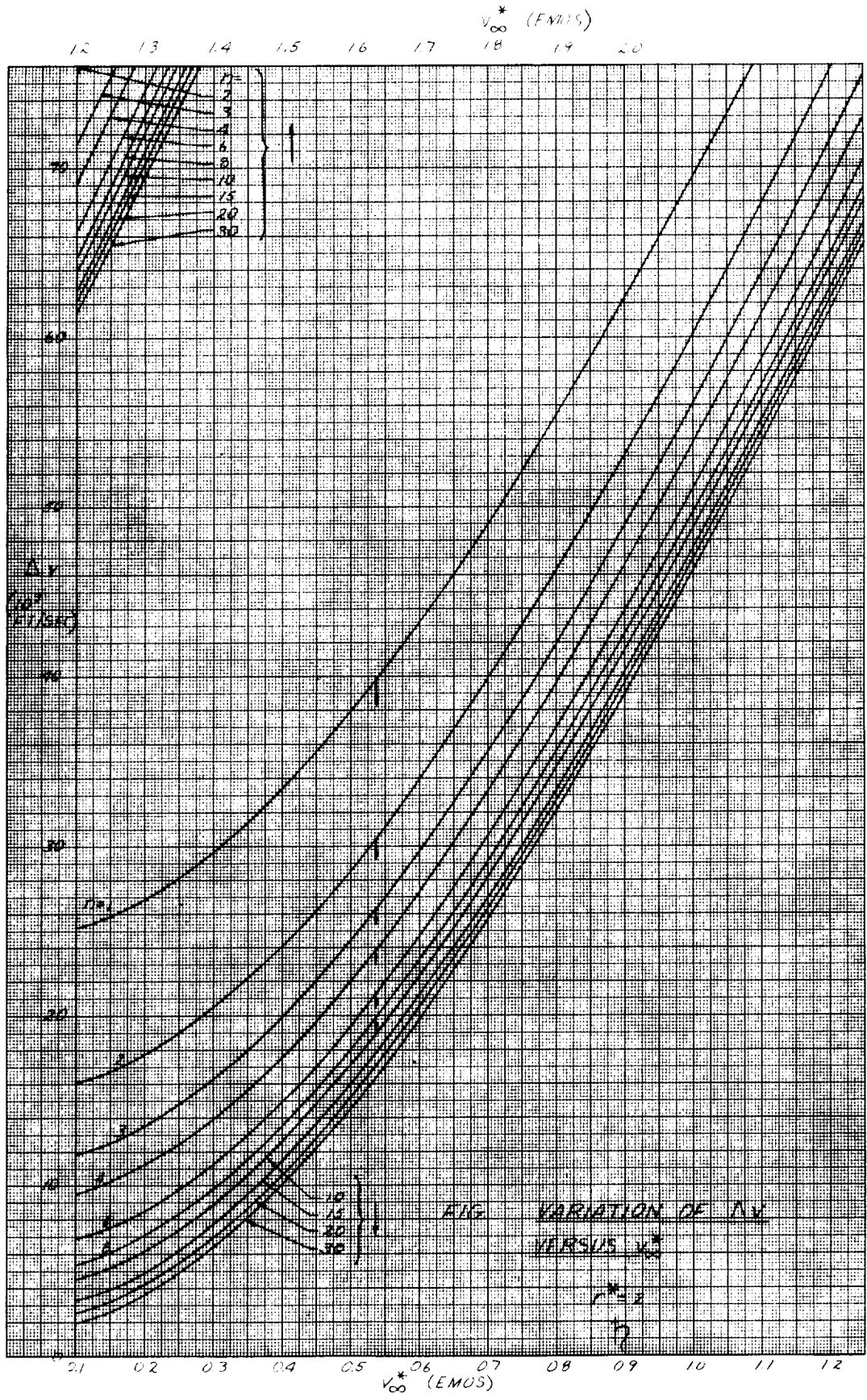


FIG. VARIATION OF $\frac{\Delta v^*}{v_\infty^*}$ VERSUS v_∞^*







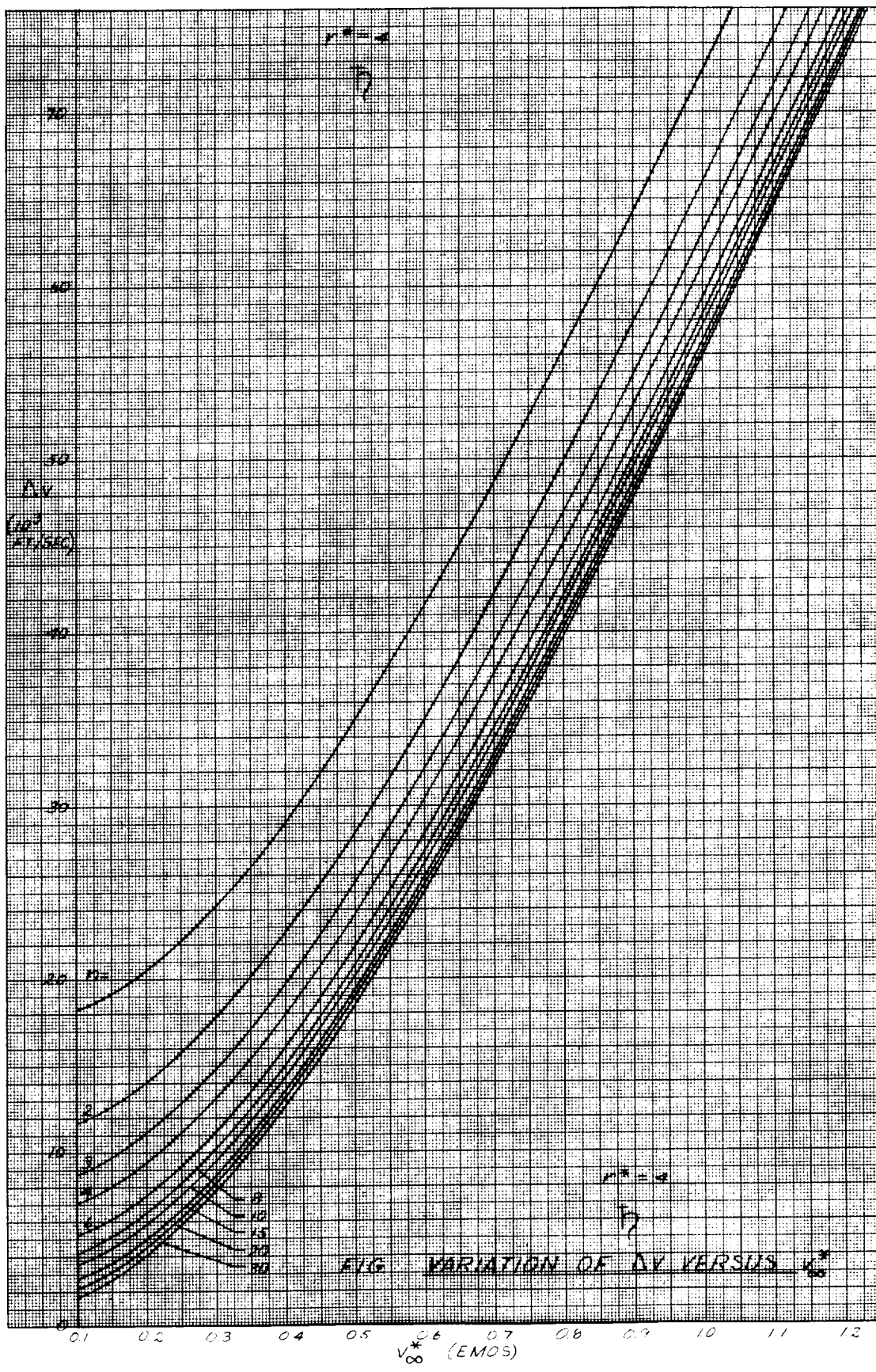
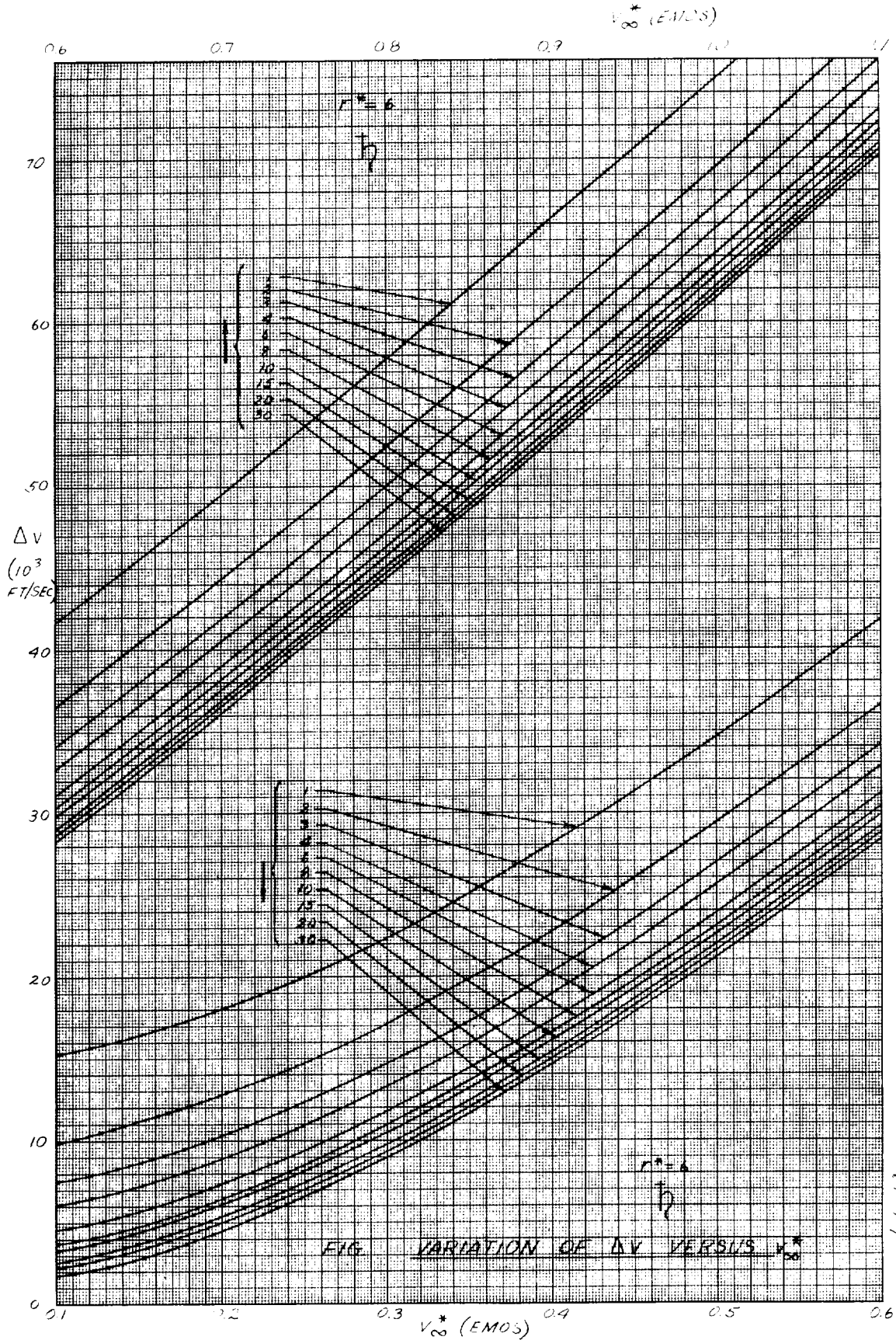


FIG VARIATION OF A_v VERSUS V_{∞}^*



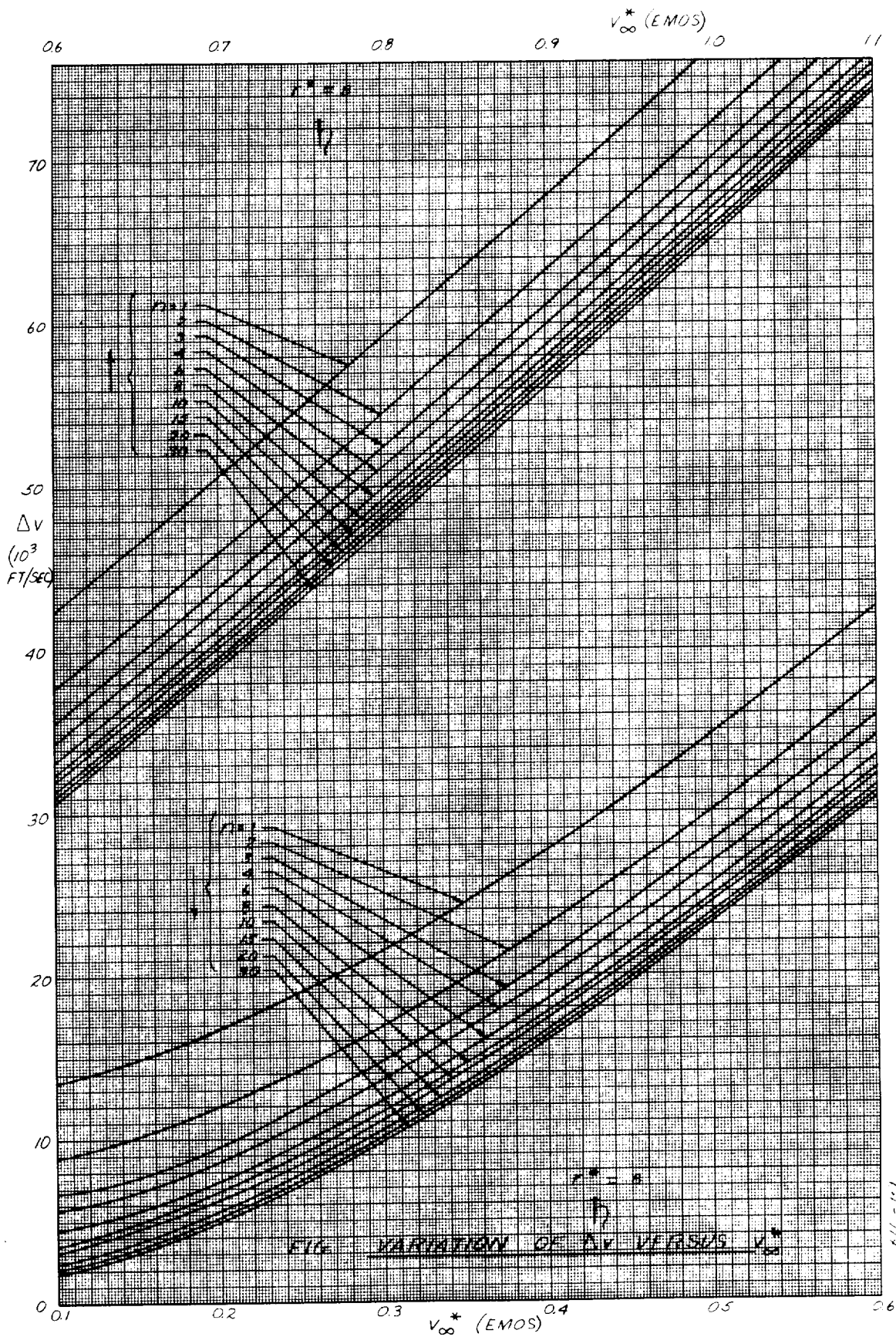
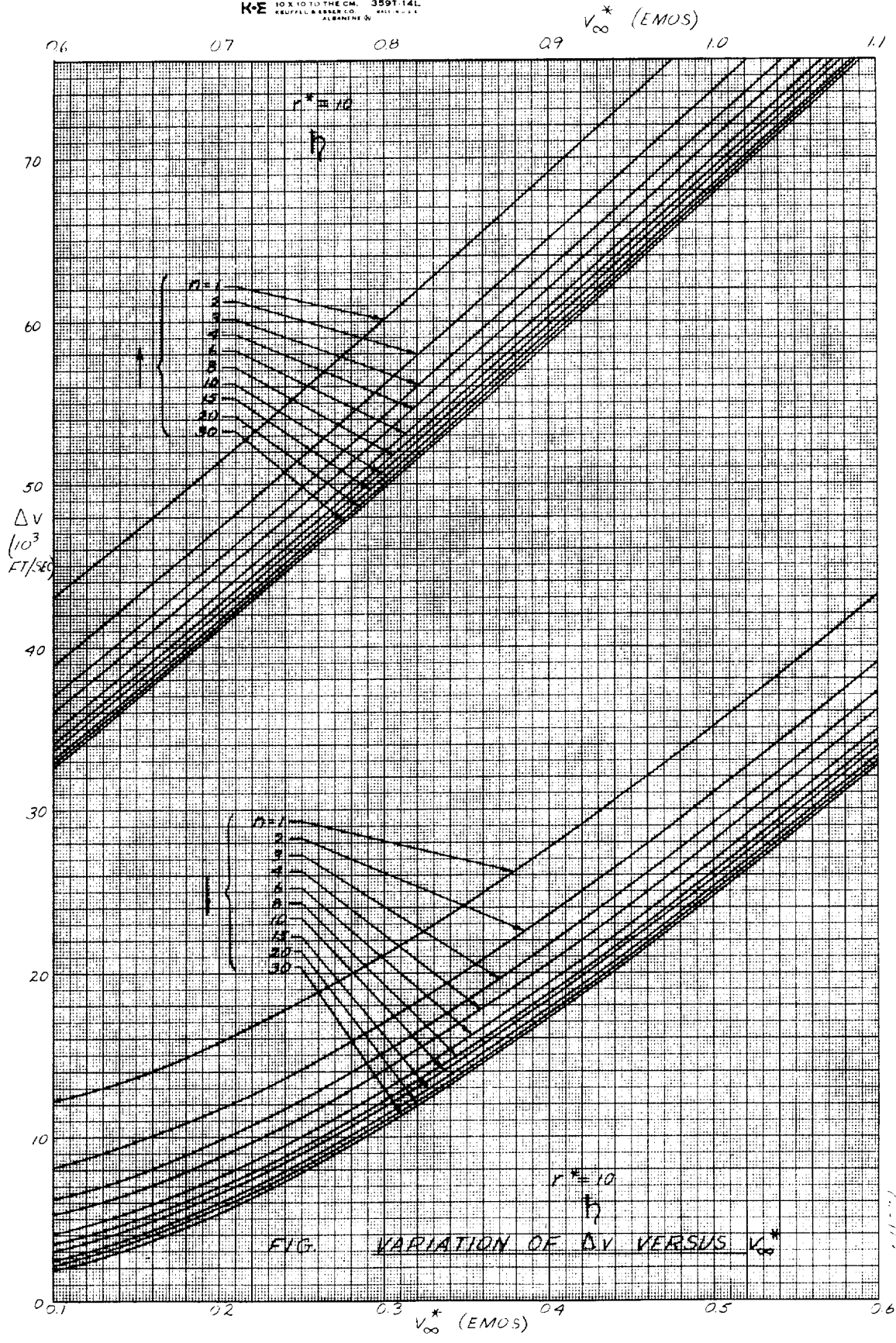
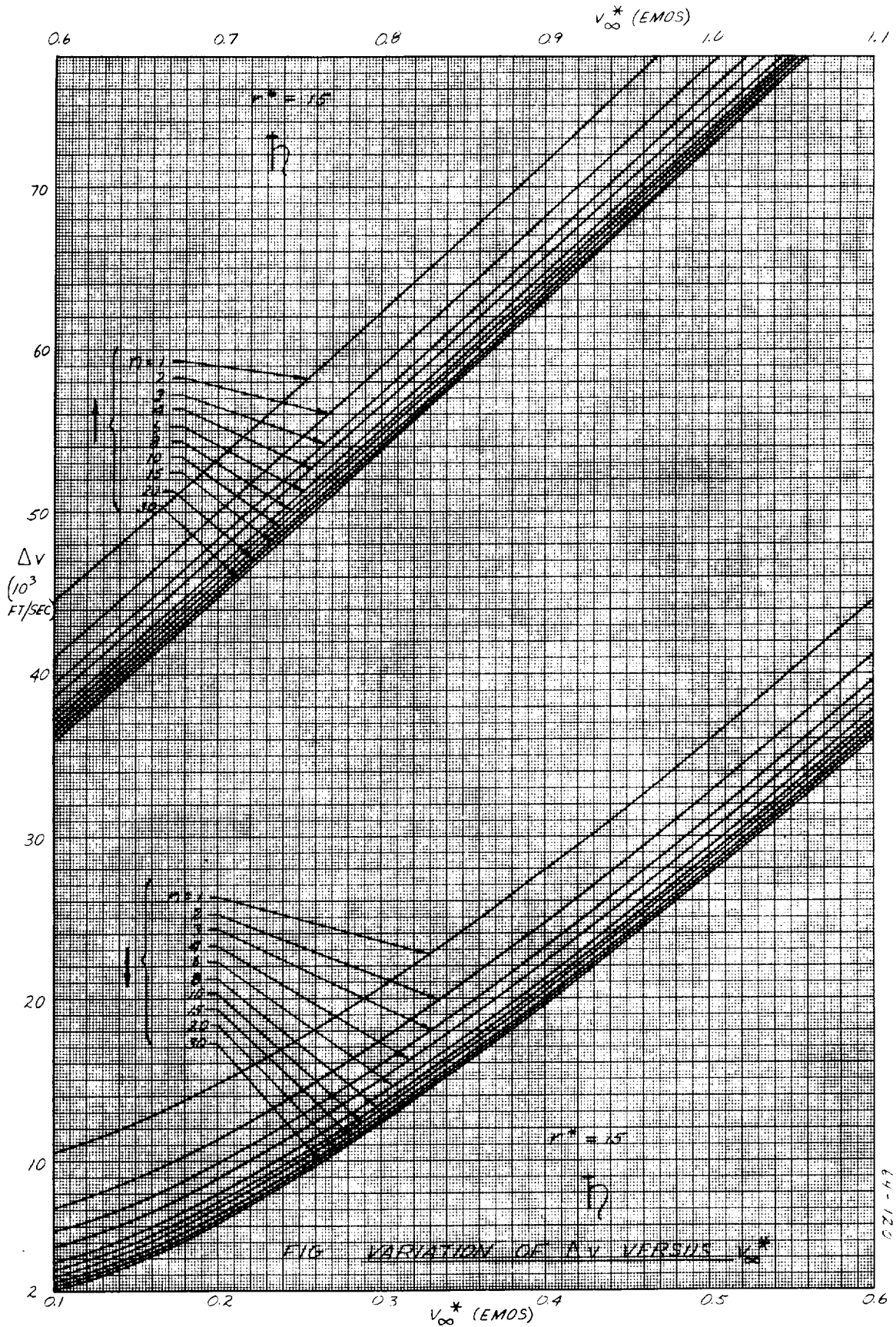
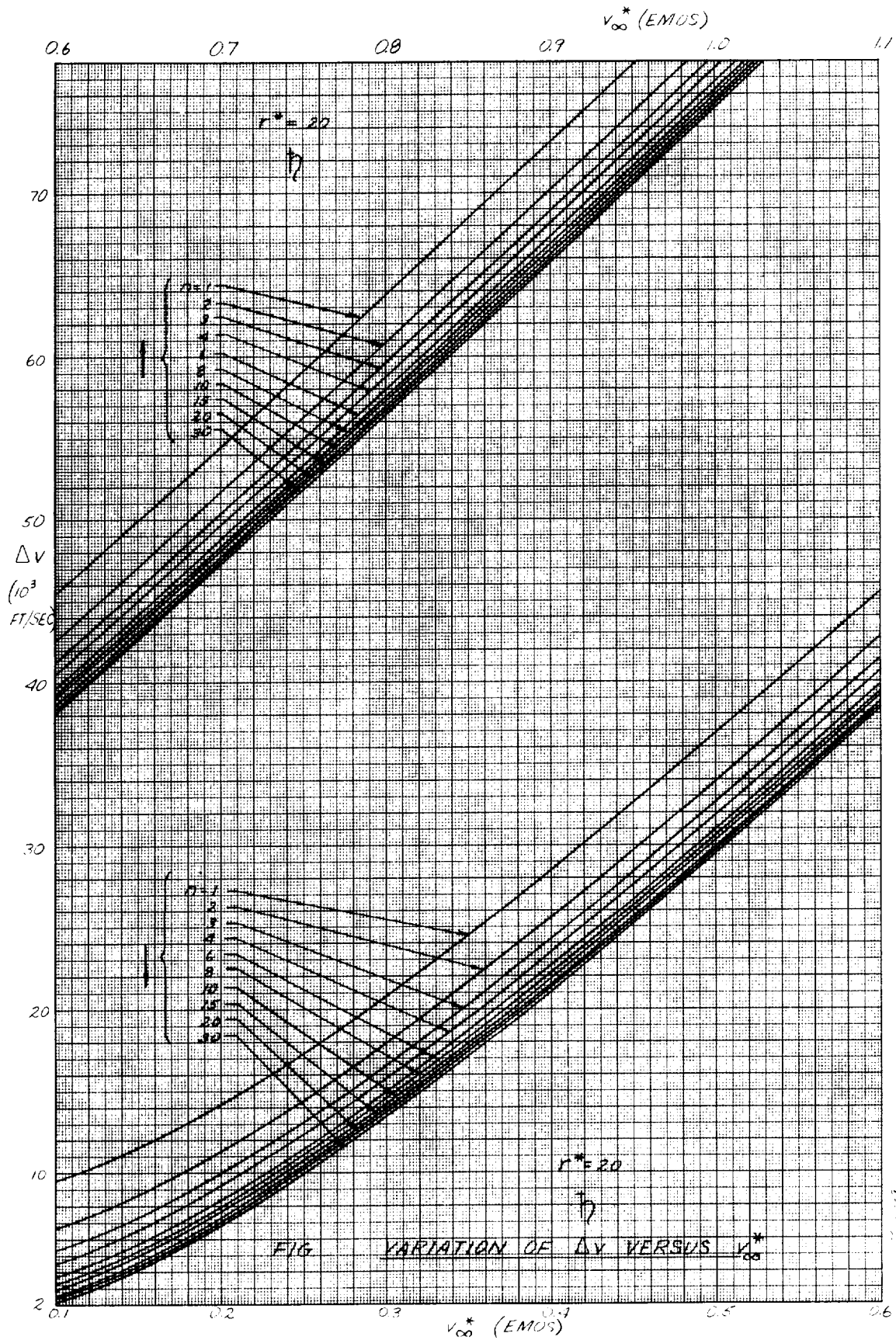


FIG. VARIATION OF ΔV VERSUS V_∞^*







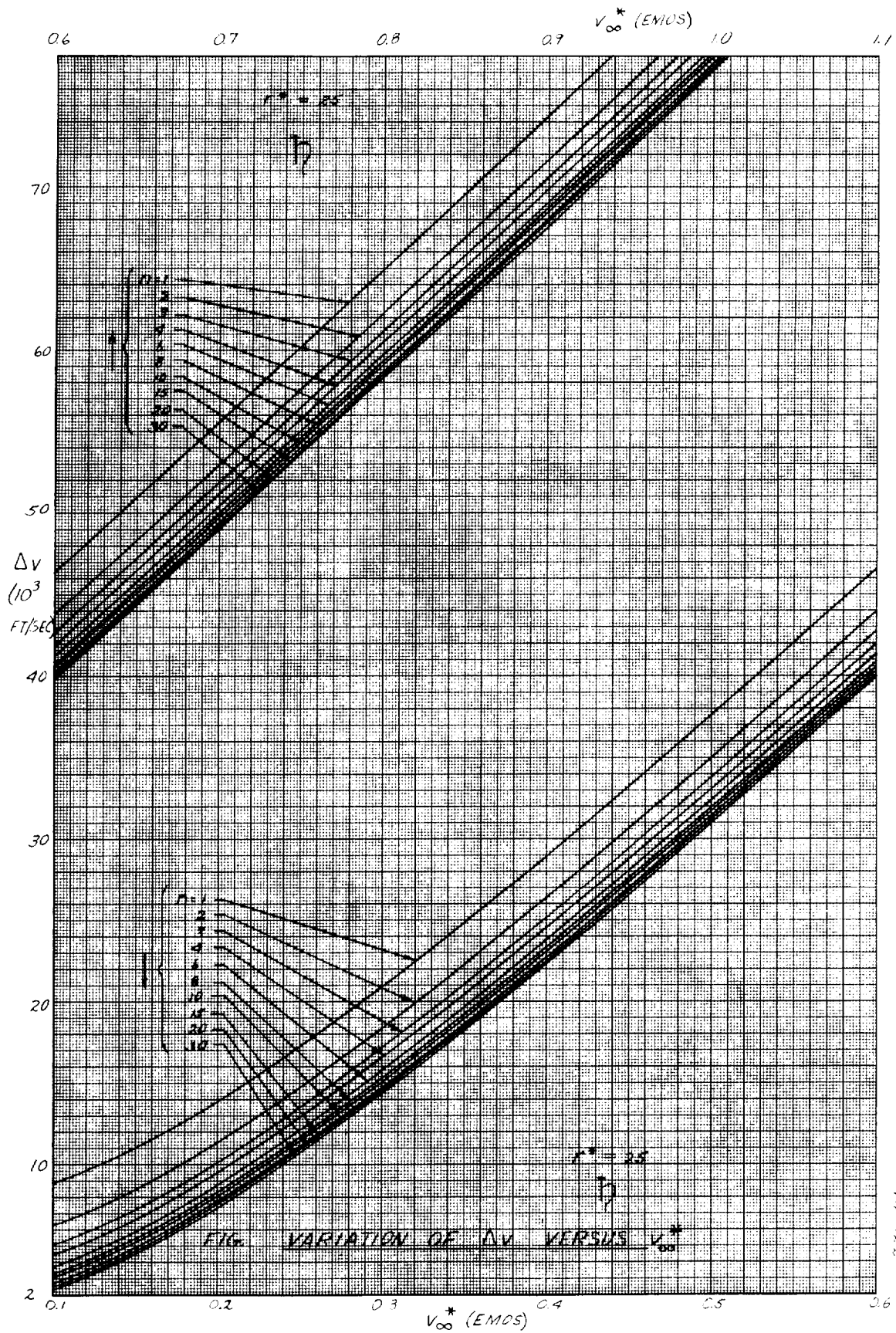


FIG. VARIATION OF ΔV VERSUS V_∞^*

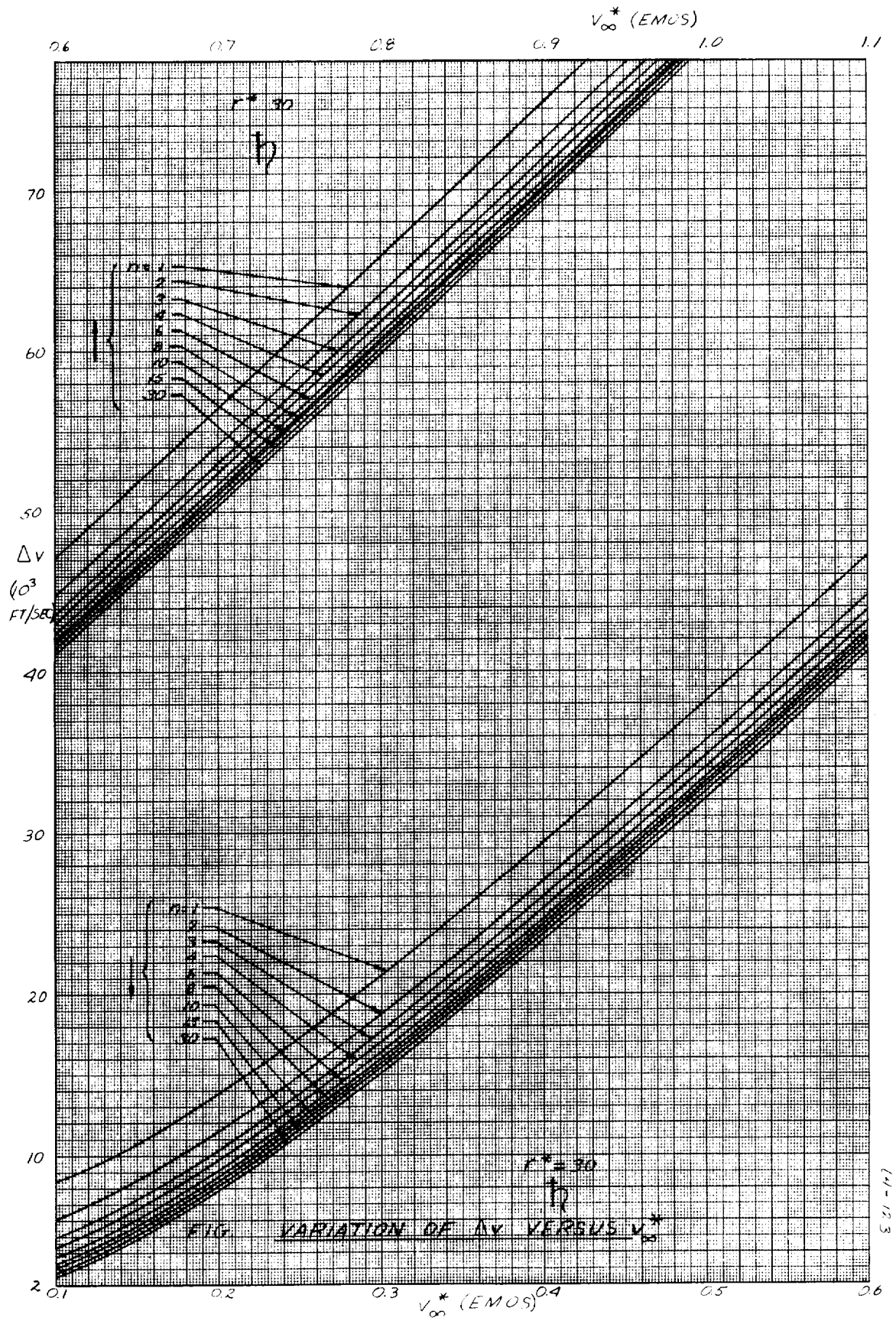


FIG. VARIATION OF Δv VERSUS V_∞^*

14-123

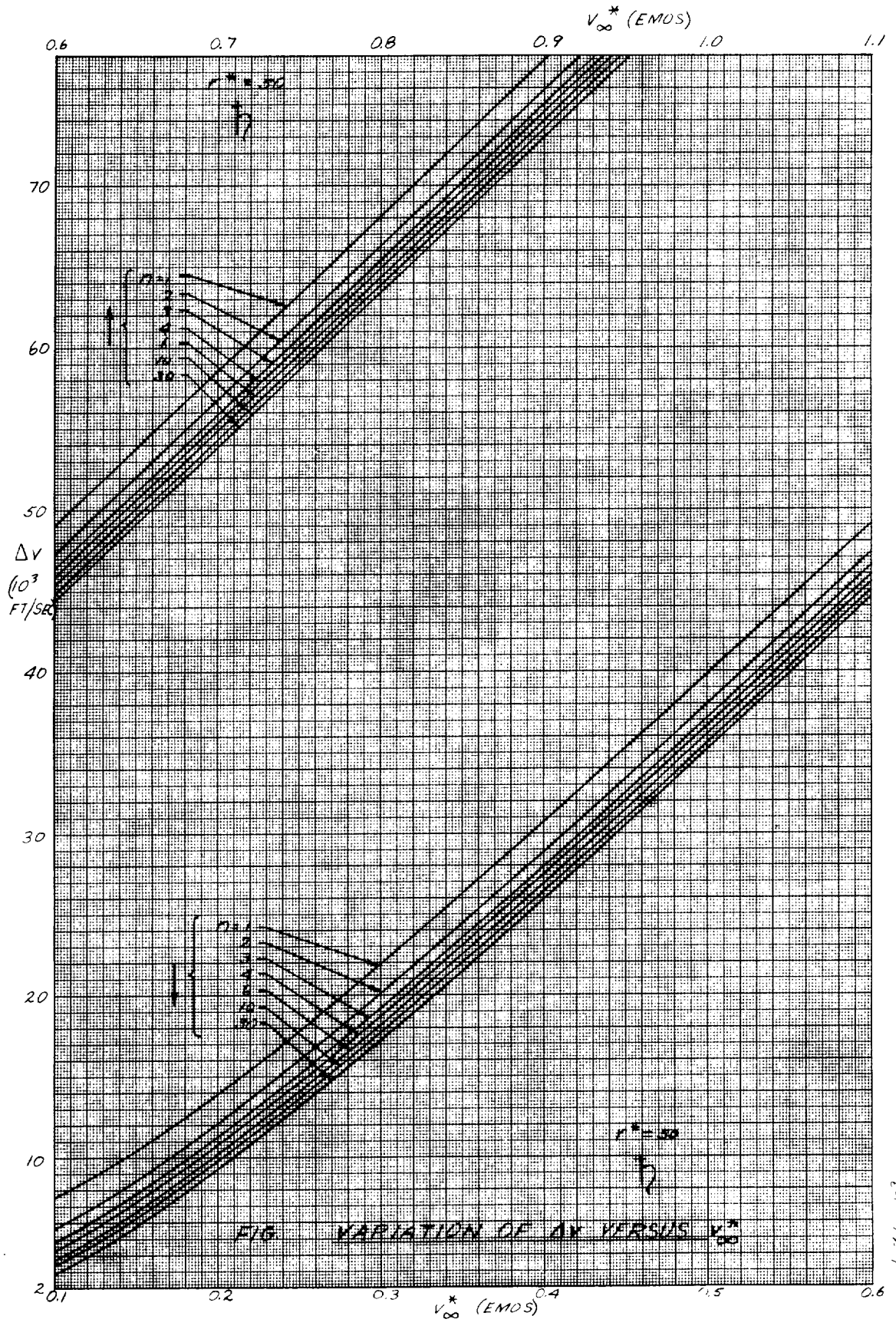


FIG. VARIATION OF ΔV VERSUS V_∞^*

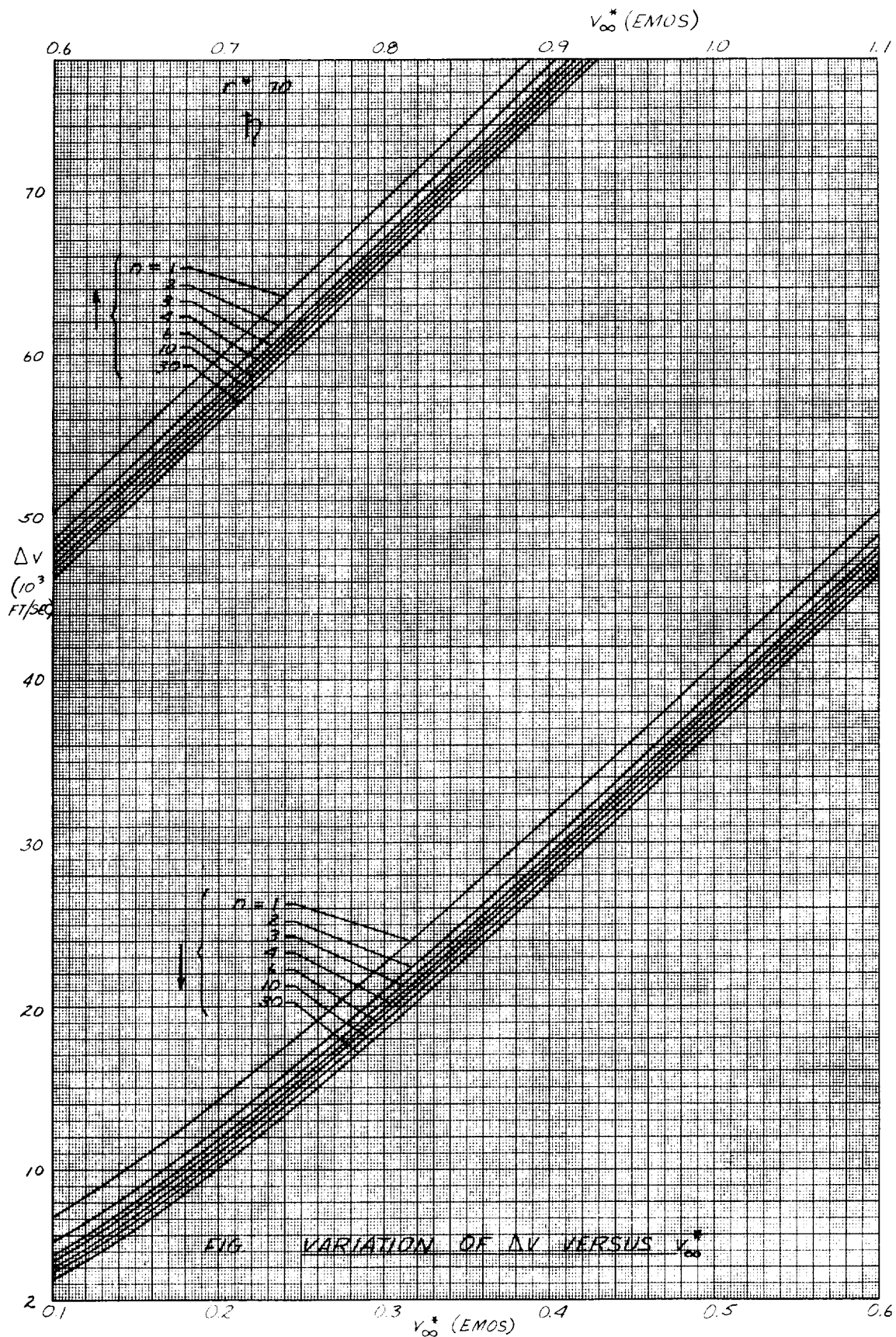


FIG VARIATION OF ΔV VERSUS V_∞^*

64-126

